A STUDY OF THE MORPHOLOGY-PROPERTY RELATIONSHIPS OF POLYMER-LAYERED SILICATE NANOCOMPOSITES

Khangelani Methuli Mbanjwa

Not for loan

A study of the morphology-property relationships of polymer-layered silicate nanocomposites

By

Khangelani Methuli Mbanjwa

Dissertation presented for the Degree Master of Technology

(Chemistry)

at the

Cape Peninsula University of Technology

Promoter:
Prof V. Hugo

Co-promoter:
Prof. R. D. Sanderson

Cape Town
May 2007

Declaration

I, the undersigned, hereby declare that the work contained in this thesis is my own original work and that I have not previously, in its entirety or part, submitted it at any university for a degree or examination, and that all the parts used or quoted have been acknowledged by complete references.

Signature: 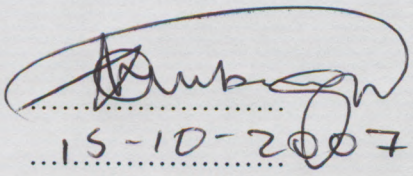

Date: 15-10-2007

Abstract

The continuous development of new materials and the improvement of existing ones ensure a balance between technological growth and environmental sustainability. With the above trade-offs, the quality of life for humankind is continually being improved. Polymeric materials are some of our most valued commodities in our everyday lives. They continue to be developed and improved in a variety of ways; one of which is to improve their properties by preparing nanocomposites. Polymer-based nanocomposites (PNCs) is a way of getting novel properties and enhancing existing one in polymer matrices, by incorporating additives on a nano-scale. The most significant advantage of PNCs is the potential to design and tailor properties for a specific application, since the control of the structure can be done at the molecular level. Therefore, a fundamental understanding of the relationships between the structure and the properties of PNCs is of utmost importance. Amongst the most studied and researched PNC materials, polymer-layered silicate nanocomposites (PLSNs) have recently enjoyed attention from academia and industry.

In the current study structure-property relationships of PLSNs were investigated. Polystyrene (PS) was chosen as the base polymer due to its wide use in many articles such as in packaging. It was also a material of choice based on its poor mechanical properties in its natural state (unfilled), so as to contribute in its property improvement. Montmorillonite (MMT) was a layered silicate (clay) of choice, as much research has been done on it, and it is available worldwide, as a main component in Bentonite (a natural material).

Clays are composed of sheet-like, layered particles, which, when in a suitable environment, can delaminate into single, nano-sized sheets. The sheets are held together by van der Waals forces and between the sheets are exchangeable cations. The clays are hydrophilic in nature and cannot readily delaminate in a hydrophobic polymer matrix due to the differences in surface energies. A MMT surface was functionalized to be hydrophobic by conducting an ion exchange reaction with alkyl ammonium surface active agents (surfactants). Polymerizable surfactants (surfmers) were used to enhance the interfacial interaction between the PS matrix and MMT silicate layers.

The organically modified clays (organoclays) were used in synthesizing polystyrene-layered silicate nanocomposites (PS-LSN) by an in-situ intercalative polymerization method. The polymerization of the nanocomposites was conducted in bulk. The morphologies of the nanocomposites were characterized using small-angle X-ray scattering (SAXS), transmission electron microscopy (TEM), Fourier transform infrared spectroscopy (FTIR) and gel permeation chromatography (GPC).

The study was further expanded to the investigation of the effects of the nanocomposite structure, type of organic modifier, and amount of clay loading on the properties of the materials. The properties were studied by dynamic mechanical analysis (DMA), thermomechanical analysis (TMA) and dielectric analysis (DEA). The properties were dependent on the interfacial processes between the clay layers and the polymer matrix. The changes in properties compared to the PS homopolymer showed time and temperature dependent effects, as determined by DEA. Even though the dynamics of the interfacial interactions are still not fully understood, the nanocomposites showed improvements in properties compared to the homopolymers.

Acknowledgements

I would like to give sincere thanks and the highest regard to the **Almighty** for the endless prospects, courage and inner strength.

The most important point for me is to acknowledge the people who have contributed to the success of the study and have not been thanked enough, the people who have been forgotten, and I realize I could never thank all the people enough here but I have the regard for their contribution.

My promoters, **Professors Ron Sanderson** and **Victor Hugo** are greatly acknowledged for believing in me, and their tireless support and advices during the course of my study.
This study was, indeed, meant to be a success with their ideas and mentorship.

The **Division of Polymer Science (Chemistry and Polymer Science Department, Stellenbosch University), Cape Peninsula University of Technology** and the **National Research Foundation** are acknowledged and gratefully thanked for the financial support.

Dr Patrice Hartmann and **Valeska Cloete** are gratefully acknowledged for giving me opportunities to explore and break boundaries in the scientific field. The experimental part of my research would have been non-existent if there was no space for me in the Paper Coatings/ Mondi Packaging Research Laboratory. Extra-thanks to Dr Hartmann for mentorship and the SAXS results. **Austin Samakande** is sincerely thanked for sharing knowledge and discoveries in the clay nanocomposites subject and for being a good friend. The discussions we had were always fruitful.

Dr Godfrey Sauti is acknowledged for sharing expertise in dielectric analysis and for opening a 'window in the world of Physics'. Sharing of ideas always fitted well in our discussions. **Prof David Maclachlan** is unreservedly acknowledged for allowing the use of the dielectric instrumentation whose results comprise a very important part of this thesis. I also would like to thank him for support and mentorship.

I would like to extend my gratitude to **Dr Margie Hurndall** for helping with proof-reading of the thesis script, and for her untiring patience.

The **staff and students** at the Institute for Polymer Science are thanked for tireless assistance during the course of the study. The administrative staff; **Erinda Cooper**, **Johan Bonthuys** (late), **Adam Keuler** and **Aneli Fourie** have been of great assistance in all the three years I have spent at the institute. **Calvin Maart** and **Hennie Groenevald** are gratefully thanked for their kindness and assistance.

Mohamed Jaffer of Electron Microscope Unit at the University of Cape Town is greatly acknowledged for the TEM analyses.

Dr Andy Roediger and staff at Roediger Agencies are acknowledged for their unreserved assistance and support.

I acknowledge an endless list of my **friends and relatives** that I cannot mention one by one in a single paragraph; who have always been a support and a source of inspiration for the 'cause'. All work and no play would have made me very dull. I thank everyone for putting in a share of amusement and delight in my days.

The last but not least of acknowledgements goes to **my family**, which has given a real measure of love, and the meaning of oneness and support. **Joyce Bulelwa Mbanjwa**, my mother, whose aspirations and struggles have blossomed into this success, is forever appreciated, and this paragraph could never be sufficient to give the thanks she deserves.

TABLE OF CONTENTS

CHAPTER 3

CHAPTER 4

List of Figures

List of Schemes

List of Tables

Notations and Abbreviations

Notations and symbols

α	aspect ratio
E'	storage modulus
E"	loss modulus
tan δ	tan delta
10^{-9} m	nanometer
Hz	hertz
d-spacing	basal spacing
q	diffraction wave vector
λ	radiation wavelength
θ	scattering angle
n	diffraction order
d_{hk}	basal spacing between reticular planes *hkl*
q_{hkl}	wave vector corresponding to planes *hkl*
τ	dielectric relaxation time
ε^*	complex permittivity
ε''	imaginary permittivity or dielectric loss
ε'	real permittivity
tan δ	*loss tangent* (tan delta)
i	square root of -1
ω	angular frequency
X	coefficient of linear expansion
ϕ	volume fraction
$\sigma(\omega)$	conductivity
$M(\omega)$	modulus
$Z(\omega)$	electrical impedance

Abbreviations

AIBN	2,2-azobis (isobutyronitrile)
A/L	Area-to-thickness ratio
A/V	ratio of surface area-to-volume
CEC	cation exchange capacity
CLTE	coefficient of linear thermal expansion
CTAB	cetyl trimethyl ammonium bromide
CTABMMT	CTAB-modified MMT
DEA	dielectric analysis
DMA	dynamic mechanical analysis
DRS	dielectric relaxation spectroscopy
DTG	first derivative of percentage weight loss
EGA	evolved gas analysis
EM	electromagnetic radiation
ethylMMT	ethyl surfmer-modified MMT
ethyl surfmer	11-acryloyloxy undecyl dimethyl ethyl ammonium bromide
FTIR	Fourier transform infrared spectroscopy
GPC	gel permeation chromatography
HDT	heat deflection temperature
FTIR	Fourier transform infrared spectroscopy
hydroxyethylMMT	hydroxyethyl surfmer-modified MMT
hydroxyethyl surfmer	11-acryloyloxy undecyl dimethyl hydroxyethyl ammonium bromide
l	filler width/radius
L	filler length
M^+	adsorbed alkali cations in the interlayer space
M_w	average molecular weight
Na-MMT	sodium montmorillonite

NMR	nuclear magnetic resonance
oganoclay	organically-modified clay
P	polarization
P_A	atom polarization
P_E	electron polarization
P_I	induced dipoles
P_O	dipole orientation
PAS	photo-acoustic spectrometry
PDI	polydispersity index
PLSN	polymer-layered silicate nanocomposite
PMMA	poly(methyl methacrylate)
PNC	polymer-based nanocomposite
PS	polystyrene
PS-LSN	polystyrene-layered silicate nanocomposite
Pyr-GC	pyrolysis-gas chromatography
R_g	radius of gyration
RAFT	reverse addition fragmentation chain transfer
rpm	rotations per minute
SAXS	small-angle X-ray scattering
SEM	scanning electron microscopy
Surfmers	polymerizable surface-active agents
T_g	glass transition temperature
$T_{onset,1}$	first peak onset of degradation
T_{max}	temperature point/s at which the DTG peak shows a maximum
TD	thermodilatometry
TEM	transmission electron microscopy
TG	percentage weight loss
TGA	thermogravimetric analysis

TMA	thermomechanical analysis
T:O	Ratio of tetrahedral sheets to octahedral sheets
UHP	ultra-high purity
vol%	volume percent
WAXS	wide angle X-ray scattering
wt%	weight percent
XRD	X-ray diffraction

Chapter 1

Introduction

1.1 General introduction

We live in a constantly changing world. The one thing that changes at a very fast rate is technology. Technological changes are sustained by constant improvements and new developments in many scientific disciplines. These developments generally ensure that the quality of life for humankind is continually embraced and improved.

Materials science and polymer science, in particular, have always been amongst the scientific fields that have a considerable impact in everyday life, especially after the drastic increase in the world production of plastics after 1930.[1] Looking around us, we see many articles that are a direct and/or indirect result of the progress in these fields. The influence of these fields was eminent as early as when synthetic materials substituted conventional materials such as metals. Synthetic materials complemented clothing made from natural sources such as cotton and wool.

Composite technology improves the properties of materials, such as polymers, by adding enhanced properties and new characteristics. Polymer composites include metals for electrical conductivity, glass fibers for mechanical properties, bioactive ceramics for medical applications, natural fibers for biodegradable polymers, semiconductors for electronic properties, carbon fibers for mechanical and electrical properties and ceramics for insulating properties. The incorporation of different materials into polymers results in the use of such composites in an increasing variety of applications. These include aircraft and aerospace, construction, marine technology, automotive, electronics, medical applications and packaging.[2-8]

Recently, a lot of focus has been on nanotechnology as one of the ways of incorporating fillers and additives into polymers. The resulting product is known as a nanocomposite. The essence of nanotechnology is described by Schmidt et al.[9] as "the ability to work at the molecular level to create large structures with fundamentally new molecular organizations". Nanotechnology is based on the understanding of phenomena at dimensions equivalent to a nanometer (10^{-9} m). This means that steps towards the understanding of phenomena on an even smaller scale than conventionally known to date are leading to a more precise and focused way of improving and controlling material properties.

One of the ways to improve polymer properties, which has received much attention from research and industry, is by the incorporation of organically modified silicates (organoclays).[9-11] Control of the resultant structures is of utmost importance when it comes to the improvement of the properties. The interactions between the incorporated filler and the polymer are at very small dimensions (at least one dimension in nanometers). For this reason, the interactions influence the improvement of properties more significantly than larger scale interactions such as microcomposites and macrocomposites do.

Layered-silicates or clays (also known as phyllosilicates) are usually modified by organic molecules to make their surfaces more hydrophobic and hence compatible with hydrophobic polymer matrices.[10,11] The surface modification promotes the penetration of the packed (stacked) silicate layers by the polymer chains (intercalation) and subsequently delamination/dispersion of the layers in the polymer matrix (exfoliation). Exfoliated clay nanocomposites have a larger surface area interaction with the polymer matrix. This is the basis of improved properties exhibited by polymer-layered silicate nanocomposites (PLSNs).

1.2 Rationale

Ever since the polymer-layered silicate nanocomposites were reported to be successfully synthesized on nylon-6 matrix by the Toyota Research Group in 1993, a lot of work has been done by other researchers on this type of nanocomposite.[10-12]

Although the morphology and properties of nanocomposites of different types of polymer matrices have been studied, there is, as yet, no full understanding of the fundamental principles, such as structure-property relationships, volume fraction-property relationships, driving factors to total exfoliation, as well as the 'fine tuning' of the morphology to yield very specific properties.[9,13,14] Data gathered for the systems that have been studied do not apply universally to other systems.[13] Uncertainty still exists in understanding the important interactions that are vital to future research into applications of these new materials.

The Department of Chemistry and Polymer Science, University of Stellenbosch, has recently taken an interest in layered-clay nanocomposite research. New polymerizable surface-active agents (surfmers) were successfully synthesized and it was found that they could be used to modify layered clays for PLSN synthesis.[15] Although PLSNs have been studied for specific polymer matrices[10,11], fundamental principles in understanding the structural interactions are still not well understood. This is because the nanocomposite materials are very dependent on specific factors such as the polymer matrix, type of clay, organic surfactant and the preparation conditions. The fact that each polymer-clay nanocomposite material is a unique system opens a wide window of investigation.

1.3 Objectives

The study is a follow-on from work done by our group on surfmers to organically modify layered clay surfaces for nanocomposite synthesis. In this study, modified layered

silicates, the structure and properties of the subsequent polymer-clay nanocomposites are studied further. The principal objectives of this study are:

1. To synthesize organically modified clays (organoclays) for nanocomposites using in-house synthesized, polymerizable surfactants; a commercial, classical surfactant; and montmorillonite clay (MMT), and then characterize the organoclays using Fourier transform infrared spectroscopy (FTIR), thermogravimetric analysis (TGA) and scanning electron microscopy (SEM).
2. To synthesize polystyrene-based clay nanocomposites using bulk polymerization and to characterize their structures using small-angle X-ray scattering (SAXS), transmission electron microscopy (TEM), FTIR and gel permeation chromatography (GPC).
3. To study the relationships between the nanocomposite structure and the properties using a variety of classic and state-of-the-art analytical techniques, namely dynamic mechanical analysis (DMA), thermomechanical analysis (TMA) and dielectric analysis (DEA).
4. To establish new and/or improved properties due to changes in the nanocomposite structure.
5. To establish whether these new/unique properties can be used to explain the specific nanocomposite structure.

The above objectives are sub-divided into smaller, more specific goals, and are elucidated as objectives in the relevant chapters.

The flow chart (Scheme 1.1) illustrates the focus and the main objectives of this study. The area inside the segmented line shows the topics that will be covered, while the part outside the area shows a topic that is considered to be a key element in the current research but was not included in this study. The synthesis of surfmers for clay modification was studied by co-workers in the previous study.[16] The initial synthesis of

the surfmers, which led to the modification of clays, opened opportunities for the study of the subsequent nanocomposite materials.

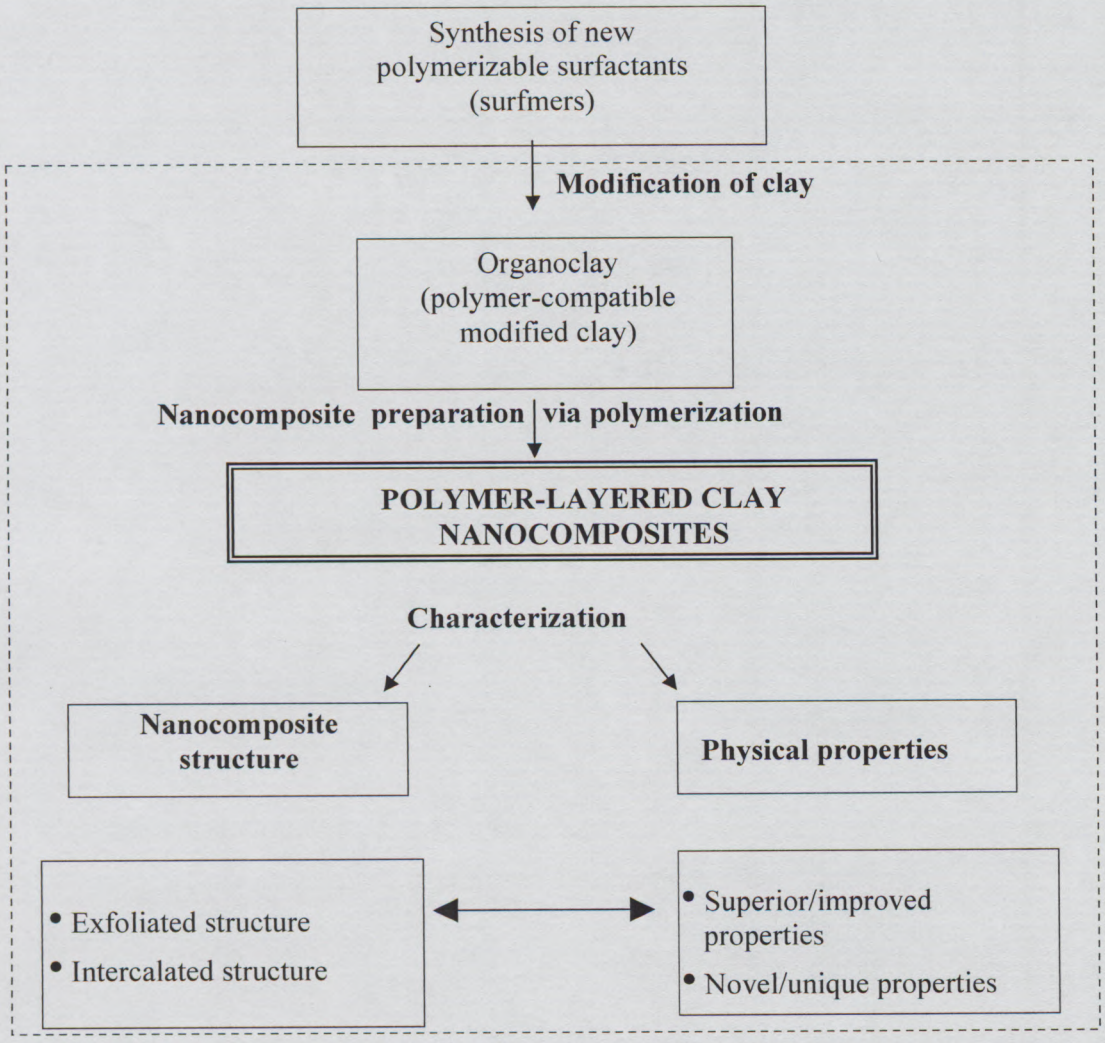

Scheme 1.1: Schematic chart showing the focus and objectives of the research on the study of structure-property relationships in polymer-clay nanocomposites.

1.4 Thesis layout

Chapter 1 provides an overall introduction to the study and also includes objectives and the motivation for the study. Chapter 2 gives a detailed background to clay materials, composites and polymer-layered silicate nanocomposites. It includes a literature review of chemical background and fundamental principles of layered silicates, nanocomposite synthesis and their characterization. In Chapter 3 different analytical techniques used for the characterization of PLSNs are reviewed and discussed.

Chapters 4, 5 and 6 cover the experimental work carried out in this study, and the discussions of the results obtained. The synthesis of organoclays and their properties are covered in Chapter 4. Chapter 5 focuses on the synthesis of polystyrene-layered clay nanocomposites, and also their structural characterization. The effects of the nanocomposite structure on its physical properties are discussed in Chapter 6. Also, correlations between new characteristic properties and structure are discussed. Chapter 6 also focuses on dielectric properties of polymer-layered clay nanocomposites. Correlations between nanocomposite structure and the observed dielectric properties are discussed. Dielectric analysis is a field of research that has not yet received much attention in the field of polymer-layered silicate nanocomposites; this thesis explorers some aspects of dielectric studies.

Conclusions and recommendations are given in chapter 7. Possible further developments for the field are stated.

1.5 List of references

1. Imperial Chemical Industries Ltd., *Landmarks of the Plastic Industry*. 1st ed.; Imperial Chemical Industries, Ltd.: **1962**; p 126.

2. Soutis, C. *Materials Science and Engineering: A* **2005,** 412, 171-176.

3. Mills, D. M.; Smith, S. W. *IEEE on Ultrasonics, Ferroelectronics, and Frequency Control* **2002,** 49.

4. Kawada, H.; Kobiki, A.; Koyanagi, J.; Hosoi, A. *Materials Science and Engineering: A* **2005,** 412, 159-164.

5. Barton, B.; Wobbe, E.; Dharani, L. R.; Silva, P.; Birman, V.; Nanni, A.; Alkhrdaji, T.; Thomas, J.; Tunis, G. *Materials Science and Engineering: A* **2005,** 412, 129-136.

6. Lua, J.; O'Brien, J.; Key, C. T.; Wu, Y.; Lattimer, B. Y. *Composites Part A: Applied Science and Manufacturing* **2006,** 37, 1024-1039.

7. Tharanathan, R. N. *Trends in Food Science & Technology* **2003,** 14, 71-78.

8. Quilter, A. *Composites In Aerospace Applications*; IHS Company (engineers.ihs.com/pdf/litcenter/444.pdf) Accessed 07 July **2006**: pp 1-3.

9. Schmidt, D.; Shah, D.; Giannelis, E. P. *Current Opinion in Solid State & Materials Science* **2002,** 6, 205-212.

10. Alexandre, M.; Dubois, P. *Materials Science and Engineering: R (Reports)* **2000,** 28, 1-63.

11. Ray, S. S.; Okamoto, M. *Progress in Polymer Science* **2003,** 28, 1539-1641.

12. Kojima, Y.; Usuki, A.; Kawasumi, M.; Okada, A.; Fukushima, Y.; Kurauchi, T.; Kamigaito, O. *Journal of Materials Research* **1993,** 8, 1185-1189.

13. Vaia, R. A.; Wagner, D. H. *Materials Today* **2004,** 7, 32-37.

14. Zeng, H. Q.; Yu, A. B.; LU(Max), G. Q.; Paul, D. R. *Nanoscience and Nanotechnology* **2005,** 5, 1574-1592.

15. Samakande, A.; Hartmann, P. C.; Sanderson, R. D. *Journal of Colloid and Interface Science* **2005,** 269, 316-323.

16. Samakande, A. Synthesis and Characterization of Surfmers for the Synthesis of Polystyrene-Clay Nanocomposites. MSc Thesis, University of Stellenbosch, Stellenbosch, **2005**.

Chapter 2

Clay Materials and Composites:

A brief overview and history of layered-silicates, their use in composites, and the properties of polymer-based clay nanocomposites

2.1 Introduction

This section of the literature study (2.1) includes consideration of the mineralogy and chemistry of clay materials in order to highlight their properties and use in composites. Clay materials come from different types of mineral sources worldwide.[1] Clays are a very diverse group of materials in terms of composition, structure and chemistry. The term 'clay' refers to components of minerals that are mainly silicates. There is a wide range of silicate-type minerals, classified in different groups. Silicate structures and chemistry are the main categorizing phenomena for the different types of clay materials (by international agreement).[2] A framework is used to guide the classification of the clays, as it is a complex study that is continually being improved.

2.1.1 Mineralogy, chemistry and classification of clays

Clays are constituted in crystallographic structures, forming sheets that are arranged in layers, and hence they are also called phyllosilicates.[1] Each individual sheet consists of two, three, or four layers, based on aluminum (Al) and silicon (Si) crystal groups (alumnosilicates). These crystal sheets are organized in structures where tetrahedral and octahedral groups are the main components. The tetrahedral sheet has a chemical structure comprising a central silicon atom and four adjacent oxygen atoms, based on the formula: $[SiO_4]^{4-}$. The octahedral formula is $[AlO_3(OH)_3]^{6-}$. It comprises a small metal

cation at the centre (e.g. aluminum) and six adjacent oxygen atoms, some of which have bonded protons, to form hydroxyl groups. The octahedral groups form a hexagonal network in each sheet. Magnesium (Mg) and iron (Fe) may substitute Al in varying degrees.[2] Konta[1] reported the classification of clay minerals based on the number and the ratio of sheets (tetrahedral to octahedral) in a fundamental layer. He classified the minerals into seven groups, as shown in Table 2.1 below.

Table 2.1: Classification of clay minerals according to the number and ratio of octahedral (O) and tetrahedral (T) sheets[1]

Classification (group name)	**T:O ratio[π]**	**Sheet layer**	**Charge**	**Sub group name General chemical formula (example)**
Kaolinite and serpentine group	1:1	two-sheet	0	Kaolinite $Al_4[Si_4O_{10}](OH)_8$ Halloysite $Al_4[Si_4O_{10}](OH)_8.4H_2O$ Serpentine $Mg_6[Si_4O_{10}](OH)_8$ (crysotile)
Micas	2:1	three-sheet	≤ 2	$K_{<2}Al_4[(Si_{>6}Al_{<2})O_{20}](OH)_4.nH_2O$ (illite)
Vermiculite	2:1	three-sheet	1.2 – 1.8	$(Mg, Fe^{2+}, Fe^{3+})_6[(Si>Al)_8O_{20}](OH)_4.nH_2O$
Smectite	2:1	three-sheet	0.5 – 1.2	Montmorillonite $M^+_{x+y}(Al,Fe^{3+})_{4-y}(Fe^{2+},Mg)_y[Si_{8-x}Al_xO_{20}](OH)_4.nH_2O$ Beidellite $M^+xAl_4[Si_{8-x}Al_xO_{20}](OH)_4.nH_2O$ Nontronite $M^+_xFe_4{}^{3+}[Si_{8-x}Al_xO_{20}](OH)_4.nH_2O$ Saponite $M^+_xMg_6[Si_{8-x}Al_xO_{20}](OH)_4.nH_2O$
Pyrophyllite and talc group	2:1	three-sheet	0	Pyrophyllite $Al_4[Si_8O_{20}](OH)_4$ Talc $Mg_6[Si_8O_{20}](OH)_4$
Chlorites	2:1:1 (T:O:O)	four-sheet	1.1 – 3.3	$Al_4[Si_8O_{20}](OH)_4Al_4(OH)_{12}$ (donbassite)
Palygorskite and sepiolite group		random		Palygorskite $Mg_5[Si_8O_{20}](OH)_2(OH_2)_4.4H_2O$ Sepiolite $Mg_8[Si_{12}O_{30}](OH)_4(OH_2)_4.nH_2O$

[π] T:O is the ratio of the tetrahedral layers to the octahedral layers as the basic composition of a clay mineral.

In the table above, for the smectite group, M^+ represents adsorbed alkali cations in the interlayer space. It is reported that alkali earth and alkali cations (Ca^{2+}, Mg^{2+}, Li^+ and Na^+) often occur, generally $M^{2+}_{x/2}$.[1,2] The charge for M^+ is mostly around 0.7. Murray[3] also acknowledges the possibility of the presence of M^+ as Fe^{2+}.

Based on past and more recent studies, it is eminent that man has long benefited from the unique properties possessed by clay materials.[1,3-5] These properties emanate from different clay material types and chemical compositions. Over the years, the applications of clays ranged from agricultural (plant nutrition), domestic (porcelains and fine china), construction (bricks and roof tiles), coatings (pigments), environmental protection (organic contaminant absorbents) to medical (drug vehicle) and the plastic manufacturing industry (fillers in rubbers and plastics).[1] One of the prominent applications of clay is its use as filler in composite materials. Clays such as talc[6,7], mica[8] and the smectites[9] have been used as fillers in polymer-based composites.

In an expansion to the use of clays in polymeric materials, the smectite-polymer composites have recently received considerable attention in academia and industry due to the enhanced properties achieved with less than 5 wt% filler.[9-11] The silicate layers delaminate into nano-sized sheets in the polymer matrix, hence the products are known as polymer-layered silicate nanocomposites. The dispersion of the silicate sheets in the polymer matrix provides extraordinary reinforcement. The smectites are also known for the expansion properties, and the ability to form complexes with organic molecules, which is critical in the fabrication of the nanocomposites. Furthermore, being natural materials, they are widely available worldwide and therefore less expensive than other filler materials (e.g. synthetic glass fibers).

2.1.2 2:1 Smectite clays

The term "smectite" is given to a group of alumnosilicates based on sodium (Na), calcium (Ca), iron (Fe) and lithium (Li), to which the individual layered silicates such as montmorillonite, nontronite, saponite and hectorite belong.[3]

In this group of alumnosilicates, the crystal structure of a single clay layer has a configuration of two-dimensional alumnosilicates with two tetrahedral groups (T) on either side of the octahedral group (O) (hence 2:1, also T-O-T). The octahedral sheet (of Al or Mg) is fused to the tetrahedral sheets (of Si) by the lateral atoms so that the oxygen ions of the octahedral sheet are shared by the tetrahedrons, as illustrated[12] in Figure 2.1. Stacking of the layers leads to a regular packing with van der Waals forces between the adjacent layers, and the space in between is referred to as the interlayer or gallery. The layer thickness is around 1 nm and the lateral dimensions range from 30 nm to several microns, or larger.[12] The sheets have a permanent negative charge that results from an isomorphic substitution, mainly in the octahedral layer.[13] Isomorphic substitution is a natural phenomenon in which an atom is substituted by a different atom of similar radius. The isomorphic substitution normally involves Si, Al and Fe^{3+} at the tetrahedral sites and Al, Fe^{3+}, Mg and Fe^{2+} at the octahedral sites. The net charge on the layers, as a result of the isomorphic substitution, lies between 0.50 and 1.20 for general 2:1 smectites. However, layer charges of 0.7 and 1.0 are known for the smectite clays that have a formula unit $O_2(OH)_4$.[2] The charge is located at the surface of the alumnosilicate and is non-homogenously distributed on different layers. The charge is balanced by counter cations, normally situated between the sheets. These interlayer cations are hydrated and readily exchangeable. The negative surface charge is a characteristic of silicates. It is expressed as milli-equivalents per hundred grams (meq/100 g) and known as the cation exchange capacity (CEC). The hydration of the cations is determined by the humidity of a given exposed atmosphere. It is possible to dehydrate the cations by extreme desiccation but the clays will quickly rehydrate. The interlayer space expands to accommodate the hydration layer around the interlayer cation.

The 2:1 smectites are generally known for their strong expansion ability. They swell in water, ethylene glycol and some other similar compounds.[2] According to Newman and Brown[2], no detailed explanation of the factors involved in the swelling of the silicates is yet available, but there is a general agreement that one of the factors influencing swelling

is the balance of the attractive and repulsive forces between adjacent alumnosilicate layers.

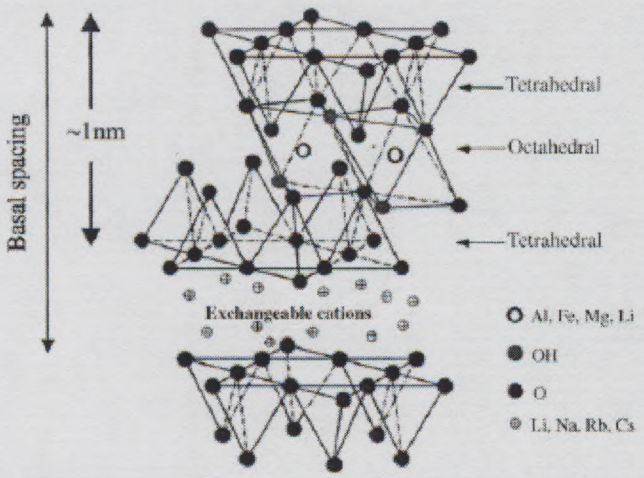

Figure 2.1: A crystal structure of 2:1 layered silicates with each layer comprising an octahedral group sandwiched in-between two tetrahedral groups.[12]

There are three commonly used 2:1 smectite clays for nanocomposite synthesis: saponite, hectorite and montmorillonite (MMT). If in the gallery of pristine clay, such as montmorillonite, the interlayer cation is only sodium, then the material is known as the sodium-montmorillonite (Na-MMT). A similar notation is used for Ca-MMT, Mg-MMT and Li-MMT, and so forth. MMT is widely available, worldwide, as the main component of bentonite.[3] Na-MMT has been widely studied for its use in the synthesis of PLSNs. MMT can have a surface area of about 700 m^2/g when exfoliated, which is an advantage for the dispersion of small amounts thereof in a polymer matrix.[14]

2.2 Review of ion-exchange of interlayer cations in clays with organic moieties

The hydrated interlayer cations in silicate galleries are readily exchangeable with organic molecules. There is a wide range of organic molecules that are exchangeable with the interlayer cations to form organic-inorganic complexes. Organic-inorganic hybrids have been researched for different potential applications such as rheology modifiers, drug-delivery agents and for polymer-based nanocomposites synthesis.[5] Other areas of research under which the modification of clay has been studied include colloid science, sedimentary geology and petroleum technology.[15]

Traditionally, the organic modification of layered silicates is studied by X-ray diffraction (XRD). This technique is used to determine the basal spacing or *d*-spacing (see Figure 2.1) of the layered silicates and gives information about the size of the interlayer spacing. When interlayer cations are replaced with organic molecules through ion-exchange, the interlayer spacing increases to accommodate them. The arrangement and orientation of the molecules in the gallery (intercalated) are determined by the combination of the subsequent interlayer spacing and the molecule geometry.[15] A traditional understanding is that the molecules can form monolayers or bilayers in the galleries. The molecule orientation is such that they can lay flat parallel to the silicate layers, or stand upright at an angle.[9]

Infrared (IR) spectroscopy techniques are used to study the molecular orientation in the interlayer space, and the mechanisms by which the organic molecules interact with the silicate surface and between themselves. IR spectroscopy is also used to determine other effects such as interaction with the residual water.[15] It has recently been reported that Fourier transform infrared (FTIR) spectroscopy has been used to establish the arrangement of alkylammonium cations inside the galleries of layered silicates, contrary to the traditional understanding of monolayers and bilayers.[12] The study established that the alkyl chains form arrangements that are *liquid-like* and *solid-like*. The liquid-like character is dominant as the chain length decreases or as there are fewer adsorbed

molecules in the galleries, or as the temperature increases.[12] It is further explained that the molecules assume the *trans* and *gauche* conformations rather than the traditional assumption which only depicts all *trans* conformations. There are relatively small energy differences between the two conformations, which makes it feasible to achieve both molecular arrangements. When there are longer chain alkylammonium cations in the silicates, they can show thermal transition upon heating. This transition is said to be similar to melting or liquid-crystalline to liquid-like transition.[12]

The alkyl ammonium salts can be primary, secondary, tertiary or quaternary, which directly relates to the number of bonds to the ammonium groups. The most widely studied complexes are those of long chain quaternary alkylammonium and alkylphosphonium salts, which are known for their organophilic character.[15] They are categorized as surface active agents (surfactants). Surface active agents are organic molecules with an alkyl, hydrophobic tail (non-polar) and charged hydrophilic head.

In the preparation of PLSNs, surfactants play a major role in compatibilizing the polymer matrix with the silicate layers. Layered silicates are naturally hydrophilic and hence it is necessary to modify their surfaces in order to make them compatible with the most generally used polymers, which are hydrophobic. Different types of organic molecules and alkylammonium surfactants have been used in the modifications of clay for PLSN synthesis.[16-19]

2.3 Structures and properties of polymer-layered silicate nanocomposites

2.3.1 Polymeric materials

The term polymer was first used to describe large molecules (macromolecules) with the same composition, but they could have different molecular weights.[20] A polymer is,

basically, a natural or synthetic macromolecule with many repeating units (monomers), linked to each other through covalent bonding. The monomers can be connected to each other in a simple two-way link to form a linear chain. Depending on the functionality (valency) of the monomers, the chains can be branched or non-linear. Some polymers may be highly branched to form two-dimensional (planar) or three-dimensional networks. In the same polymer there maybe varying degrees of polymerization, simply defined as the number of monomers connected together. The degree of polymerization describes the molecular size and that can vary, leading to molecular weight distribution of different chain sizes within the same polymer. This phenomenon is common in synthetic polymers.[20] Many different synthetic polymers have been studied and developed over the years. Their ability to be used in different application across the entire industrial spectrum makes them very interesting materials to study and further develop.

The molecular and structural constitution of polymers has a direct effect on their physical properties, and subsequently their applications. Polymers can be categorized into thermoplastics and thermosets. Thermosets are polymers in which the chains are inter-linked by other chains to form an irreversible network, referred to as cross-linked network. The latter are highly resistant to solvents and do not melt on heating. On the other hand, thermoplastic polymers melt on heating and resolidify on cooling. The softening and melting properties of thermoplastics are affected by molecular weight and chain orientation.[21] The effect of the molecular weight is observed in the different phases of a polymer system. At a given temperature a polymer will be in a certain phase. It may be soft and pliable or it may be hard and brittle. The phases shown in Figure 2.2 determine the physical state and properties of the polymer. Orientation affects the type of phases that a polymer possesses. A polymer may have an ordered chain arrangement and will have a transition point at which those chains are disrupted, namely the melting temperature (T_m). These are known as crystalline polymers. On the contrary, polymers with highly disordered chains are known as amorphous polymers and are usually brittle at temperatures below their softening points.

The choice of a polymer for a particular application depends, among other factors, on its properties in the chosen temperature range. Some polymers, for example, are "usable" below their softening point and some are better at temperatures where they are hard. The softening point is the temperature at which a polymer becomes soft and rubbery, from being hard and brittle, and is known as the glass transition temperature (T_g). In the case of some polymers under the ambient conditions, the T_g may be below room temperature and the polymer useable for soft materials in that state. This is advantageous for applications such as coatings and rubbers. Some polymers such as polystyrene are better usable at temperatures below the T_g. However, the polymer may be brittle and therefore exhibit poor impact loading for mechanical uses. It is, therefore, necessary to modify and improve its properties for it to be suitable for the intended application.

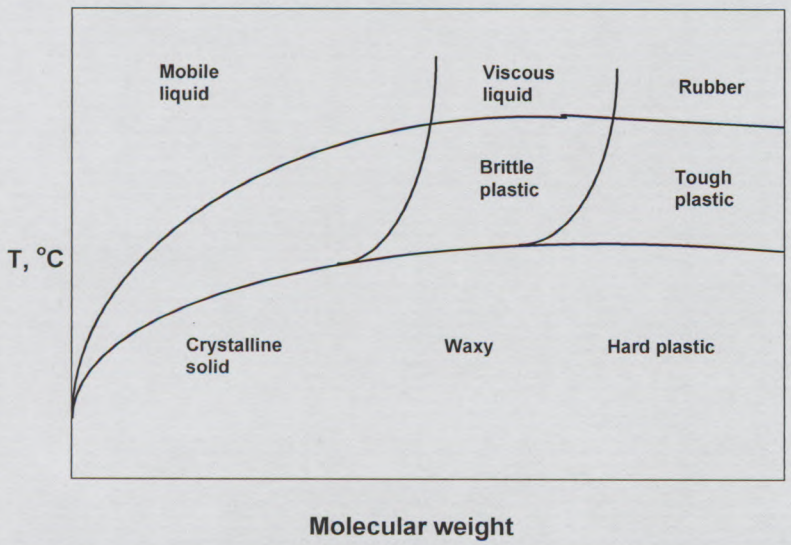

Figure 2.2: A schematic presentation of polymer phase dependence on molecular weight and temperature.[20]

A polymer can be modified to supplement its molecular nature by the addition of modifiers or additives. Additives include thermal/ultraviolet stabilizers, colorants, plasticizers, cross-linking agents and mineral fillers. In order to improve mechanical properties in thermoplastic polymers, inorganic mineral fillers, amongst others, have been used.[6-8] Currently, layered clays are one of the preferred types of mineral inorganic materials to improve polymer properties. This is because of the ability to have modifiable

surfaces and to allow polymer chains to intercalate for better interfacial interaction. Other inorganic materials, natural and synthetic, are known to allow the intercalation of polymer chains (See Table 2.2).[9]

Table 2.2: Example of host crystals susceptible to intercalation by polymer chains.[9]

Chemical nature	Examples
Element	Graphite
Metal chalcogenides	$(PbS)_{1.18}(TiS_2)$, (MoS_2)
Carbon oxides	Graphite oxide
Metal phosphates	$Zr(HPO_4)$
Clays and layered silicates	Montmorillonite, hectorite, saponite, fluorohectorite, vermiculite, kaolinite, magadiite, ...
Layered double hydroxides	$M_6Al_2(OH)_{16}CO_3.nH_2O$; M=Mg, Zn

2.3.2 Nature of nanocomposites compared to microcomposites

To begin the discussion of properties of polymer-layered clay nanocomposites and their structural relations, it is important to first provide a background to the fundamental aspects of polymer reinforcement by the addition of fillers. One of the critical aspects related to describing the properties of a PLSN is the emphasis of the differences and the advantages they have over the classical micro-scale composites. Vaia and Wagner[22] set up a "framework" defining the dynamics of polymer-based nanocomposites (PNCs) in comparison to the traditional type of fillers. They based their discussion on carbon nanotubes and layered silicate nanocomposites, chosen as the most studied of nanocomposites. It is understood that the fundamental aspects of PNCs are different to those of the conventional materials. The main characteristics of PNCs, which are interrelated, that distinguish them from the classically filled systems, are:

- Low percolation threshold exhibited at a volume fraction (ϕ) of approximately 0.1 – 2 volume percent (vol%);
- Particle-particle correlation (orientation and position) arising at a low volume fraction (critical volume fraction, $\phi_c < 0.001$);
- Large density of particles per particle volume ($10^6 – 10^8$ particles/μm^3);

- Extensive interfacial area per volume of particles ($10^2 - 10^3$ m^2/ml);
- Short distances between particles (10 – 50 nm at $\phi \sim 1 - 8$ vol%); and
- Comparable size scales among rigid nanoparticle inclusion, distance between particles, and the relaxation volume of polymer chains.

One of the most advantageous features of nanocomposites is that the particles, of 1 – 100 μm, are introduced into the polymer matrix or polymer matrix precursor which contain a number of associated nano-sized particles. These nano-sized particles are usually in excess of ten million, and they become isolated into individual nano-particles in the matrix.

The following example, in Figure 2.3, is given to illustrate the comparison of a microcomposite to a nanocomposite material when micro-sized (l =1 μm, L=25 μm) and nano-sized (l =1 nm, L=25 nm) fibers are dispersed in equal volume fractions in different polymer based systems. Dimensions are represented with l for width or radius and L for length, respectively. When a filler is dispersed in a polymer matrix, there are three main composite material constituents: (1) the matrix, (2) the dispersed paticle (fiber), and (3) the interfacial region, which interlinks the polymer matrix to the fiber, as illustrated in Figure 2.3. This region has different properties to the bulk matrix because of its closeness to the fiber. The key to the improvement of properties is when the filler is introduced into the polymer matrix and is associated to a parameter known as the radius of gyration (R_g). Radius of gyration is a parameter, relating to the surrounding space of the polymer matrix, which the majority of the static and dynamic properties of the polymer can be linked to.[22] The interfacial area of the nanocomposite material extends to four times the value of R_g, which is a few tens of nanometers.

The distance between the nano-sized particles is about 10 nm and that value corresponds to the size of the interfacial region. As there are a higher number of particles in the matrix of the nanocomposites than the microcomposite, the relative volume fraction of the interfacial region is also considerably higher. A homogenized nanocomposite loses the

bulk properties of the virgin polymer and is dominated by the characteristics of the interfacial region, and hence the impact on the overall physical properties.

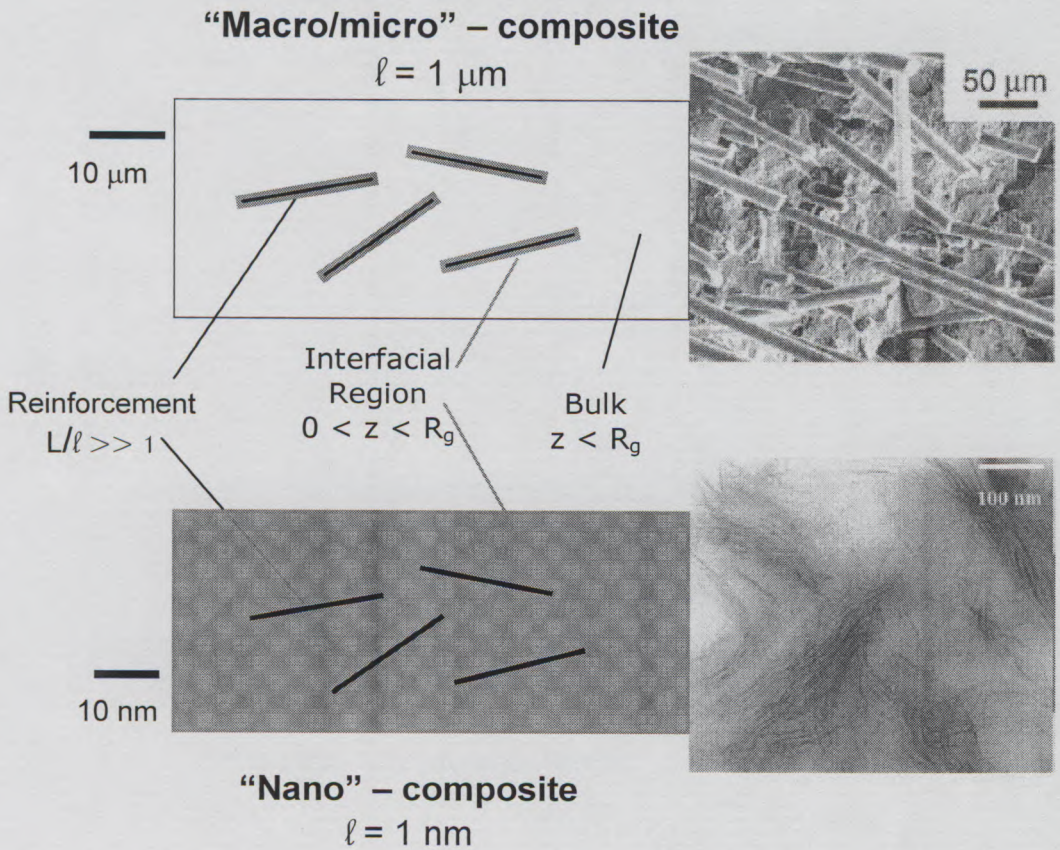

Figure 2.3: An illustration of a microcomposite in an amorphous matrix compared to a nanocomposite containing the same volume fraction. (Insert pictures show scanning electron micrographs of a glass fiber (15 μm) reinforced polyolefin (top) and a transmission electron micrograph of an epoxy-montmorillonite nanocomposite (1nm thick layers) (bottom).[22]

In addition to the defining aspects encompassing different PNCs, it is sufficient to acknowledge the complexity of each PNC system. Also, the dynamics of PLSNs may not always be relevant to another system with nano-sized dispersed phase. These differences arise from the nature of the dispersed phase to its shape, and the type of interaction with the polymer matrix. The aspect ratio (α) is a factor based on the shape of the filler, determining the extent of physical interaction with matrix. It is the ratio of the length (for rods) or thickness (for plates/sheets) to the radius of the particle.

Figure 2.4 shows the range of the value of α for composites: for rods with $\alpha > 1$ and for plates with $\alpha < 1$. The plot also illustrates the ratio of surface area-to-volume (A/V) versus the aspect ratio of cylindrical particles with a given volume. A/V is a raio of the surface area to the volume of the filler particle, which is related to the aspect ratio, and to the total surface area in contact with the polymer matrix. The A/V value increases much quicker (as a function of α) in the case of the sheet compared to the rod. The layered silicates are 1-nm-thick plates with width or radius ranging from a few nanometers to several microns. The layered silicate sheets have a relatively larger surface area-to-volume ratio compared to fiber-like fillers. This means that there would be less particle-particle contact in the fiber-like filler compared to the sheet. However, the larger contact ability in sheet-like fillers may also present itself as disadvantageous to practical PLSNs systems as the sheets will tend to agglomerate.[23] This hinders the formation of a well-dispersed phase in the matrix. Despite the latter, the larger surface area still renders the use of layered silicate sheets in nanocomposites more advantageous compared to classical mineral fillers.

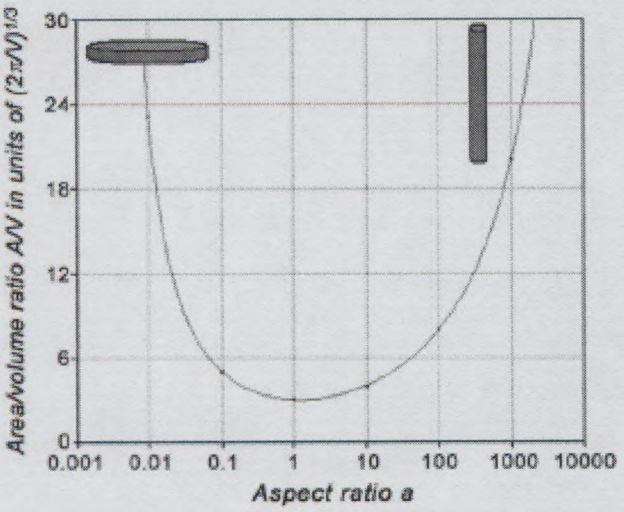

Figure 2.4: A plot of surface area-to-volume (A/V) versus aspect ratio of cylindrical particles describing the quick change in sheet-like fillers compared to rod-like particles.[23]

2.3.3 Structure of polymer-layered silicate nanocomposites

When a layered silicate is mixed with a polymer or a polymer precursor (e.g. monomer), there are generally three types of nanocomposites morphologies that are likely to be obtained (Figure 2.5), viz tactoids, intercalated/flocculated and exfoliated morphologies, which are further discussed below. The layered silicates are normally added as micron-sized powders (1 – 100 μm). The polymer/polymer precursor is usually in liquid, melt or in solution, depending on the method used to prepare the composite material (see Section 2.4).

The first morphology possible is one where the dispersed clay particles in the final composite material are settled as aggregated, micron-sized units (tactoids) encompassed in the polymer matrix. Each tactoid has many layers packed adjacent to each other and held close by van der Waals forces. This is the morphological characteristic of the traditional microcomposite materials, and the morphology is known as *phase-separated*. Gao[24] reported that the tactoids in the conventional composites are a possible point of weakness of the composites because of the weak interlayer bonding.

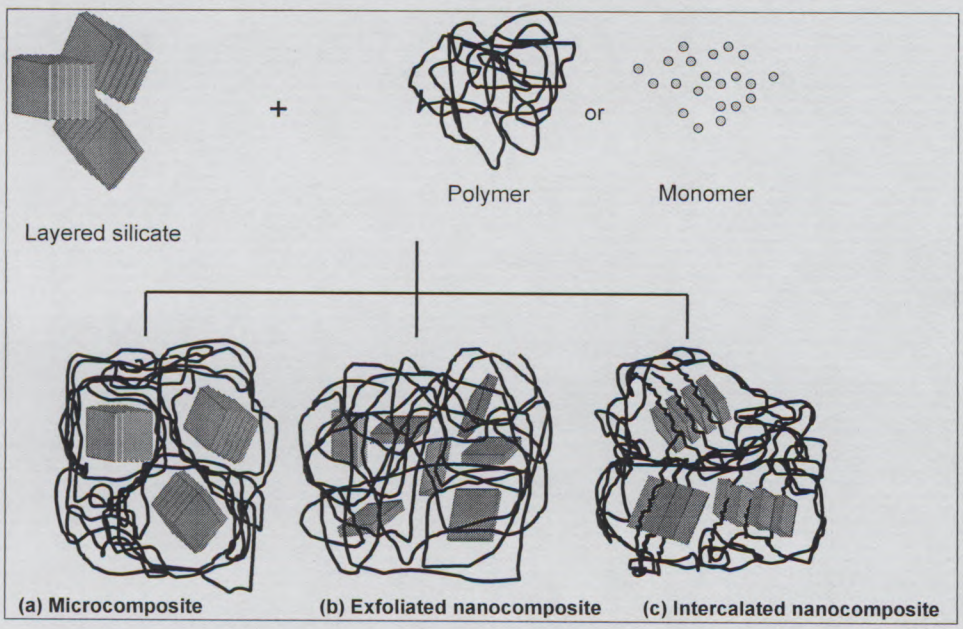

Figure 2.5: A schematic presentation of three main types of composites obtained when clay is incorporated into a polymer matrix.

The second possible morphology is where the polymer chains are extended into (intercalate) the gallery of the nano-sized silicate layers. When the polymer chains intercalate the gallery, the spacing between the layers subsequently increases and each layer moves away from another, without losing the ordered, crystal structure. This type of morphology is known as the *intercalated nanocomposite* morphology. The morphology can be also be configured as intercalated with silicate layers positioned adjacent to one another by edges. This is influenced by what is known as the hydroxylated edge-edge interaction, where edges of the silicate layers come close to neighboring layers because of the hydroxyl groups at the edges.[12] This type of sub-morphology occurs in a composite known as *flocculated nanocomposite*, which is similar to the intercalated morphology, but characterized by the latter feature.

A third type of morphology is where the layers totally delaminate from the crystal and disperse in the polymer matrix (exfoliate). This type of morphology leads to single, isolated silicate layers being randomly distributed in the polymer matrix. This is known as *exfoliated nanocomposite* morphology. It allows for maximum interfacial interaction between the silicate sheets and the polymer matrix and according to the literature, it generally leads to better properties than the intercalated nanocomposites.[9,12,17,25] However, it should be noted that in practical systems a *partially exfoliated (quasi-exfoliated)* morphology can be obtained where the exfoliated morphology is dominant but an intercalated structure is also present.[10] The homogenous dispersion is not always easy to achieve; the smaller the particles, the larger their internal surface will be, which promotes their tendency to agglomerate than to disperse homogenously in the matrix.[23]

2.4 Preparative methods of polymer-layered silicate nanocomposites

When preparing a material such as a polymer composite, it is very important to define the expectations of the final product, in terms of composition and properties (also possible applications). This will better enable one to establish a suitable preparation method. An understanding of the required structure (physical and chemical) should be the first consideration when devising this pathway.[12] The ability to control the structure is of utmost importance when the aim is to control the eventual properties. Control of the particular preparation process will strongly depend on the understanding and knowledge of the relationship between the structure and the properties for a particular material. Currently, the extent to which a preparative process can be controlled with precision, to engineer and tailor specific properties of the final clay-based nanocomposite material, is generally still not well understood. However, different types of nanocomposite materials have shown that there are endless possibilities of controlling the structure in order to obtain the application-designed structure.[22]

In the case of PLSNs, control of the structure is guided by an understanding of the interfacial interaction between the polymer matrix and the surface of the modified clay layers. Three methods to prepare PLSNs have been established. They have been allocated according to the starting materials and preparation technique. These methods have been developed in a smaller, lab-scale environment, but also relevant to larger industrial processes. This is to ensure the eventual product can be manufactured on an industrial scale. The three basic methods used for the preparation of PLSNs are: (1) solution-mediated intercalation, (2) melt-intercalation and (3) in-situ intercalative polymerization.

Depending on the constituent materials (e.g. surfactant, type of clay, polymer precursor, monomer, and polymer matrix), preparation conditions (e.g. temperature, pH, reaction type, free radical, catalysts and medium, solvent) and the selected preparative method, the composites may be intercalated, exfoliated or agglomerated. Since the study of PLSNs is a relatively new and complex field, properties have not been widely tailored, but depend on the obtained structure, which is controlled by the above-mentioned factors. However,

the exfoliated structure has always been a highly sought after structure compared to the intercalated nanocomposite structure. This is because in the former type of structure the clay layers are truly delaminated and dispersed in the polymer matrix, and hence higher interfacial interaction and better properties are achieved. The choice of the method of preparation is usually based on its ability to produce exfoliated nanocomposites.[17,26,27]

2.4.1 Solution-mediated intercalation

In this type of preparation method a polymer or polymer precursor (if the polymer itself is insoluble) is dissolved in an appropriate solvent and the intercalation occurs by diffusion of the dissolved molecules into the silicate galleries. This technique has been widely used with water-soluble polymers. The clay material is first swollen by dispersion in a solvent, such as water, chloroform, or toluene to allow swelling to take place. The solvent soluble polymer is then dissolved, allowing for the intercalation of the polymer in the galleries to displace the solvent. On drying, the nanocomposite structure is obtained. The clay material used in the solution preparation of water-soluble polymers is usually unmodified since the polymer matrix is polar in nature. Non-aqueous solvents have also been used in this type of preparation. A single solvent or a mixture of solvents can be used depending on the solubility of the polymer in the selected solvent or solvent mixture. Nevertheless, the solvents play a critical role in the preparation and the structure of the eventual nanocomposite.[12] This method allows for preparation of thin films with intercalated clay layers.

2.4.2 Melt intercalation

In this method the clay material is mixed with a polymer melt and, on curing, the nanocomposite material is formed. This is a more viable method for industrial processes because the process involves only mixing and heat treatment of the components.[12] The polymer material is already in its final form and the clay is readily mixed in its powdered

form. The clay can be pre-modified (organically) before the melt-intercalation to make the surface organophilic if a hydrophobic polymer is used to prepare the composite. The interaction involves the alkyl chains of the organic ammonium surfactants in the galleries and the polymer chains, as illustrated in Figure 2.6.[12]

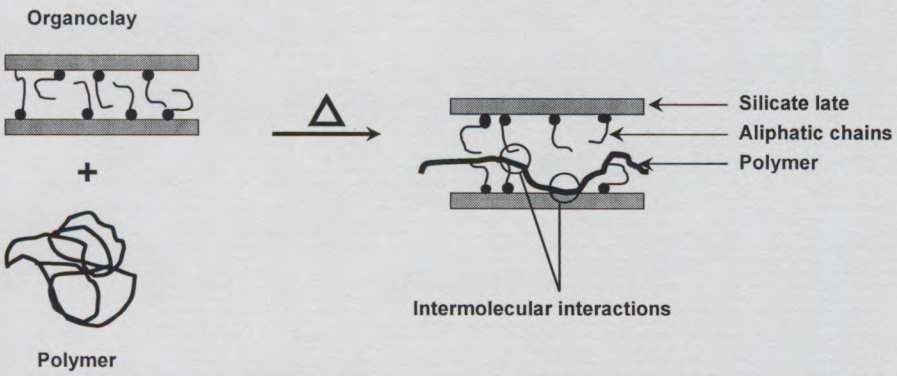

Figure 2.6: A schematic presentation of melt intercalation of a polymer using an organically-modified clay.[12]

The thermodynamics of the molten state processes have been explained by lattice-based mean-field theory.[9] This involves the enthalpy and entropy factors that determine the interaction processes between the molten polymer matrix and the organically-modified silicate layers. The intercalation of the polymer matrix confines the chains, which leads to reduced overall entropy of the chains. However, this entropy reduction is compensated for by the increase in conformational freedom from the alkyl ammonium surfactant chains as they relax because of the separation of the silicate layers. The total intercalation is highly influenced by enthalpic changes since the small changes in the gallery spacing do not strongly influence the total entropy change. The enthalpic changes arise from the interaction between the polymer and surfactant chains, and between the polymer and the layered silicate layers.

Melt intercalation is more advantageous than other methods of preparation; it is environmentally sound and industrially viable.[24] The absence of solvents and/or monomers makes it more environmentally preferable compared to other methods. The pre-mixing and melt compounding is the currently used method of processing polymer materials on industrial scale. This method of preparing nanocomposites is, therefore,

compatible with techniques currently used in the industry such as injection molding and extrusion.

2.4.3 In-situ intercalative polymerization

In this method a liquid monomer or a monomer solution is intercalated in the modified clay. The clay swells as the monomer is intercalated in the galleries. A free-radical polymerization reaction is initiated inside the galleries by radiation activation, heating, or through the use of an initiator. In other cases a polymerization reaction is activated by a fixed organic initiator or catalyst that is pre-introduced into the galleries through ion exchange.[12] Organoclays modified using longer-chain surfactants intercalate larger amounts of monomers. This is due to the fact that the intergallery spacing of clays modified using longer-chain surfactants are larger.

When a polymerization reaction progresses inside the galleries, the increasing chain lengths and expanding polymer network pushes the alumnosilicate layers apart. As a result, delamination of the layers is obtained, leading to a break down of the packed lattice. The exfoliated structure is obtained when the layers disperse in the polymer matrix. The reaction can take place in a solvent or a mixture of solvents, or it can be in bulk (liquid monomer). The presence of a solvent aids the dispersion, as the free-radical polymerization reaction method is characterized by high viscosities. This means that the free-radical reaction in solution will provide better mixing of the composite than a reaction in bulk. However, the presence of the solvent is known to either positively or negatively influence the interaction of the polymer with the organoclay, as is the case with solution-mediated intercalation method.[9]

In some studies, cationic organic moieties with a polymerizable group have been used to modify the silicate surfaces. On polymerization, these modifiers take part in the polymerization reaction.[16,19,28] However, a pure polymer is not obtained since the polymer chains co-polymerize with the polymerizable organic cation. These copolymers

are an intermediate network, anchoring on the silicate surface and inter-joining into the polymer matrix, as illustrated in Figure 2.7.[19]

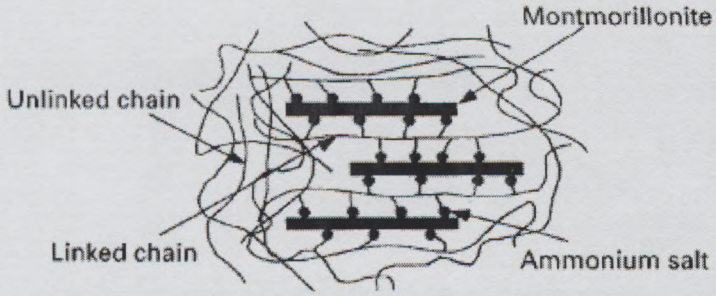

Figure 2.7: Schematic structure of nanocomposites from a reactive organically modified clay.[19]

2.5 Review of structure-property relationship of polystyrene-layered clay nanocomposites

2.5.1 General aspects

The general structure of PLSNs is characterized by two techniques: X-ray diffraction (XRD) and transmission electron microscopy (TEM). These two techniques are used complementarily as each outcome cannot give definitive results about the structure of the nanocomposites. The XRD technique provides information about the position, shape and intensity of the basal reflections of the silicate layers in the polymer matrix. However, TEM is needed to confirm the type of morphology deduced from XRD by giving a visual perspective. The morphology can be determined from these two techniques, as seen from Figure 2.8.

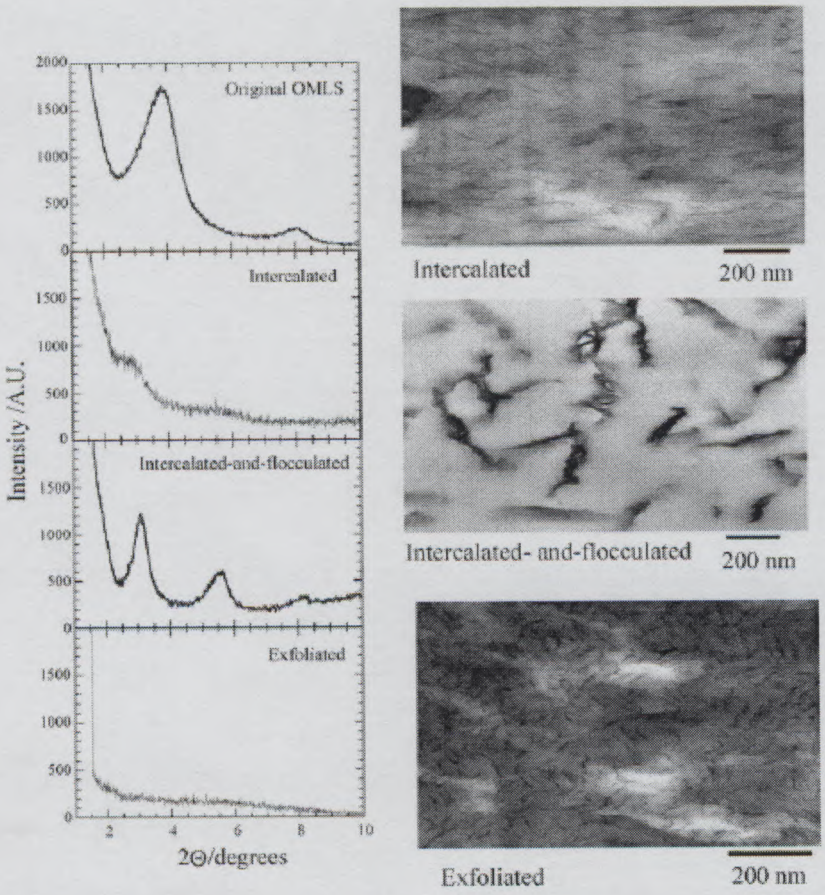

Figure 2.8: Morphologies of polymer-layered silicate nanocomposites as determined by XRD (left) and TEM (right).[12]

XRD gives quantitative information about the changes in the interlayer spacing of the nanocomposite in relation to the original layered silicate, based on basal reflections. Wide-angle X-ray diffraction (WAXD) gives information if the layer spacing is in the dimension range lower than 6 – 7 nm. If this range is exceeded, due to an increase in the interlayer spacing or exfoliation, the WAXD is ineffective, but small-angle X-ray scattering (SAXS) is a better tool. Simultaneous SAXS-WAXD techniques have also been used to obtain quantitative results of the crystalline structure in nanocomposites based on polyamide-6.[12] XRD does not give information about the distribution of the silicates, homogeneity, or the internal structure of the nanocomposites. On the other hand, TEM gives direct and pictorial insight into the internal structure of the composite and the distribution of the dispersed phase in the polymer matrix. It also allows qualitative

determination of the homogeneity of the nanocomposites. Details of the techniques are discussed in detail in Chapter 3.

Studies on the dynamics of polymer/filler interface, morphology, and macroscopic properties have been done.[11,29,30] In two selected reviews on PLSNs by Alexandre and Dubois[9] and Ray and Okamoto[12], structure-property relationships of different PLSNs are reviewed. The general outlook is that layered silicate nano-fillers lead to tremendous improvements in properties with less than 5 weight percent (wt%) loading compared to the traditional composites and pristine polymers. These properties include an increase in tensile (Young's) modulus and flexural modulus, fire retardancy and thermal stability, decreased gas and solvent permeability. These properties have been reported for thermoplastics [Nylon-6[31], polypropylene (PP)[32,33], polystyrene (PS)[16,29,34] and poly(methyl methacrylate) (PMMA)[26,35]] and for thermosets [epoxy[36] and polyurethane (PU)[37]].

Mechanical properties are said to be mostly improved through exfoliation, while improved thermal, fire barrier properties and decreased thermal expansion coefficients may be expected without complete exfoliation, based solely on properties of layered silicate and path blocking in matrix (tortuosity).[38] An increase in modulus is directly related to the high aspect ratio of clay.[10] Mechanical properties that are improved through nanoclay dispersion include impact strength, tensile modulus, flexural modulus, stress at break, elongation at break, and thermomechanical and dynamic mechanical characteristics. Thermal stability properties, barrier properties and electrical conductivity properties are also improved.

2.5.2 Polystyrene-based layered silicate nanocomposites

The current study focuses on the thermal, mechanical and dielectric properties of polystyrene-based layered silicate nanocomposites (PS-LSNs). More emphasis is placed on the latter two, which have not been extensively researched to date. Extensive research has already been done on PS-LSNs.[16,17,19,26-28,39-42] The structure of different PS-LSNs

fabricated using various methods, and some based on organically modified and unmodified MMT, and their subsequent properties, have been investigated. Results of these studies have shown disagreement in some aspects of the structure-property relationship. This finding further expands the issue that each nanocomposite system is unique, and its subsequent properties further demonstrate that acumen. It further reinforces the understanding that each system should be thoroughly examined and extensively understood before a general description can be compiled for PLSNs even if based on the same polymer. Property improvements in PLSNs are said to be maximized when the clay nanocomposite system is exfoliated but, have also been achieved in intercalated and intermediate systems.[23,30]

Factors that have effects on the structures of the PS-LSNs and subsequent properties include the method of preparation[26], the type of layered silicate and its properties[42] and the type and nature of the organic cation.[17,19,39,41] Different fabrication methods expose the components to different conditions, which influence the bounds within which each nanocomposite is formed. These include thermodynamic conditions, which are critical factors in the formation of the PLSNs.[12]

Wang et al.[26] investigated the effect various polymerization methods on the nanocomposites based on PS and PMMA. This study showed that PLSNs of exactly the same composition can yield different morphologies and different properties. For example, a PS-LSN fabricated by bulk polymerization from an organoclay with a polymerizable modifier yields an exfoliated morphology, whereas an intercalated morphology is obtained by solution polymerization. From the same study, and other studies on PS-LSNs, it has been shown that different organic modifiers will not produce similar nanocomposite morphologies.[16,19,25,27] It is hypothesized that organic cations with polymerizable groups lead to exfoliated nanocomposite morphology.[17] This has a direct effect on the morphology of the PS-LSN that is formed.

There are numerous possibilities to the variations that can be found in organic modifiers. As mentioned earlier, alkylammonium and alkylphosphonium salts are the most well-

known. They can have long-chain alkyl groups with a chosen number of carbons in the chain. The ammonium or phosphonium head could also have alkyl groups or a chosen substitution of a functional molecule. An example of a substitution is a phosphonium ion with three benzyl groups.[41] The latter (phosphonium) was compared to a long-chain alkylammonium surfactant and found to be more effective in producing exfoliated PS-LSNs. Polymerizable groups can be included in an organic molecule to increase the interfacial interaction between the polymer and the layered silicate. The polymerizable group in a molecule can be positioned at different parts of the molecule, and the effect may vary.

The type of layered silicate also has a role to play in the type of morphology of a nanocomposite material. First of all, the ability of the clay material to expand, and which differs from one to another, may influence the ease of intercalating an organic material in the galleries. In addition, the ability of the clay material to exchange a larger quantity of organic modifier is mostly influenced by the clay CEC. CEC, as mentioned in Section 2.1.2, is characteristic of a particular clay material and varies within the same clay type. Aphiwantrakul et al.[42] investigated the role of the cation-exchange capacity in the formation of PS-LSNs by in-situ polymerization. Two types of interlayer packing were observed when an alkylammonium surfactant was intercalated in two types of layered clays. One clay type (Wyoming) showed liquid and solid phase configurations of the alkylammonium surfactant but the other (Bentonite H) showed only the liquid phase packing. Liquid phase packing is observed when the density (due to relatively lower CEC) of the intercalated molecule is low, as discussed in Section 2.2. This study also showed that the layered silicate with lower CEC led to exfoliated PS-LSNs while the higher CEC led to an intercalated morphology. All of the above-mentioned factors can, directly or indirectly, affect the properties of the PS-LSNs and other PLSNs.

Thermogravimetric analysis (TGA) of PS-LSN is a tool to determine thermal stability of the nanocomposites and degradation-related phenomena. A comparison with pristine polystyrene polymer is usually done to observe the effects of the added filler on the thermal properties. Thermal and mechanical properties of PS-LSNs have received a lot of

attention in the literature, whereas dynamic mechanical and dielectric properties have not enjoyed similar focus.

The following sub-sections are a literature review of the properties that will be investigated for PS-LSNs in the current study. More information on all the analytical techniques that were used are discussed in Chapter 3.

2.5.2.1 Dynamic mechanical properties

Dynamic mechanical analysis (DMA) is an analytical technique in which a sample is subjected to an oscillating force and the sample response recorded. The technique gives information about relaxation processes and molecular mobility of a polymer under sinusoidal test at a given temperature and frequency. An elasticity factor of the sample response is measured and is reported as storage modulus (E'), and a viscosity factor is expressed as loss modulus (E''). Tan delta (tan δ) denotes the overall damping properties of the material and is the ratio of the loss modulus to the storage modulus (E''/E').

Qutubuddin et al.[16] used a three-point bending technique to measure the dynamic mechanical properties of a PS-LSN synthesized by one-step emulsion polymerization using a reactive surfactant. One-step emulsion polymerization combines a cationic exchange reaction with polymerization in one step. A nanocomposite with 5 wt% clay loading showed a considerable increase in the onset temperature of the storage modulus (flexural) compared to the homopolymer, corresponding to an increased T_g. The value of the storage modulus was also found to be higher than that of a pure PS. The morphology of the nanocomposites obtained by the emulsion polymerization method was depicted as partially exfoliated, as determined by XRD and TEM.

The presence of the polymerizable surfactant leads to covalent bonding with the polymer chain, which increases the interfacial interaction with the silicate layers. Earlier work by Fu and Qutubuddin[25] showed that the increase in loading of the MMT clay modified with a polymerizable surfactant led to an increase in the storage modulus. The increase was achieved with 3.6 wt%, 5.6 wt% and 7.6 wt% loading and was higher than that of pure

PS. However, the onset temperature decreased with increasing clay loading, meaning a decline in T_g, as shown in Figure 2.9. The decrease was associated with viscosity-polymerization factors that had affected the diffusion of the initiator molecules and chain propagation. This, evidently, led to the decrease in the molecular weight of the nanocomposite material.

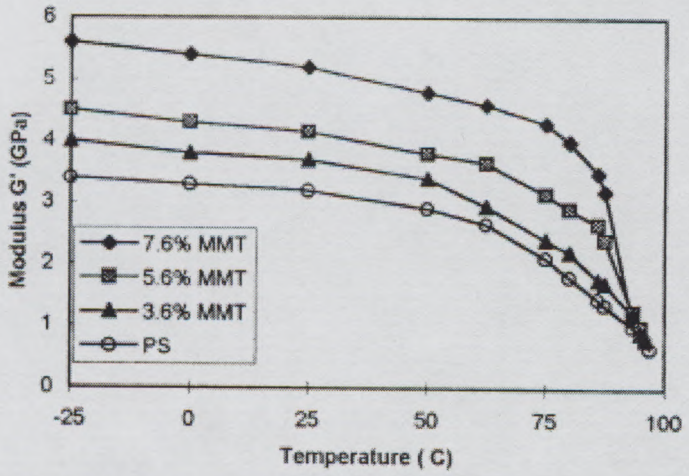

Figure 2.9: Increase in the storage modulus and decrease in the onset temperature at T_g with an increase in clay loading.[25]

Noh and Lee[40] showed that there was no change in the onset of the storage (tensile) modulus of a PS-LSN material synthesized by emulsion polymerization. However the tan δ peak showed some broadening and a shift to the higher temperatures. The shift towards the higher temperatures denotes an increase in the T_g. An increase in T_g and tan delta peak broadening are associated with restricted motion of the polymer chains near the layered silicate surface. The nanocomposites were synthesized without an organic pre-modification of the layered silicate. Na-MMT clay was prepared for the synthesis only by ultrasonic pre-treatment. This study showed that a hydrophobic PS can be intercalated in a hydrophilic clay material, as supported by XRD studies. However, it is not clear what the exact morphologies of the nanocomposites were, since a TEM study was not included.

In 1998 Laus et al.[19] synthesized PS-LSNs using a reactive quaternary ammonium salt and (chloromethyl) styrene, by emulsion polymerization. Na-MMT clay was pre-modified with the latter compound which contained a styryl group attached to a quaternary ammonium group. The DMA results showed an increase in T_g with a clay loading up to 15 wt%, as shown in Figure 2.10. The overall increase in the T_g was estimated to be about 12 °C, compared to the homopolymer. One unavoidable factor is the decrease of the average molecular weight (M_w) of the nanocomposites as the amount of clay is increased. This decrease may be due to chain transfer or termination during the polymerization reaction. It was therefore concluded that the effect of reinforcement was higher than observed in the DMA results, as the T_g of PS decreases with decreasing molecular weight.

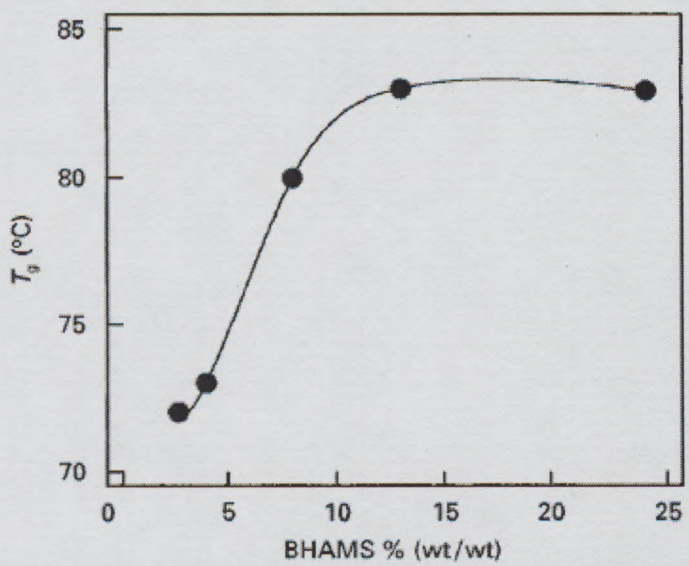

Figure 2.10: Trend of the glass transition temperature of PS-LSNs as a function of an increasing weight percent of modified clay (BHAMS).[19]

2.5.2.2 Thermogravimetric analysis

Thermogravimetric analysis (TGA) is a technique in which a sample is exposed to elevated temperatures, usually under an inert atmosphere, to determine its thermal

stability characteristics by measuring the loss in mass due to thermally-induced evolved species.

TGA analysis of PS-LSN based on different preparation methods was investigated by Wang et al.[26] Results showed considerable inconsistency between the different methods. The onset of degradation, 10% mass loss, 50% mass loss and an involatile fraction at 600 °C were determined. The following results were obtained for the onset degradation for materials obtained by each synthesis method: bulk polymerization showed an increase in the degradation onset; solution polymerization showed a decrease in the onset, which led the authors to question the state of their materials as no results in the literature had shown such trend; suspension polymerization showed only a slight increase; and the emulsion polymerization did not show any change in the onset of degradation.

TGA results of PS-LSNs from a study by Wang et al.[41] showed an increase in the onset of thermal degradation. The nanocomposites were synthesized by solution polymerization using clay modified by a long-chain quaternary ammonium surfactant, hexadecyltrimethylammonium chloride (HTAC). The nanocomposites were exfoliated at 3 wt% clay and partially exfoliated at 5 wt%. The nanocomposites were all more thermally stable than the pure PS polymer. A similar tendency was observed for the nanocomposites synthesized by emulsion polymerization using unmodified clay but prepared by sonication.[40] The increase in the thermal degradation onset shows that the silicate layers protect the polymer chains from the thermally-induced degradation.

A study by Su and Wilkie[17] showed that the TGA degradation onset of PS-LSNs polymerized by bulk polymerization increased by 50 °C, compared to a PS homopolymer. An organic cation with two styryl groups (polymerizable) was used as a modifier for the clay. In their study, they also solvent-extracted the polymer from the nanocomposite material. From the TGA measurements of the insoluble components, the amount of polymer polymerized to the organic cation was determined.

The same group carried out an investigation into PS-LSNs fabricated from carbazole containing surfactants as an organic modifier in a layered silicate.[39] The main focus of this study was to investigate the effect of more than one long alkyl chain in the organic modifier molecules (surfactants). Nanocomposites were obtained by bulk polymerization and by melt-blending. The TEM results showed that the dispersion of bulk polymerized nanocomposites was excellent compared to the nanocomposites obtained from melt blending, which showed a rather poor dispersion. This was attributed to overcrowding of the intergallery spacing due to the intercalated bulky molecules with increased chain numbers per molecule. It is easier for a monomer to migrate into the gallery spacing compared to the polymer melt. TGA analysis of the bulk polymerized nanocomposites showed variable findings, where the most bulky organic modifier was the least stable and its subsequent nanocomposites. For melt-blended composites there was little or no change in the onset of degradation compared to the homopolymer. This finding was attributed to the immiscibility of the organically-modified clay with the polymer matrix.

Noh and Lee[40] investigated the addition of clay (up to 30 wt%) to a polystyrene matrix which showed an increase towards higher temperature in the onsets on degradation in the TGA study of PS-LSNs based on unmodified Na-MMT. The shift towards higher temperature was dependent on the amount of clay added. The onset of degradation temperature increased for all the composites even though the higher percentages might not have yielded nanocomposite materials.

In most of the TGA data the increase in the onset of degradation is dependent on the amount of clay loading in the nanocomposite. However, it has been reported that the clays can contribute to the degradation of the nanocomposites. Silicates can catalyze the degradation reaction of the polymers they reinforce due to the oxide surfaces.[38]

2.5.2.3 Dielectric analysis

Dielectric analysis (DEA) measures, in simplified terms, resistive/conductive properties, dipolar orientations and capacitive properties of polymeric materials. Dielectric constant and dielectric loss are determined as a function of frequency or temperature.

Dielectric studies on PS-LSNs have not been widely explored. Wang et al.[28,41] studied the dielectric properties of polystyrene-based clay nanocomposite films with clay loadings from 1 wt% to 5 wt%. The measurements were done at frequencies of 100 Hz to 1MHz in the temperature range 25 °C to 70 °C. The dielectric constant and dielectric loss of the nanocomposites were significantly reduced compared to the PS homopolymer, as shown in Figure 2.11. These findings were attributed to confinement of the polymer chains due to the presence of the inorganic silicate hosts. The confinement was said to be within 1.5 nm to 2.0 nm of the silicate layers. This was directly reflected in their reorientation dynamics, meaning that the dipole orientation from the benzene side of PS was constrained and was not easily changed due to the confinement.

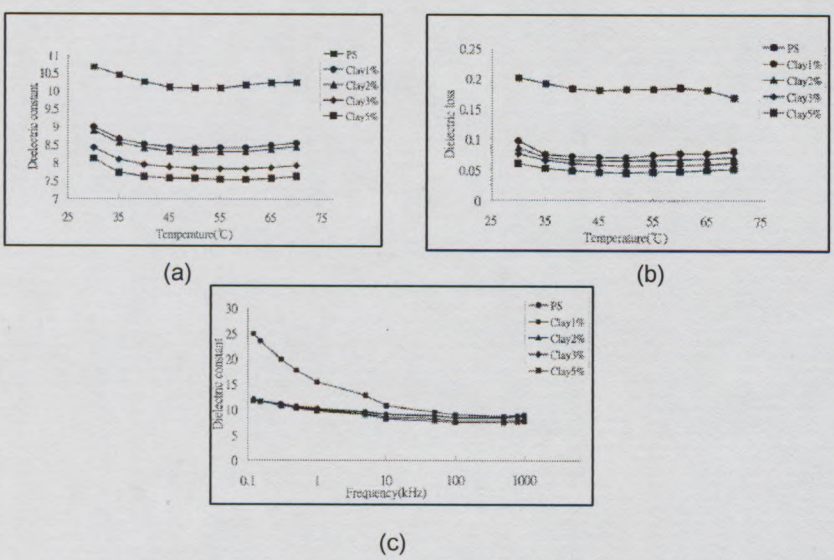

Figure 2.11: DEA graphs of PS homopolymer and PS-LSNs showing (a) the dependence of dielectric constant on temperature (10 kHz), (b) dielectric loss on temperature and (c) dielectric constant on frequency (30°C).[41]

2.5.2.4 Differential Scanning calorimetry

Thermal properties are also investigated by differential scanning calorimetry (DSC). DSC measures the energy changes in a sample due to endothermic and exothermic processes, where those energy changes are directly caused by specific transitions in the polymer.

Information such as T_g, melting point, crystallization and other transitions that absorb or release energy are determined on the DSC. Heat flow to the sample is measured as a function of sample temperature, in a specified atmosphere.[43] The change in the heat flow curve is associated with the transitions and can give information, on peaks and their sizes or deflection points, about curing, degree of crystallinity, molecular weight distributions, degree of branching, copolymer blend ratio, and/or processing history.

A DSC study of clay-based composites gives information about the effect of the filler on the thermal stability of the material, usually depicted as an increase in the T_g. It is evident that the silicate layers lead to the enhancement of the composite, regardless of whether the underlying morphology is exfoliated or intercalated. A study in which clay loading was increased to 30 wt% in the polymer matrix showed that an increase in the endothermic deflection (T_g) was dependent on the amount of clay used.[40] In this study it was shown that intercalation could be achieved with hydrophobic PS and hydrophilic Na-MMT using emulsion polymerization. The composites were intercalated from 5 wt% to 30 wt% and the T_g was thus dependant on the loading. However, when the composites were extracted for 5 days in toluene by means of the Soxhlet technique, the DSC thermograms did not show any T_g endothermic changes. This was ascribed to the confined polymer chains intercalated between the silicate layers. An emulsion polymerized PS-LSN with 5 wt% clay modified by a polymerizable surfactant, vinylbenzyldodecyl dimethylammonium bromide (VDAC), also showed an increase in T_g compared to pure PS.[16] The increase was attributed to various factors: a higher molecular weight achieved by emulsion polymerization, enhanced interaction between the polymer and the clay, and copolymerization with VDAC.

An increase in the T_g of PS-LSNs with 1 wt%, 2 wt%, 3 wt%, and 5 wt% surfactant-modified clay has been reported.[41] This increasing trend was observed even though the exfoliation was up to 3 wt%, as determined by WAXD. At 5 wt% there was a peak in the X-ray diffraction pattern meaning that the nanocomposite had some unexfoliated clay. The DSC results confirmed the fact that the increase in the T_g was not dependent only on the exfoliated morphology of the nanocomposite.

2.6 List of references

1. Konta, J. *Applied Clay Science* **1995,** 10, 275-335.

2. Newman, A. C. D.; Brown, G., The Chemical Constitution of Clays. In *Chemistry of Clays and Clay Minerals*, 1st ed.; Newman, A. C. D., (Eds). Wiley-Interscience: New York, 1987; pp 1-116.

3. Murray, H. H. Clays In *Ullmann's Encyclopedia of Industrial Chemistry;* Wiley-VCH Verlag GmbH & Co. Online: http://www.mrw.interscience.wiley.com/. (12 June 2006),

4. Grim, R. E.; Guven, N., *Bentonites: Geology, Mineralogy, Properties and Uses*. 1st ed.; Elsevier Scientific Publishing Company: Amsterdam, 1978; p 256.

5. Patel, H. A.; Somani, R. S.; Bajaj, H. C.; Jasra, R. V. *Bulletin of Materials Science* **2006,** 29, 133-145.

6. Hadal, R. S.; Dasari, A.; Rohrmann, J.; Misra, R. D. K. *Materials Science and Engineering: A* **2004,** 372, 296-315.

7. Hadal, R. S.; Misra, R. D. K. **2004,** 374, 374-389.

8. Kuelpmann, A.; Osman, M. A.; Kocher, L.; Suter, U. W. *Polymer* **2004,** 46, 523-530.

9. Alexandre, M.; Dubois, P. *Materials Science and Engineering: R (Reports)* **2000,** 28, 1-63.

10. Zeng, H. Q.; Yu, A. B.; LU(Max), G. Q.; Paul, D. R. *Nanoscience and Nanotechnology* **2005,** 5, 1574-1592.

11. Schmidt, D.; Shah, D.; Giannelis, E. P. *Current Opinion in Solid State & Materials Science* **2002,** 6, 205-212.

12. Ray, S. S.; Okamoto, M. *Progress in Polymer Science* **2003,** 28, 1539-1641.

13. Cadene, A.; Durand-Vidal, S.; Turq, P.; Brendle, J. *Journal of Colloid and Interface Science* **2005,** 285, 719-730.

14. Hackman, I.; Hollaway, L. *Composites: Part A - Applied Science and Manufacturing* **2005,** 37, 1-10.

15. Raussell-Colom, J. A.; Serratosa, J. M., Reactions of Clays with Organic Substances. In *Chemistry of Clays and Clay Minerals*, 1st ed.; Newman, A. C. D., (Eds). Wiley-Interscience: New York, **1987**; pp 371-422.

16. Qutubuddin, S.; Fu, X.; Tajuddin, Y. *Polymer Bulletin* **2002,** 48, 143-149.

17. Su, S.; Wilkie, C. A. *Journal of Polymer Science Part A: Polymer Chemistry* **2003,** 41, 1124-1135.

18. Uthirakumar, P.; Song, M.-K.; Nah, C.; Lee, Y.-S. *Europian Polymer Journal* **2005,** 41, 211-217.

19. Laus, M.; Camerani, M.; Lelli, M.; Sparnacci, K.; Sandrolini, F.; Francescangeli, O. *Journal of Materials Science* **1998,** 33, 2883-2888.

20. Stille, J. K., *Introduction to Polymer Chemistry*. 1st ed.; John Wiley & Sons, Inc.: New York, **1962**; p 248.

21. Turi, E. A., *Thermal Characterization of Polymeric Materials: Vol 1*. 2nd ed.; Academic Press, Inc.: San Diego, California, USA, **1997**; p 1378.

22. Vaia, R. A.; Wagner, D. H. *Materials Today* **2004,** 7, 32-37.

23. Fischer, H. *Materials Science and Engineering: C* **2003,** 23, 763-772.

24. Gao, F. *Materials Today* **2004,** 7, 50-55.

25. Fu, X.; Qutubuddin, S. *Polymer* **2001,** 42, 807-813.

26. Wang, D.; Zhu, J.; Yan, Q.; Wilkie, C. A. *Chemistry of Materials* **2002,** 14, 3837-3843.

27. Fu, X. A.; Qutubuddin, S. *Journal of Colloid and Interface Science* **2005,** 283, 373-379.

28. Wang, H.-W.; Chang, K.-C.; Yeh, J.-M.; Liou, S.-J. *Journal of Applied Polymer Science* **2004,** 91, 1368-1373.

29. Park, C. I.; Choi, W. M.; Kim, M. H.; Park, O. O. *Journal of Polymer Science Part B: Polymer Physics* **2004,** 42, 1685-1693.

30. Jordan, J.; Jacob, K. I.; Tannenbaum, R.; Sharaf, M. A.; Jasiuk, I. *Materials Science and Engineering: A* **2005,** 393, 1-11.

31. Uribe-Arocha, P.; Mehler, C.; Puskas, J. E.; Altstadt, V. *Polymer* **2003,** 44, 2441-2446.

32. Filho, F. G. R.; Mélo, T. J. A.; Rabello, M. S.; Silva, S. M. L. *Polymer Degradation and Stability* **2004,** 89, 383-392.

33. Perrin-Sarazin, F.; Ton-That, M.-T.; Bereau, M. N.; Denault, J. *Polymer* **2005,** 46, 11624-11634.

34. Samakande, A. Synthesis and Characterization of Surfmers for the Synthesis of Polystyrene-Clay Nanocomposites. MSc Thesis, University of Stellenbosch, Stellenbosch, **2005**.

35. Ratinac, K. R.; Gilbert, R. G.; Ye, L.; Jones, A. S.; Ringer, S. P. *Polymer* **2006,** 47, 6337-6361.

36. Sarathi, R.; Sahu, R. K.; Rajeshkumar, P. *Materials Science and Engineering: A* **2007,** 445-446, 567-578.

37. Xiong, J.; Zheng, Z.; Jiang, H.; Ye, S.; Wang, X. *Composites Part A: Applied Science and Manufacturing* **2007,** 38, 132-137.

38. Schmidt, D.; Mead, J.; Barry, C.; Chen, J., Nanomanufacturing with Polymers. In *Handbook of Plastics Technologies*, ed.; (Eds). McGraw-Hill (Digital Engineering Library): **2006**.

39. Chigwada, G.; Jiang, D. D.; Wilkie, C. A. *Thermochimica Acta* **2005,** 436, 113-121.

40. Noh, M. W.; Lee, D. C. *Polymer Bulletin* **1999,** 42, 619-626.

41. Wang, H.-W.; Chang, K.-C.; Chu, H.-C.; Liou, S.-J.; Yeh, J.-M. *Applied Polymer Science* **2004,** 92, 2402-2410.

42. Aphiwantrakul, S.; Srikhirin, T.; Triampo, D.; Putiworanat, R.; Limpanart, S.; Osotchan, T.; Udomkichdecha, W. *Journal of Applied Polymer Science* **2005,** 95, 785-789.

43. Shah, V., *Handbook of Plastics Testing Technology*. 2nd ed.; John Wiley & Sons, Inc: New York, **1998**; p 527.

Chapter 3

Analytical and characterization techniques

3.1 Introduction

Polymer-layered silicate nanocomposites (PLSN) are a diverse group of materials that have attracted a lot of attention recently. They are of a particular interest because their properties are improved with relatively low filler loadings. Hence the focus will not only be on the synthesis of these materials, but also on their characterization. Characterization of the PLSNs is divided into two categories: structural/morphological characterization and physical (functional) property characterization. Structural characterization is directed at determining how the clay layers are dispersed in the polymer matrix, and whether a composite is a nano dispersed system or a micro dispersed system. A nano dispersed system will either be intercalated or exfoliated. Structural and morphological characterizations are carried out by transmission electron microscopy (TEM) and X-ray diffraction (XRD) techniques.

Functional properties are the performance properties of a material. Determination of performance properties (such as mechanical) is used to determine how much improvement is achieved for the nanocomposite, compared to a homopolymer, or microcomposite (where applicable). These properties are studied to determine novel features in the PLSNs, and to determine how effective they will be in specific applications. These properties include mechanical properties, thermal properties, dielectric properties, decreased solvent and gas permeability, increased biodegradability in biodegradable polymers and flame retardant properties. These properties need to be measured by standard and specialized techniques, and sometimes by newly developed techniques or by the modification of existing ones.

This chapter focuses on techniques and instrumentation used in this study to characterize the polystyrene-based layered silicate nanocomposites (PS-LSN). Background information of each technique is briefly given and their experimental information, such as sample preparation, instrument calibration and operation. In some instances, very elementary definitions of fundamental principles are given for the purposes of clarity, and where necessary, the subject discussed in depth.

In cases where measurements were made and results provided by other researchers limited mention is made of the instrumentation.

3.2 Structural characterization

3.2.1 X-ray diffraction

3.2.1.1 Background on X-ray diffraction

X-rays are beams of electromagnetic radiation (EM) produced by the sudden deceleration of fast moving particles (usually electrons). Being components of the EM, X-rays possess both wave and particle properties.[1] This means that when interacting with a medium they can be partly transmitted, partly refracted and scattered, and/or partly absorbed. The particle property comes from components of particle nature known as photons, which are energy packets that can bounce or transfer momentum. X-rays can be diffracted by a grating of appropriate size, and have wavelengths that can be measured. This property gives the X-rays the nature of waves. They are usually produced by emission from a target of X-ray tubes or can be produced from synchrotron radiation. Synchrotron radiation is the name given to radiation that occurs when charged particles are accelerated in a curved path or orbit, usually at high speeds.[2] Classical X-ray tubes produce radiation by electrons emitted from a tungsten filament (cathode) at high voltage (between 15 kV and 60 kV), accelerated through a vacuum to strike a target metal (anode). As electrons collide with the atoms of the target and decelerate suddenly, a broad continuous spectrum of wavelengths is produced, termed white (also *Bremsstrahlung* or continuous) radiation.

The high energy electrons also eject inner shell electrons in atoms through the ionization process. The energy from collisions of electrons appears as X-rays is represented by:

$$E = h.\upsilon \qquad (3.1)$$

$$\upsilon = c/\lambda \qquad (3.2)$$

where h is Planck's constant, υ is the frequency, c is the speed of light and λ is the wavelength of the radiation.

When the electrons fill the shell, X-ray photons with energy characteristic of the target material are emitted. The characteristic radiation produces a spectrum with sharp peaks of discrete wavelengths. Common targets in X-ray tubes include copper (Cu) and molybdenum (Mo), which emit 8 keV and 12 keV X-rays with corresponding wavelengths of 1.54 Å and 0.8 Å, respectively.[3]

For diffraction applications only short wavelength X-rays are used. They are also known as hard X-rays, with a wavelength range of a few angstroms to 0.1 angstrom, with energies ranging from 1 keV to 120 keV respectively. The wide choice of wavelengths to use is based on the size of the atoms and molecules to be analyzed. The energy in the X-rays allows them to penetrate deep into the materials and provide information about the bulk structure. When the X-rays interact with electrons of the atoms of the material they collide with, the photons are deflected away from the direction they initially come from. If they do not lose their initial wavelength it means that they have not lost energy from the collision and the process is known as the elastic scattering (Thompson scattering). Only momentum gets transferred in the scattering process. These are the X-rays measured in the scattering/diffraction experiments, as they carry information about the electron distribution in materials.

On the contrary, in the inelastic scattering (Compton scattering), X-rays transfer some of their energy to the electrons and the scattered radiation will have a different wavelength to that of the incident rays. Diffracted waves from atoms can interfere with each other and the resultant intensity distribution is strongly modulated by this interaction. If the

atoms are arranged in a regular fashion, such as crystals, the diffracted waves will consist of sharp interference peaks with the same symmetry as in the atom distribution. Measuring the diffraction pattern therefore allows the study of the distribution of the atoms of a material.

The peaks in a X-ray diffraction pattern are directly related to the atomic distances. If an incident X-ray beam interacts with atoms in a periodic manner, as illustrated in Figure 3.1 (a), the beam will be reflected according to the arrangement of the atoms in the lattice. Atoms, represented by the dots can present different set of planes in a particular crystal, such as the illustrated two-dimensional planes in Figure 3.1(b). For a given lattice distance, d, between planes can be determined from a diffraction peak by Bragg's Law (equation 3.3).

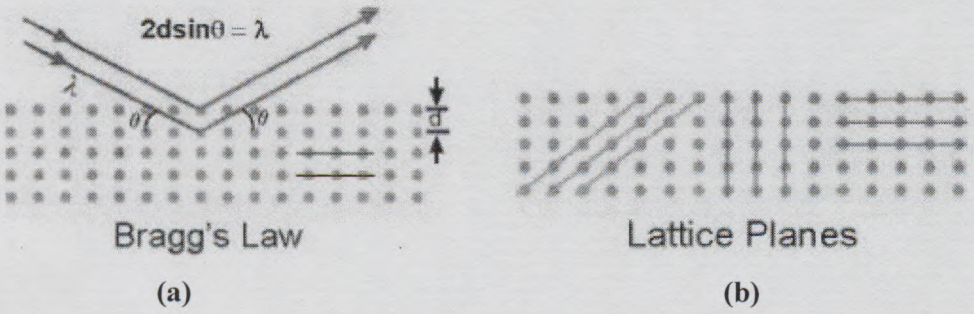

Figure 3.1: An illustration of (a) X-ray scattering through a lattice showing the interlayer distance as determined by Bragg's Law and the (b) different planes in a lattice.[3]

$$2d\sin\theta = n\lambda \qquad (3.3)$$

where λ is the wavelength of the X-ray, θ is the scattering angle, and n is the integer representing the order of the diffraction peak.

3.2.1.2 X-ray analysis of clays and clay nanocomposites

X-ray diffraction (XRD) techniques have been widely used for the study of clay minerals.[1,4] The crystalline phases in clay are studied by XRD, and their components

quantitatively evaluated. The X-ray diffraction patterns give information about variations in the basal interlayer distances. X-ray studies have been used in the evaluation of organic modification of the clays and to evaluate the changes in the interlayer spacing due to the organic modification. XRD is also used to characterize PLSNs and evaluate the structure of the materials.[5,6] By monitoring the position, shape, and the intensity of the basal reflections from the distributed silicate layers, the nanocomposite structure may be identified. To a larger extent, wide-angle X-ray diffraction (WAXD) has been used in the structural characterization of the PLSNs. In an exfoliated nanocomposite the extensive layer separation associated with total delamination of the original silicate layers in the polymer matrix leads to the total disappearance of any X-ray reflection. This is deduced from the disappearance of the peak in the WAXD diffraction pattern. Whereas, in the intercalated nanocomposite, the layer expansion associated with polymer penetration inside the galleries leads to the appearance of a new peak due to basal reflections corresponding to larger gallery height. WAXD determines the interlayer spacing of the layered silicates and the intercalated nanocomposites within 1 – 4 nm.[5] However, when the layer spacing exceeds 6 – 7 nm, or the layers become disordered, WAXD is not very efficient. In that case, SAXS is a better tool. Simultaneous WAXD-SAXS has been reported to give more quantitative results in the study of the nanostructure of clay-nylon-6 (N6) nanocomposites.[5] In the determination of the structure of PLSNs, XRD techniques are always combined with TEM. An important factor to consider when determining the structure of PLSNs is that XRD alone cannot give an accurate conclusion. For instance, the absence of a diffraction peak may not always be due to an exfoliated structure.[7] The absence of a peak in the diffractograms may be due to an undetectable amount of clay (low clay loadings), an immiscible system, and the sample type (e.g solid versus powder).

For the purposes of the current study, SAXS which has been complemented by TEM was used to study the nanostructure of organically-modified silicates and the nanocomposites.

3.2.1.3 Small-angle X-ray scattering

SAXS measurements were performed at 25 °C ant the diffraction measurements were carried out in a transmission configuration. A rotating copper and X-ray source (functioning at 4 kW) with a multilayer focusing "Osmic" monochromator giving high flux (10^8 photons/sec) and punctual collimation was used. An "image plate" 2D detector was used. Diffraction curves were obtained, giving diffracted intensity as a function of the wave vector q.

For crystalline compounds, the d-spacing d_{hkl} between reticular planes hkl can be determined from the position of the corresponding Bragg peaks observed on the diffraction curve. d_{hkl} was calculated from Bragg's law, analogous to (3.3):

$$2d_{khl}\sin\theta = \lambda \qquad (3.4)$$

where 2θ is the diffraction angle and $\lambda_{Cu} = 1.54$ Å.

The wave vector, q, is related to θ by the relation:

$$q = \frac{4\pi \sin\theta}{\lambda} \qquad (3.5)$$

From the relations (3.4) and (3.5), the following can be deduced:

$$d_{hkl} = \frac{2\pi}{q_{hkl}} \qquad (3.6)$$

where q_{hkl} is the q value corresponding to the associated Bragg peak position.

3.2.2 Transmission Electron Microscopy

3.2.2.1 Background

Microscopy is a technique in which objects are converted into images. The main function of microscopy is to magnify object to levels that are not possible with a naked human eye. The fundamental principles of magnification in electron microscopy are similar to those for light optics.[8] Electrons and light can be viewed as electromagnetic radiation with energy (photons) and wave properties. The difference between light and electron beams lies in the size of their wavelengths: electrons (useful for microscopy) have a wavelength ranging between 0.001 and 0.01 nm and visible light has a wavelength between 400 and 700 nm. The essence of the electron beam is that its wavelength is sub-atomic, making it feasible to interact with particles of those particular sizes. The difference in the wavelengths is transferred to the sizes of particles that can be detected by the corresponding radiation sources. The difference in the wavelengths (by thousands of factors) is also one of the main differences between the electrons and light. Through a combination of the fundamental principles of physics and mathematical techniques, electron microscopy provides high magnifications (1 000 000 x), higher resolution, greater depth of focus and greater versatility than would have been possible with light microscopy. Electrons, in the modern instrumentation, are sourced from systems that produce thermoionic emissions from a heated filament and are known as electron guns.[8] High voltage is applied across a material, such as tungsten, at high temperatures (excess of 2700K).

There are two types of electron microscopy techniques commonly known: transmission electron microscopy (TEM) and scanning electron microscopy (SEM). SEM provides images of external morphology that can be referred to as similar in appearance to those seen by the eye. On the other hand, TEM is used to probe the internal microstructure/ultrastructure of the materials.

3.2.2.2 TEM analysis of PLSNs

TEM analyses of PLSNs have been well studied, as it is a very vital technique in studying the nanostructure of the materials.[7,9] The technique provides a qualitative study of the dispersed particles in the matrix. It provides a better view when there is a mixed morphology (intermediate) between exfoliated and intercalated. Morgan and Gilman[7] defined a method of getting valuable information from the TEM images. This method includes getting the global representation of the material by observing different local points and drawing a conclusion thereafter. The TEM technique can help clarify differences within the same morphology. For instance, exfoliated morphology can be ordered or disordered. Ordered exfoliated morphology is where single sheets are delaminated but they still have a layered lattice, in a long range (very large *d*-spacing). Disordered exfoliated morphology will have all the layered lattices interrupted and single layers will be randomly dispersed in the matrix. It is vital to note that, with SAXS, a diffraction peak could be observed in the case of the ordered exfoliated morphology if the distance is within the techniques detection limit. TEM, therefore, gives an advantage in accurately describing the morphology of the PLSNs, where XRD could have led to a different conclusion.

3.2.2.3 Experimental

Each nanocomposite sample to be analyzed was stained for 24 hours in osmium tetroxide (OsO_4). A Spurr's resin (epoxy) was used to embed the sample and it was then left for 24 hours to cure at 60 °C. A Reichart Ultracut ultratome (Leica, Austria) was used to microtome 100-nm sections (nominal thickness) with a glass and a diamond blade at ambient conditions.

The sections were picked up on 200-mesh square copper grids from water and injected into a cryo-system of a LEO 912 – Omega (Zeiss, Germany). Electron micrographs of different magnifications were recorded digitally. Other TEM instrumentation used was a JEOL 1200EXII (Tokyo, Japan). Images were taken on a photographic film. The photos were digitized by scanning for the purposes of reporting and digital analysis.

3.3 Characterization of physical properties of PLSNs

3.3.1 Dynamic mechanical analysis

3.3.1.1 Background

Dynamic mechanical analysis (DMA) is a technique in which a sample is subjected to a sinusoidal (oscillating) force and the sample response measured as a function of time, temperature, frequency, stress, strain, or a combination of these parameters. DMA can be used for the understanding of the molecular processes from the measured physical properties. Properties determined by DMA are time-dependant, meaning that they change as a function of time or frequency. DMA is a thermal analysis technique and temperature is programmed or controlled while the sample property is measured. Functionally, the technique is based on rheometric principles, where deformation and flow properties of materials (e.g. liquid, melt or solid form) are measured. The deformation of a material is determined based on accurate measurement of the applied stress and strain sustained by the sample.[10]

There are two main types of responses exhibited by polymeric materials when subjected to stress: elasticity and damping (viscous behavior). Elasticity is the ability of a material to store deformational energy. In simple terms, it is the ability of a sample to retain its original shape after deformation. On the other hand, damping is the ability of a material to dissipate mechanical energy. This is due to the rheological (flow) properties of the measured sample. Most polymeric materials are viscoelastic in nature, since they have phases characterized by both elastic and viscous properties. During dynamic testing, as in DMA, an oscillating (sinusoidal) force is applied to a sample and the response (deformation and recovery) will also be sinusoidal.[10] The elasticity factor is reported as the *storage modulus* (E') and the viscosity factor is represented by the *loss modulus* (E''), both calculated from dynamic constants, dynamic forces and sample geometries.[11] *Tan delta* (tan δ) is the ratio between the loss modulus and the storage modulus (see equation 3.7) and is independent of geometrical factors of the sample.

$$\tan \delta = E''/E' \qquad (3.7)$$

When the storage modulus value is high, the mobility of the molecules is restricted, and when the value of the modulus is low, the mobility of the molecules is relatively high. This is because there is free volume available for molecular chains to be mobile. On the other hand, loss modulus denotes the ability of a material to dissipate mechanical energy. The molecular mobility is unrestricted when the loss modulus value is high. The material exhibits viscous properties. Tan δ denotes the overall mechanical properties of a material. It is sometimes referred to as the mechanical loss factor.[11] Tan delta also indicates how energy is lost due to molecular relaxation and internal friction.[10]

3.3.1.2 DMA analysis of PLSNs

DMA analysis of polystyrene-layered silicate nanocomposites is discussed in detail in Chapter 2, Section 2.4.4.2.1

3.3.1.3 Instrumentation

A Perkin Elmer Dynamic Mechanical Analyzer was used to carry out the experimental measurements in this study. The DMA system comprises three major components:

- Perkin Elmer *Dynamic Mechanical Analyzer* (DMA7e)
- Perkin Elmer *Thermal Analysis Controller* (TAC7/DX)
- *Pyris Software for Windows* version 3.81 (Software)

These three components are interconnected and function interactively, to form a functional DMA system. The DMA7e unit is the main component, where measurements are done, and is interfaced with the computer (software) through the TAC7/DX controller. The software takes control of the instrument and is responsible for data acquisition and data analysis. The DMA7e unit is divided into four functional components: motor, detector, measuring system and environmental system an all of these contribute to the functionality and versatility of the system. The functionalities they provide include inert gas atmosphere (nitrogen gas), cooling with an intercooler refrigerator that can cool up to -55 °C or a liquid nitrogen dewar (very low temperature).

A full calibration of the instrumentation was done when either the cooling system or furnace were changed. The instrument did its own internal calibration of the electronics, and then a set of assisted calibrations was done. A minor calibration was done when small changes were done in the system, such as the measuring system and sample holders. Temperature calibration of the instrument is set to use metal melting onset for calibration. However, this temperature calibration technique was found to be ineffective and external digital references were used. External thermocouples were set up next to the instrument thermocouple to verify calibration accuracy.

3.3.1.4 Sample preparation

Samples for DMA, thermomechanical analysis (TMA) and thermodilatometry (TD) were prepared by compression molding. The samples were compression molded in a steel die at ~130 °C (see Figure 3.2) under hydraulic pressure. A cycle of compression was done, in order to prevent air voids and thermal stresses. The compression-heating cycle was as follows:

20 MPa pressure was applied to compact a powdered/flake sample, followed by immediate release. Heating was done at ~ 30 °C for 40 minutes at zero force. 15 MPa pressure was then applied for about a minute. Room temperature cooling of the pressing die was allowed for slow cooling. The method that was subsequently used was developed after a number of trials. The main concern was to achieve the molding of the sample without voids or air packets, which would affect the quality of the measurements. Sample masses between 0.1 g – 0.3 g of the polymer powders were used, and yielded samples with thicknesses of about ~1 – 3 mm.

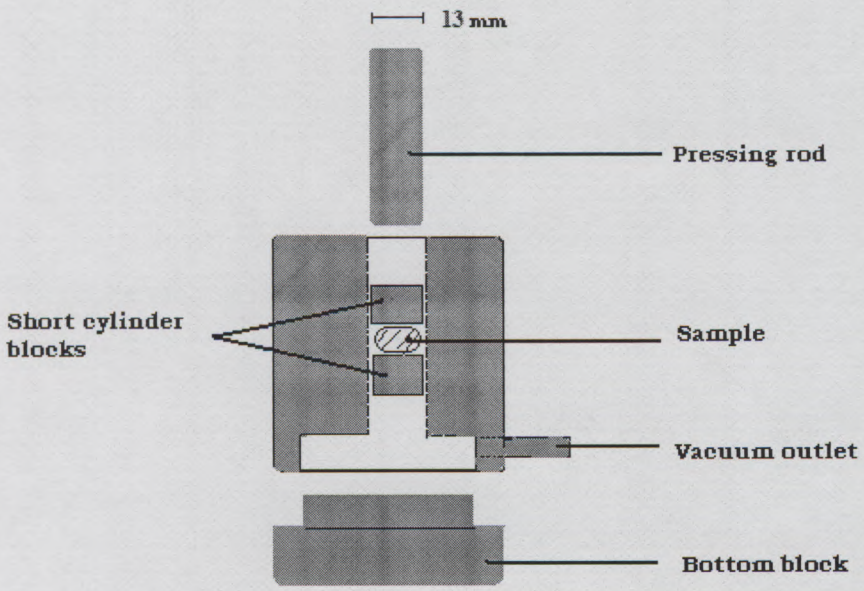

Figure 3.2: In-house manufactured steel die for compression molding of polymer samples.

3.3.2 Thermomechanical analysis

3.3.2.1 Background

Thermomechanical techniques are the classical techniques on which DMA techniques are based. Constant forces/stresses are applied as a function of programmed/controlled temperature and dimensional changes are determined. The most commonly known thermomechanical techniques are vicat softening point and heat deflection temperature (HDT). These techniques are related, because they both involve applying load to a specimen and measuring the change in the position of the rod/pin on it. In some instances, zero force is applied to a sample as a function of temperature and the change in sample dimensions determined. This technique is known as thermodilatometry (TD). TD is best used for the determination of the coefficient of linear thermal expansion (CLTE).

The CLTE is the one-dimensional coefficient of thermal expansion, defined as the fractional change in length or volume of a material for a unit change in temperature.[12]

Determination of the expansion properties in polymers is important as polymers have different behaviors compared to metals or ceramics. Expansion behavior of polymer is very critical for processing and for failure prediction. Differences in the coefficient of thermal expansion in polymers could lead to the development of internal stresses and stress concentrations in the matrix, thereby leading to premature failure.[12] Classically, materials such as fiberglass are used as fillers in polymers to lower the expansion coefficient. Linear expansion is measured using a dilatometer with a programmed temperature and the change in sample dimension monitored. CLTE (or X) is related to the measured parameters by the following equation:

$$X = \frac{\Delta L}{L_o \Delta T} \qquad (3.8)$$

where X is the coefficient of linear expansion (/°C), ΔL is the change in length of the sample due to heating or cooling, L_o is the initial length of the sample and ΔT is the temperature difference over which the change in the sample length is measured.

3.3.2.2 TMA analysis of PLSNs

HDT studies of PLSNs have been carried out, even thought they have generally not received much attention.[5] A study on polymer-silica nanocomposites showed that the coefficient of thermal expansion of polymers can be greatly reduced through the incorporation of inorganic nanofillers.[13] In a review article, the thermal expansion coefficient of a poly(imide)-based PLSN was said to be greatly reduced with 10% clay addition.[6] The nanocomposite was prepared from montmorillonite clay organically modified with a long-chain cation. A decrease of 45% in the thermal expansion coefficient was observed with a 1% clay loading.

3.3.2.3 Instrumentation

The DMA7e is equipped with options for static force measurements; therefore TMA measurements were carried out on the same instrumentation.

A 1-mm-diameter probe was used for the penetration measurement and a 3-mm-diameter probe was used for the thermal expansion measurements.

3.3.3 Dielectric analysis (DEA)

3.3.3.1 Background

Dielectric analysis (DEA) or dielectric relaxation spectroscopy (DRS) is an analytical technique for investigating the physical, chemical and electrical behavior of polymers and other organic materials through the measurement of their dipolar and conductive properties. Energy in a polymer, besides mechanical factors, can also be dispersed by electrical interaction. Dipoles attempt to follow an applied alternative electric field but may be restricted by limitations in mobility of the molecular segments to which they are attached.[14] For instance, in the T_g region, the overall mobility undergoes a major change such that the energy absorption reaches a maximum, similar to mechanical energy dissipation.

In 1997, Wunderlich[14] laid out a simple approach on the principles of DEA in homogenous polar materials. When an electric field is applied across a material, there are three types of responses the material will experience: (1) electron polarization, P_E, which is the shift of electrons in orbitals with relation to the centre of the atom; (2) atom polarization, P_A, where there is a shift of relative positions of bonded atoms in response to an electric field; (3) dipole orientation, P_O, that results from the reorientation of permanent dipoles in the material under the influence of the applied electric field. Polarizations (1) and (2) involve only a displacement of negative and positive charges relative to each other and are experienced at very fast times (10^{-16} and 10^{-15} seconds, respectively). These polarizations are known as induced dipoles, P_I, and a combination of these two takes a timescale between 10^{-12} to 10^{-10} seconds or longer for less mobile dipoles.

When the applied electric field is removed, the decay of polarization is called *dielectric relaxation.* For this reason there is a defined relaxation time, τ. Experimentally, polarization is measured via a function known as relative permittivity (dielectric constant), ε_r.

Relative permittivity or complex permittivity (ε^*), classically, is measured by placing a material between parallel plates and measuring the increase in capacitance. The dielectric constant, ε_r is defined thus:

$$\varepsilon_r = C/C_o \qquad (3.9)$$

where C is the capacitance of the material and C_o is the capacitance of the empty cell (vacuum). If the applied electric field is sinusoidal, the time scale of the experiment becomes an important factor. Figure 3.3 shows a dielectric experiment result for a polar material that shows one dispersion region. The change in real permittivity (ε') and imaginary permittivity (ε''), which are components of ε^*, are plotted as a function of frequency.

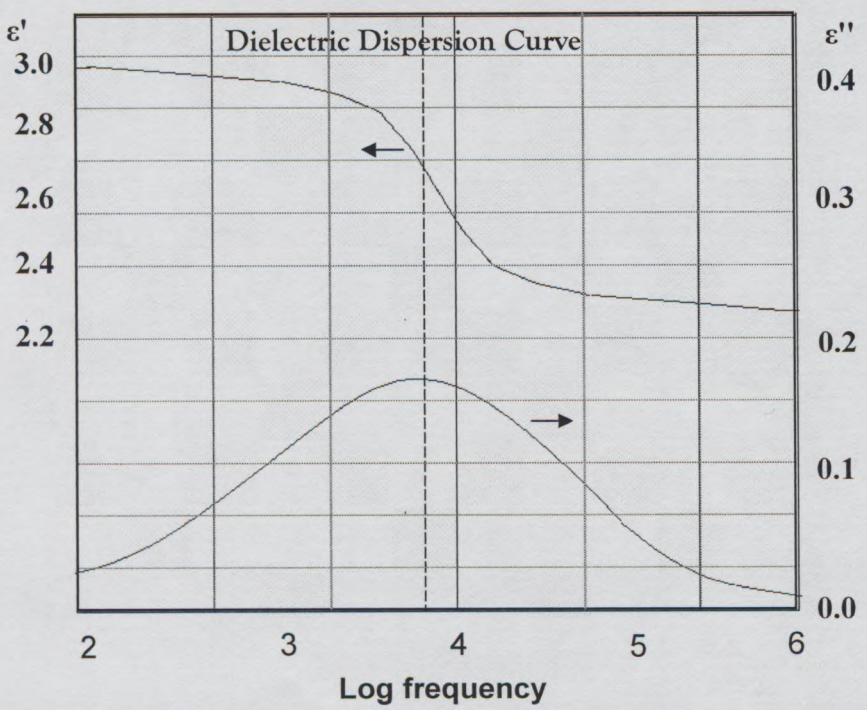

Figure 3.3: A simple dielectric dispersion curve indicating a single process relaxation as described by the Debye equation.[14]

At higher frequency the permanent dipoles cannot respond to the alternating current, meaning that the polarization contribution is mainly from induced dipoles ($P=P_I$).

The basic description of the fundamental equations of the dielectric relaxation with sinusoidal electric field resembles that of the mechanical relaxation. When the response of the dipole is in-phase with the sinusoidal field, ε' contributes to the permittivity. On the other hand, the out-of-phase component is contributed by the loss factor (*dielectric loss/imaginary permittivity*), ε". At high and low frequencies, ε" approaches zero and in the dispersion region, ε" approaches a maximum. Complex permittivity is related to both contributions by the relation (3.10) and also by the classical Debye equations (3.11) to (3.13).[14]

$$\varepsilon^* = \varepsilon' + i\varepsilon'' \qquad (3.10)$$

Where i is the square root of -1.

$$\varepsilon^* = \frac{\varepsilon_\infty' + \varepsilon_o' - \varepsilon_\infty'}{1 + i\omega\tau} \qquad (3.11)$$

$$\varepsilon' = \frac{\varepsilon_\infty' + \varepsilon_o' - \varepsilon_\infty'}{1 + i\omega^2\tau^2} \qquad (3.12)$$

$$\varepsilon'' = \frac{\varepsilon_\infty' + (\varepsilon_o' - \varepsilon_\infty')\omega\tau}{1 + i\omega\tau} \qquad (3.13)$$

where τ is the relaxation time and ω is the angular frequency. The loss factor reaches the maximum at $\omega\tau$ (marked by the vertical dashed line in Figure 3.3). At this point $\varepsilon' = (\varepsilon_o' - \varepsilon_\infty')/2$ and $\varepsilon'' = (\varepsilon_o' + \varepsilon_\infty')/2$.

The ratio between the permittivity components is known as the *loss tangent* (tan delta) and is expressed as:

$$\tan\delta = \frac{\varepsilon''}{\varepsilon'} \qquad (3.14)$$

According to Schonhals[15], tan δ is not an ideal expression to use in scientific applications because it mixes up two quantities with definite physical meanings (ε'' and ε'). However, it is very useful for technical applications where electro-technical characterization of the material is important. Equations (3.11) to (3.13) quantitatively describe the experimental curves in Figure 3.3. The explanation for the properties of the curves can be achieved by assuming a relaxation-time spectrum. If there are many prominent relaxation mechanisms with resolved relaxation times, expansion of the equations (3.11) to (3.13) would be necessary. This would be done by adding the terms describing the added processes. For instance, in the case of polymers, they may have sub-T_g transitions known as the β- and the γ-relaxations.

Generally, DEA can be determined by measurement of experimental quantities known as extensive and intensive quantities.[16] Extensive experimental quantities include electrical admittance, Y(ω) and electrical impedance Z (ω). These parameters are inversely related to one another [$Y(\omega) = Z^{-1}(\omega)$] and are dependent on the sample geometry, hence extensive.

Intensive quantities include permittivity ε(ω), modulus M(ω) and conductivity σ(ω), which are related to each other by the following relation:

$$\varepsilon(\omega) = \frac{1}{M(\omega)} = \frac{\sigma(\omega)}{i\omega\varepsilon_v} \qquad (3.14)$$

where ε_v is the permittivity of an empty dielectric cell in a vacuum.

The five dielectric experimental quantities have been used in various fields with different interpretations relating to that particular field.[16]

3.3.3.2 DEA study of PS-LSNs

DEA analysis of polystyrene-layered silicate nanocomposites is discussed in detail in Chapter 2, Section 2.4.4.2.3

3.3.3.3 Experimental

The 1- mm diameter samples were prepared by compression molding, according to the same procedure as for DMA, as discussed in Section 3.3.1.4. Electrodes on the flat side of the cylindrical samples were prepared by coating with an alcohol-based conductive silver paint (supplied by Agar Scientific). The application was done under a thermal lamp to accelerate the evaporation of the solvent. Consistency in the conductivity of the electrodes was checked using a digital multimeter (by Fluke, Netherlands).

A Schlumberger Impedance/Gain-phase Analyzer SI 1260 in combination with a Solatron Broadband Dielectric Converter (BDC) was used to run the dielectric measurements in a controlled temperature environment (to less than 0.2 °C). Measurements were done at isothermal points (with increment of 25 °C), while scanning at frequency between 10^{-2} to 10^{8} Hz. Initially, the temperature was varied from -25 °C to 250 °C. After assessing the initial data for significance, measurements were done from 25 °C to 150 °C. A data acquisition/analysis software (WinDETA) was used to record and manipulate data. Origin 7 was also used to manipulate data and to draw graphs for purposes of reporting. Conductivity, permittivity and impedance functions, and related parameters were measured in a single run.

3.4 List of references

1. Moore, D. M.; Reynolds Jr., R. C., *X-ray Diffraction and Identification Analysis of Clay Minerals*. 1st ed.; Oxford University Press: Oxford, **1989**; p 132.

2. Department of Physics and Astronomy; Georgia State University. *Hyperphysics: hyperphysics.phy-astr.gsu.edu/hbase/hph.html* **Accessed: 15 February 2007**.

3. Materials Research Laboratory; University of Califonia. *X-ray Basics: www.mrl.ucsb.edu/mrl/centralfacilities/xray/index.html* **Accessed: 15 February 2007**.

4. Grim, R. E.; Guven, N., *Bentonites: Geology, Mineralogy, Properties and Uses*. 1st ed.; Elsevier Scientific Publishing Company: Amsterdam, **1978**; p 256.

5. Ray, S. S.; Okamoto, M. *Progress in Polymer Science* **2003,** 28, 1539-1641.

6. Alexandre, M.; Dubois, P. *Materials Science and Engineering: R (Reports)* **2000,** 28, 1-63.

7. Morgan, A. B.; Gilman, J. W. *Journal of Applied Polymer Science* **2003,** 87, 1329-1338.

8. Goodhew, P. J.; Humphreys, J.; Beanland, R., *Electron Microscopy and Analysis*. 3rd ed.; Taylor and Francis: London, **2001**; p 251.

9. Morgan, A. B.; Gilman, J. W.; Jackson, C. L. *Macromolecules* **2001,** 34, 2735-2738.

10. Mernad, K. P., *Dynamic Mechanical Analysis: A Practical Introduction*. 1st ed.; CRC Press LLC: Boca Raton, Florida, **1999**; p 208.

11. Perkin-Elmer Corporation; Thermal Analysis Dept. *Dynamic Mechanical Analysis (DMA7e): Theory of Operation* **1996,** Instrument Poster.

12. Shah, V., *Handbook of Plastics Testing Technology*. 2nd ed.; John Wiley & Sons, Inc: New York, **1998**; p 527.

13. Al Arbash, A.; Ahmad, Z.; Al-Sagheer, F.; Ali, A. A. M. *Journal of Nanomaterials* **2006,** 2006, 1-9.

14. Wunderlich, B., The Basis of Thermal Anaslysis. In *Thermal Characterization of Polymeric Materials: Vol 1*, Second ed.; Turi, E. A., (Eds). Academic Press, Inc.: San Diego, California, USA, **1997**; pp 205-482.

15. Schonhals, A. *Dielectric Spectroscopy on the Dynamics of Amorphous Polymeric Systems*; Application Note Dielectrics no.3: Novocontrol GmbH: **1998**; pp 1-16.

16. Williams, G.; Thomas, D. K. *Phenomenological and Molecular Theories of Dielectric and Electrical Relaxation of Materials*; Application Note Dielectrics no.3: Novocontrol GmbH: **1998**; pp 1-29.

Chapter 4

Preparation and characterization of organically modified clays and their characterization

Abstract

The preparation and characterization of organically-modified clays (organoclays) is reported. Two polymerizable surfactants (surfmers) and a classical surfactant were used to modify the surface of montmorillonite (MMT) clay in an aqueous ion-exchange reaction. Thermogravimetric analysis (TGA), small-angle X-ray scattering (SAXS), Fourier transform infrared spectroscopy (FTIR) and scanning electron microscopy (SEM) were used for the characterization of the materials. The products were prepared for the synthesis of polymer-layered silicate nanocomposites.

4.1 Introduction

4.1.1 Background

Mineral-type inorganic materials, especially layered silicates (clays), are used in a variety of industries such as in oil-drilling industries, environmental studies, water purification, medical applications and composite material applications.[1] However these mineral inorganic materials may, at some point, need to have some organic functionality to enhance effectiveness in their applications. Organic modification is done on the oil drilling muds to improve on the rheological properties, to make the clays more absorptive of organic pollutants in water purification. Organic antibacterial surfactants were reported by He et.al[2] to show a huge potential in antibacterial applications when intercalated in montmorillonite clay (MMT). The modification of clays, especially the smectite groups, using organic molecules for dispersion in polymer matrices to make nanocomposites is a field that has recently received a lot of attention.[3-7]

Clays are hydrophilic in nature and therefore, are not readily compatible with non-polar polymers. This makes it difficult for the clay layers to disperse and delaminate in the polymer matrix, when used as filler. When delaminated into nano-sized sheets in the polymer matrix, the corresponding polymer-layered clay nanocomposite (PLSN) material possesses improved properties compared to pristine polymer or the corresponding microcomposite. This is due to optimal interaction between the dispersed clay and the polymer matrix. In order to obtain optimal interaction between the hydrophilic silicate particles, usually hydrated, and a hydrophobic polymer matrix, the surfaces of the silicate layers are modified organically to make them hydrophobic. Different types of surfactants that are known to be used in the modification of clays for nanocomposite synthesis include quaternary alkyl-ammonium cation, alkyl-phosphonium ions and amino acids.[3,6,8] MMT, of the smectite group of clays, is a commonly used material for the synthesis of

PLSNs. Different types of clay minerals and their classification are briefly discussed in Chapter 2, Sections 2.1.1 and 2.1.2.

Clays classified as smectites have a three-sheet crystal structure that forms a unit layer.[9] A unit (alumnosilicate) layer comprises of two silica tetrahedral sheets on either sides of an alumna or magnesia octahedral sheet. Many of these unit layers are packed together with Van der Waals forces holding them together. These alumnosilicate layers have cationic charges in-between them (galleries) balancing a negative surface charge originating from a crystal irregularity. This irregularity is due to a natural phenomenon known as isomorphic substitution where an ion is substituted by a different ion with a different charge but same radius (see Chapter 2, Section 2.1.2).

Modification of clay progresses by ion-exchange of surfactant (alkyl ammonium) cations with alkali/alkaline earth cations (Li^+, Na^+, Mg^{2+}) located in the galleries. The ion-exchange phenomenon is determined by the ability of the clay to exchange the cations at the surface, or its cation exchange capacity (CEC). It is elaborated by Luckham and Rossi[9] as the "total amount of cations adsorbed on the clay, expressed in milliequivalents per hundred grams (meq/100 g) of dry clay". MMT has a relatively higher CEC value in comparison to other clay minerals. In the case of sodium-montmorillonite (Na-MMT), the alkyl ammonium cations exchange with Na^+ cations in the gallery, as illustrated in Scheme 4.1 below.

Where X^- = Cl, Br

Scheme 4.1: Illustration of ion-exchange reaction of alkyl ammonium cations with intergallery cations (Na^+).

The cation exchange is carried out in an aqueous medium in which the surfactant ions in the solution diffuse into the galleries and the Na^+ ions move out of the galleries into the

solution. The Na^+ ions are then counter-balanced by the surfactant anions (usually halogen anions). The intercalation of the surfactant molecules in the galleries increases the d-spacing (also intergallery space) of the clay layers of the organically modified clays (organoclays). Since the clay layers are held together by weak Van der Waals forces, the pressure applied by the presence of the bulky, long-chain molecules is enough to push the layers further apart, leading to a larger intergallery space (Figure 4.1).

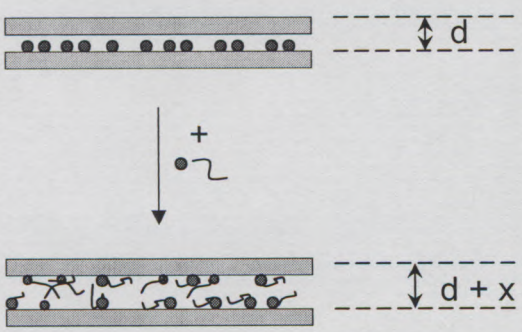

Figure 4.1: The intercalation of the long-chain cations in the galleries with increased intergallery space.

The dispersion of the clay particles in water allows wetting of the clay layer surfaces. The fact that water molecules hydrate the ions (Na^+) inside the galleries contributes to the increase of the intergallery spacing. Since the ion-exchange reaction is conducted in aqueous medium, the surfactant molecules intercalate better on wetted clay galleries. There are different configurations of the intercalated surfactant molecules in the galleries: monolayer, bilayer, pseudo-trilayer, paraffin-monolayer and paraffin bilayer. This means that the total exchanged intercalated surfactant cations may be more that the nominal CEC of the alumnosilicate. When the alkyl ammonium cations are intercalated in excess, their charge is balanced by simultaneous adsorption of anions.[10]

The most commonly used techniques for the characterization of organoclays are: X-ray diffraction (XRD), Fourier transform infrared spectroscopy (FTIR) and thermogravimetric analysis (TGA). The intercalation characteristics, such as the

interlayer spacing, is usually better determined by small-angle x-ray scattering (SAXS) and wide-angle X-ray diffraction (WAXD). In addition, FTIR used extensively for the characterization of the organoclay chemistry. The chemical phenomena are determined by the measurement of spectroscopic vibrations due to the intercalated organic material. The thermal stability of the organoclays is determined by the TGA technique.

The thermal stability of organoclays is determined by a number of factors, including the structure of the intercalated organic molecule; e.g. alkyl chain length, number of alkyls and the extent of unsaturation.[11] Fabrication of the nanocomposites involves the application of higher temperatures. Xie et al.[12] point out in their study on the thermal stability of organoclays that "elevated temperature surface chemistry complicates fundamental studies attempting to establish specific requirements for the montmorillonite/surfactant/polymer interface that is necessary for optimal dispersion and property enhancements". The thermal degradation of organoclays progresses in steps based on a range of temperatures in which specific decomposition products evolve. Table 4.1 summarizes the set temperature regions of the decomposition and the corresponding evolved products.

Table 4.1 Summary of the major species evolved from each decomposition step of clay and modified clay samples during thermal degradation.[11]

Thermal region	Region I	Region II	Region III	Region IV
Temperature range	< 200°C	200°C – 500°C	500°C – 800°C	800°C – 1000°C
Thermal decomposition products (Organoclay)	Free water	Organic water, CO_2, long-chain alkyl fragments	Water from dehydroxylation, CO_2	Water, CO_2
Thermal decomposition products (Na-MMT)	Free water	CO_2, interlayer water	Water from dehydroxylation, CO_2	CO_2

4.1.2 Objectives

The objective of this chapter is to report the processes of modifying smectite clay, in this case sodium montmorillonite (Na-MMT), using three quaternary ammonium ion organic long-chain surfactants. Two of these surfactants are similar and one is different in structure and properties. Two of these are new types of acrylate-based surfactants with a polymerizable group at the end of the hydrophobic tail. The other one is a long-chain surfactant with no polymerizable group. The modification of clay using a polymerizable surfactant has been reported in the literature.[13] The use of these types of surfactants in the preparation of PLSNs has been highlighted, in the above mentioned study, as one of the contributing factors in the exfoliation of the clay layers in the polymer matrix.

The organically modified clay will then be characterized using various techniques to determine properties and their thermal stability. An understanding of the properties of organoclays is of utmost importance as they determine the quality of the final nanocomposite material. PLSNs are synthesized by various methods, including melt blending and in-situ intercalative polymerization. The aim of the preparation and characterization of these organoclays is to obtain well understood products that are potentially ready and suitable for use in the synthesis of new PLSNs.

4.2 Experimental

4.2.1 Materials and reagents

The used deionized (DI) water was btained from a Milli-Q water purification system (by Millipore Corporation, USA). Silver nitrate salt was supplied by Merck Chemicals and Na-MMT, with CEC of 96.2 meq/100g, was supplied by Southern Clay Products Inc. Cetyl trimethyl ammonium bromide (CTAB) – a commercial surfactant, was obtained from ACROS organics. This surfactant has been previously studied and used in the

synthesis of polymer-layered silicate nanocomposites.[14] It has been used in this study for comparison purposes (comparing its use to the use of polymerizable surfactants). Nanocomposite materials produced from this surfactant are known to be intercalated, since the modification allows for easy penetration of the polymer but no dispersion of the clay layers in the polymer matrix.

'In-house'-synthesized polymerizable surfactants (surfmers), *11-acryloyloxy-undecyl dimethyl ethyl ammonium bromide* (ethyl surfmer) and *11 – acryloyloxy-undecyl dimethyl hydroxyethyl ammonim bromide* (hydroxyethyl surfmer) were the main quaternary alkyl ammonium surfactants to be studied for the intercalation of the clay materials. These surfactants are acrylate-based and have an unsaturated, polymerizable group at the end of the chain, opposite the ammonium group. The chemical structures of the surfactants used in this study are presented in Figure 4.2, and their properties are summarized in Table 4.2. A detailed study on their synthesis and characterization is reported elsewhere.[15]

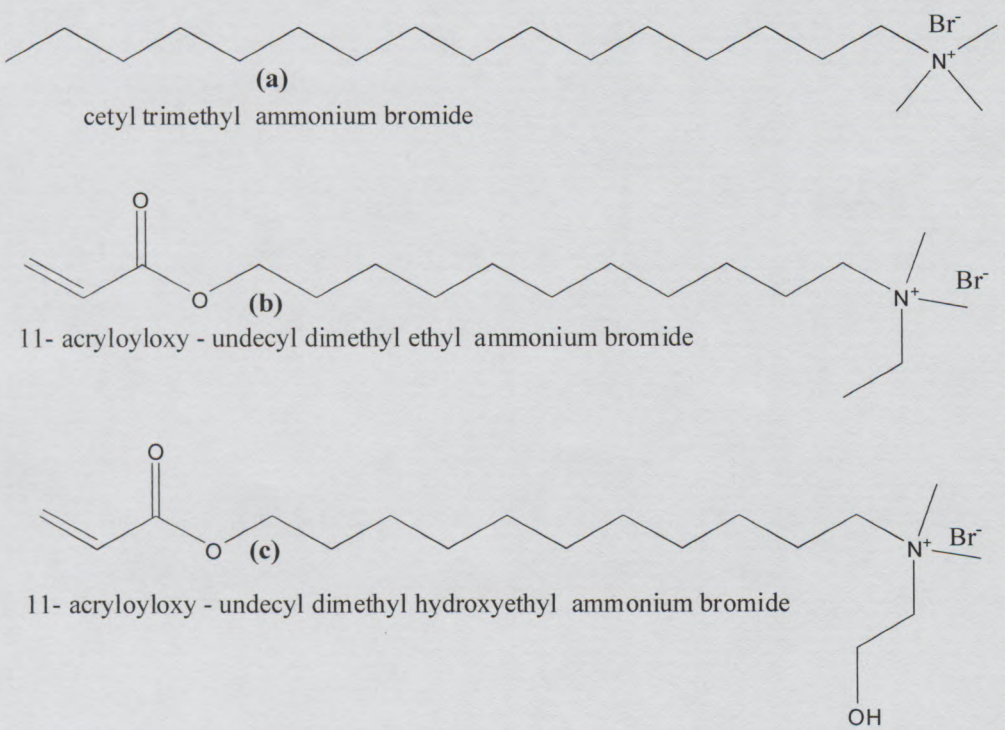

Figure 4.2: Structures of (a) CTAB, (b) ethyl-surfmer and (c) hydroxyethyl-surfmer.

Table 4.2 Summarized properties of surfactants used for clay modification.

Surfactant	Chemical formula	MW[a] (g/mol)	CMC[b] (x 10^{-2} M)	C-chains in tail	Other ammonium bonded group(s)[d]
CTAB	$CH_3(CH_2)_{15}N^+(CH_3)_3Br^-$	364.45	0.10[13]	16	None
Ethyl surfmer	$H_2CCHC(O)O(CH)_{11}N^+(CH_3)_2CH_2CH_3Br^-$	378.26	1.05[15]	14[c]	One (— CH_2CH_3)
Hydroxyethyl surfmer	$H_2CCHC(O)O(CH)_{11}N^+(CH_3)_2CH_2CH_2OBr^-$	394.26	1.16[15]	14[c]	One (— CH_2CH_2OH)

[a] Molecular weight

[b] Critical micelle concentration (measured by conductivity)

[c] Eleven carbon-alkyl bonded to an acrylic group at the end of the chain

[d] Group(s) bonded other than methyl group (s)

4.2.2 Preparation of organoclays

A specified mass of Na-MMT clay was dispersed in deionized water to make about 0.5 wt% aqueous suspension (or 1 part clay to about 200 parts by mass of DI water), typically 3 g clay in 600 g water. The suspension was stirred with a magnetic stirrer bar and continued for two hours. A precalculated (1:1.3 equivalent clay to surfactant) amount of surfactant was dissolved in about 100 ml deionized water. Table 4.3 summarizes the masses and concentrations used in the ion-exchange reaction with Na-MMT.

Table 4.3 Masses and concentrations of surfactants used in the ion-exchange reaction with 3 grams Na-MMT

Surfactant	Mol amount[§] (mmol)	Mass required (g)	Conc. in100ml (x 10^{-2}M)
CTAB	3.61	1.315	3.61
Ethyl surfmer	3.61	1.366	3.61
Hydroxyethyl surfmer	3.61	1.423	3.61

[§] 1.3 times 2.778 milliequivalent of 3 grams Na-MMT (CEC 96.2 meq/100 g)

The schematic procedure for the ion-exchange reaction is discussed below and summarized in Figure 4.3. A surfactant solution was added dropwise into the Na-MMT/water suspension while stirring was continued. The stirring continued for 24 hours to allow for maximum ion-exchange.[16] The suspension was then allowed to settle with no agitation. The modified clay moved towards the bottom of the beaker and the surfactant solution remained at the top of the beaker/flask. The solution was decanted from the organoclay.

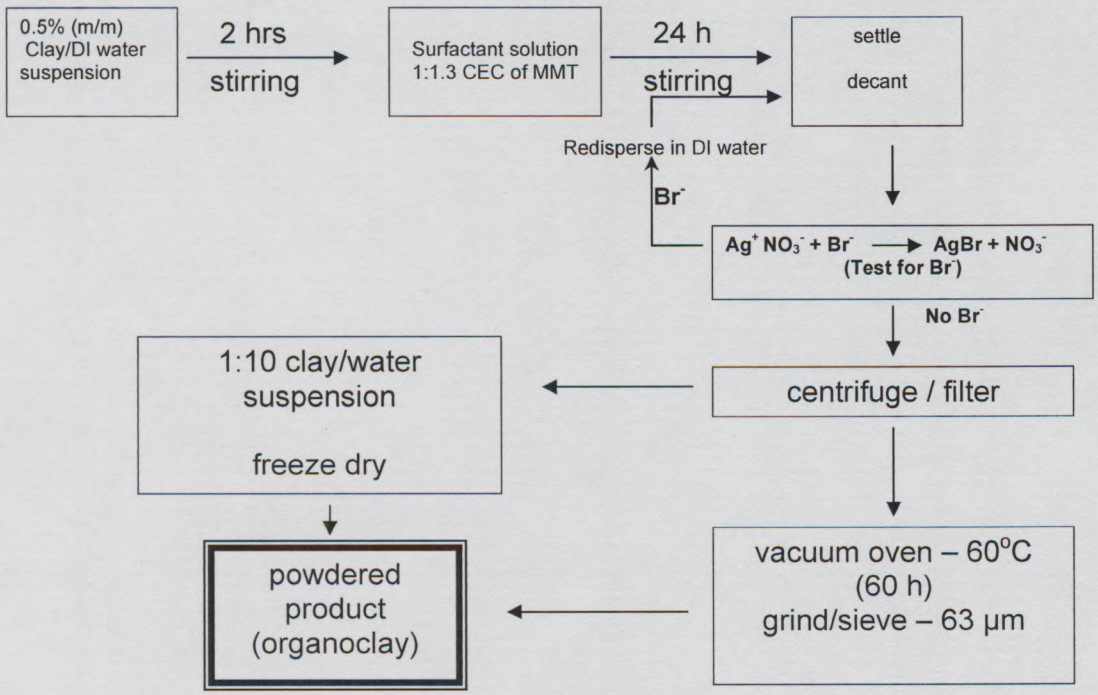

Figure 4.3: Schematic procedure for the preparation of organoclays.

The modified clay was washed free of excess surfactant by dispersing in more water and applying agitation (stirring). The suspension was then allowed to resettle and for the organoclay to separate from the solution. A 1 M $AgNO_3$ solution was used to test for the presence of bromides (Br^-) in the solution. The presence of Br^- in the solution showed precipitation in the $AgNO_3$ solution. The washing was continued until the solution

showed no presence of bromides. This meant that the solution was free of excess surfactant and also the exchanged Na^+ ions as they would be counter balanced by Br^- anions if present in solution.

After settling and decanting, the organoclay was then filtered in a 1-μm-pore Buchner funnel under vacuum suction. The obtained wet organoclay product was centrifuged in 30ml cylindrical plastic cups to speed up the separation of the product from water. A model 5702 centrifuge (by Eppendorf AG, Germany) was used with rotation speed of 3600 rotations per minute (rpm) for 20 minutes. This was a more effective method of extracting the product, than using the filtration separation which resulted in frequent blocking of the filter pores. The organoclay was dried in a vacuum oven at 60 °C for 48 hours. The product was then crushed and ground in a pestle and mortar. The powder obtained was sieved through a 63-μm mesh grain sieve.

The second procedure used to prepare the final product was to centrifuge the settled clay while washing. The suspension was allowed to settle and the supernatant liquid decanted. More deionized water was added, with stirring to wash the suspension free of excess surfactant. The washing, settling and decanting were repeated until the supernatant liquid was free of Br^- ions. The suspension was then stirred as 1:10 parts water and put in two 100-ml or 250-ml round-bottomed flasks and dipped in a liquid nitrogen bath. The suspensions were then freeze-dried in an ALPHA 1-4 LD drier (by ATR Biotech, USA). The yield products obtained by drying methods were determined and characterized by TGA, FTIR, SAXS and SEM.

4.2.3 Thermal Analysis

The synthesized organoclay samples were analyzed for thermal stability by thermogravimetric analysis (TGA). A Perkin-Elmer TGA 7 was used. Sample sizes were

about 10 mg. A temperature scan was set from 25 °C to 900 °C with a heating rate of 10 °C/min, in an inert atmosphere (nitrogen gas).

A percentage weight loss (TG) curve was plotted against temperature, complemented by its first derivative (DTG) curve. A data analysis technique of the thermal degradation was adopted from Xie et al.[12], where the total fraction of organic components in the organoclays was determined from the adjustment of weight loss of the parent Na-MMT at 400 °C to 750 °C to that of the organoclays at 150 °C to 900 °C. This difference accounted for the evolution of the decomposition products due to the dehydroxylation of the aluminosilicate crystallographic structure. The first event of organic degradation was taken from the first peak onset ($T_{onset,1}$) of the derivative curve after 150 °C. The temperature point(s) at which the DTG curve shows prominent peaks (T_{max}) denotes the deflection points (onsets) of the weight% curve, where there is a change in weight loss due to a volatile component in the organoclay. The $T_{onset,1}$ was obtained by extending the plateau and the first part of the peak slope.

4.2.4 Morphological characterization

4.2.4.1 Fourier transform infrared spectroscopy

A Fourier transform infrared spectrometry (FTIR) combined with photoacoustic spectrometry (PAS) was used to determine the characteristic absorption wavelengths of the organoclays. An FT-IR Spectrometer Paragon 1000 PC (Perkin Elmer Corporation, USA) coupled to a Model 300 photoacoustic cell (MTEC Photoacoustics, Inc. USA) was used to measure the absorbance properties of the specimens. The PAS cell was flushed with ultra-high purity (UHP) helium for two minutes before the measurements. A scan average of 128 was taken from 450 cm^{-1} to 4000 cm^{-1} with a resolution of 8 cm^{-1}. No special sample preparation was needed, except for where specified, as the PAS cell can take solid samples.

4.2.4.2 Small-angle X-ray scattering

SAXS measurements were performed at 298 K. SAXS diffraction measurements were carried out in a transmission configuration. A copper rotating anode X-ray source (functioning at 4 kW) with a multilayer focusing "Osmic" monochromator giving high flux (10^8 photons/sec) and punctual collimation was used. An "image plate" 2D detector was used to collect the diffraction patterns. Diffraction curves were obtained, giving diffracted intensity as a function of the wave vector q. The method used to calculate q is described elsewhere.[17]

4.2.5 Surface properties

Scanning electron microscopy (SEM) measurements were done on a LEO 1430 VP system fitted with backscatter. The samples were copper sputtered before measuring. This was done to make the samples more conductive for better imaging, and to prevent the accumulation of static electric fields due to electron irradiation. Variable magnifications were set and digital images of the micrographs were taken.

4.3 Results and discussion

4.3.1 Thermal characterization

The TG curve of weight-loss of the sample was plotted against temperature with the intention to observe the weight-loss onset corresponding to the degradation temperature range of the surfactants (see Figures 4.5 to 4.7). Samakande et al.[15] reported the degradation temperatures of the surfactants to be: 270°C for hydroxyethyl surfmer (taken at 10% decomposition) with a final degradation temperature of 522 °C; 240 °C for the ethyl surfmer with a final degradation temperature of 508 °C. The surfactants were of a

similar nature but with different degradation chemistry: "the differences observed between the two surfmers are probably due to the ability of the hydroxyl surfmer to form hydrogen bonds via its hydroxyl group."[15]

According to Dharaiya and Jana[18], the majority of alkyl ammonium ions have a thermal decomposition temperature starting at 200 °C to 500 °C. The initial onset of organic degradation from the DTG curve was at 238.6 °C, 213.7 °C and 227.1 °C for ethyl-MMT, hydroxyethyl-MMT and CTAB-MMT, respectively, as shown in Table 4.4. These values were comparable with those of the individual surfactant degradation onset values as the organic degradation commenced after 200 °C in all three organoclays.

Table 4.4: First organic decomposition ($T_{onset,1}$) onset and peak maxima (T_{max}) determined from the derivative curves in each thermal decomposition region for Na-MMT, ethyl-MMT, hydroxyethyl-MMT and CTAB-MMT.

Sample	$T_{onset,1}$ (°C)	Region T_{max} (°C)			
		I	II	III	IV
Na-MMT	none	57.8	None	669.7	none
Ethyl-MMT	238.58	125.9	303.3; 455.8 (Shoulder 399.0)	686	none
Hydroxyethyl-MMT	213.69	44.6	262.5; 382.6	640.0	800 °C
CTAB-MMT	227.09	56.5	332.5; 437.1	642.0	none

Table 4.4 also shows the DTG maxima of the samples at different thermal regions. The decomposition products evolved in each region corresponding to the peaks are discussed

in the Section 4.1.1 and listed in Table 4.1. Corresponding thermograms to Table 4.4 are given in Figures 4.4 to 4.7. The DTGs of the organoclays showed two T_{max} peaks at region II, which denotes that the degradation of the intercalated alkyl ammonium surfactants progressed in two steps. This was in accordance with the data published by some researchers studying the thermal degradation of organoclays.[11,19,20] It was shown that the alkyl ammonium surfactant inside the clay galleries follow a degradation regime of two, and sometimes three steps. Although the ethyl-MMT and hydroxyethyl-MMT organoclays have almost identical structures, differing only by a hydroxyl group on the latter, the ethyl-MMT organoclay showed a shoulder at 399 °C on the second DTG peak. It was rather difficult to attribute the decomposition at that point to a specific phenomenon since the TGA technique employed was not equipped to identify the products that were evolved. Techniques such as thermogravimetric-evolved gas analysis (TGA-EGA) would have been useful to identify the peak corresponding to the decomposition products.

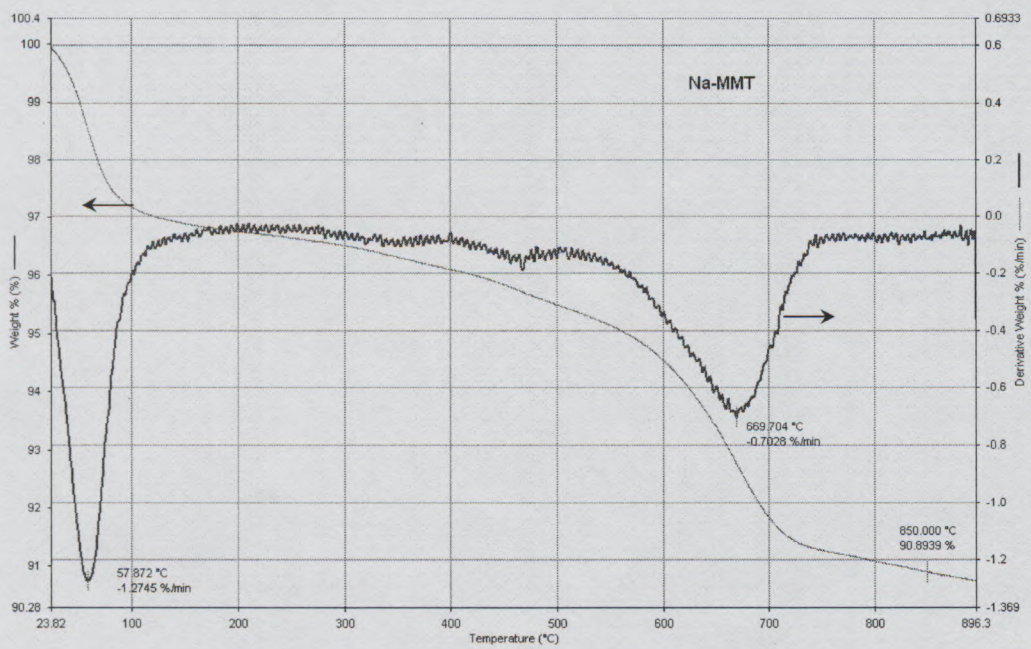

Figure 4.4: A thermogram of % weight loss and its derivative as a function of temperature for pristine Na-MMT clay.

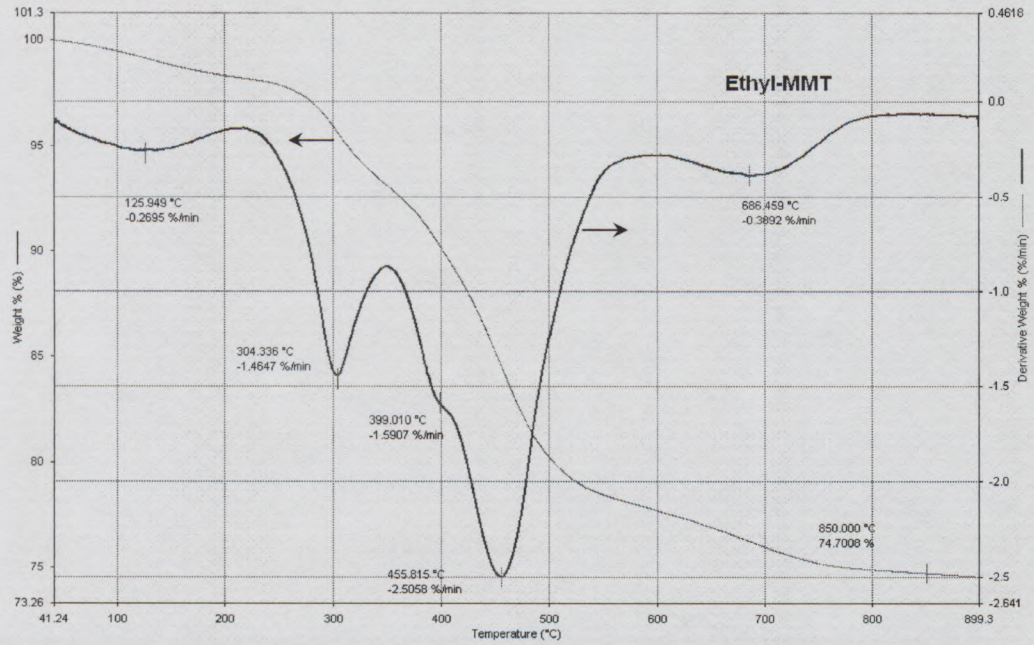

Figure 4.5: A thermogram of % weight loss and its derivative as a function of temperature for ethyl-MMT organoclay.

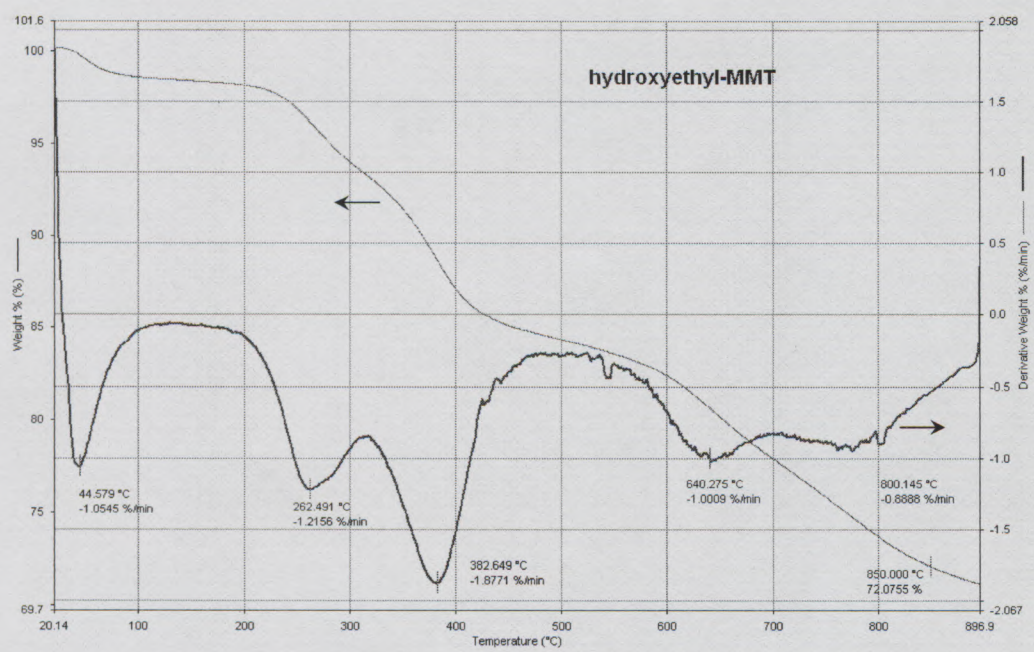

Figure 4.6: A thermogram of % weight loss and its derivative as a function of temperature for hydroxyethyl-MMT organoclay

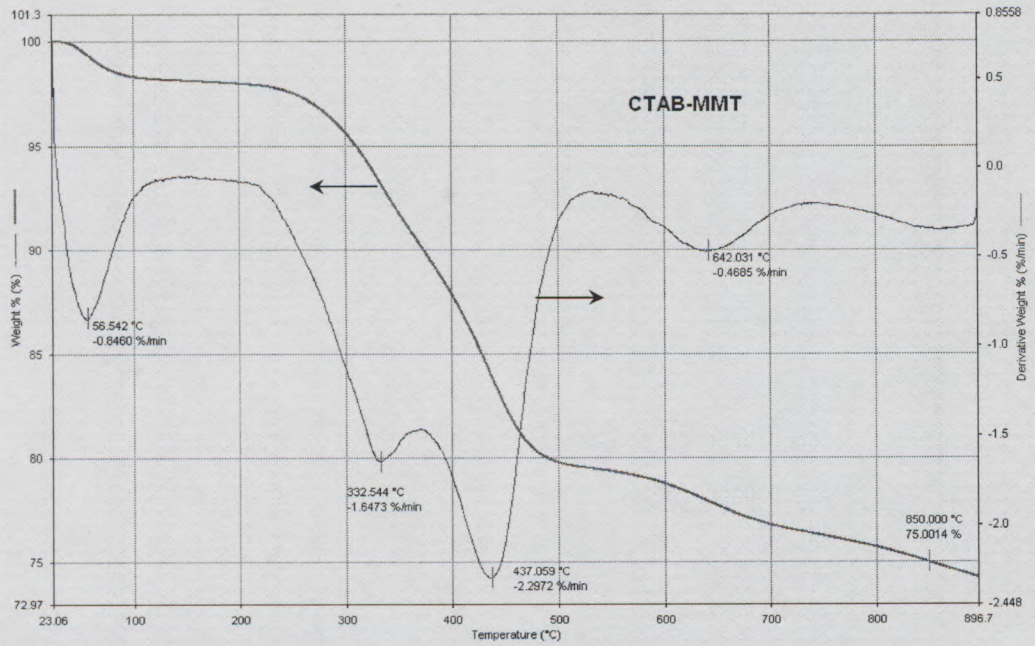

Figure 4.7: A thermogram of % weight loss and its derivative as a function of temperature for CTAB-MMT organoclay

Many studies have been done on the thermal stability of organoclays and the effect of the presence of surfactant between the clay layers[2,11,18-24]. All these studies agree on the fact that the chain length, size and the chemical structure of the surfactant have an effect on the degradability of the surfactant inside the clay galleries. Bromide based surfactants have a more stable effect on the organoclays than the chloride based ones. Also, the phosphonium ion based surfactants are more thermally stable that the ammonium ion based surfactant. Correspondingly, the phosphonium ion based organoclays are more thermally stable.[12]

The initial degradation of an ammonium surfactant in the organoclay progresses through a Hoffman elimination process. Xie et al.[19] proved this fact by pyrolysis-gas chromatography (Pyr-GC). The Hoffman elimination involves a process in which the initial degradation depends mostly on the basicity of an anion, steric environment and temperature. Table 4.5 shows the average weight losses due to water content, intercalated surfactant, first decomposition product and the corrected total organic content.

Table 4.5: A summary of the average % weight loss due to total water content, intercalated surfactant, first decomposition product and the corrected total organic content for the organoclays.

Sample	% weight loss			% total organic
	<120 °C	120 °C – 500 °C	First weight loss event	
Ethyl-MMT	0.78	19.00	5.02	19.93
Hydroxyethyl-MMT	1.58	14.17	4.85	22.71
CTAB-MMT	1.77	18.43	7.64	19.22

The ethyl-MMT clay showed the least amount of free water (0.78%) compared to hydroxyethyl-MMT (1.58%) and CTAB-MMT (1.77%) at weight loss below 120 °C. These values are lower than the determined value for the pristine clay of 2.90% weight loss (not shown). This means that the organoclays have less affinity for water than the pristine clay. However, the organoclay will still absorb some water even if isolated from ambient humidity. This was deduced from the fact that organoclays were oven dried and stored in an air-tight container but still there was a free water DTG peak appearing. The total organic content of the organoclays was 19.93% (ethyl-MMT), 22.71% (hydroxyethyl-MMT) and 19.22% (CTAB-MMT). All three values are comparative.

TGA was also used in the determination of the intercalated surfactant amount in the organoclays. Subsequently the extent of ion-exchange reaction progression, based on the amount of the surfactant in the clay, was determined.[25] The ion exchange was calculated to be 109% for the ethyl-MMT clay, 110% for the ethanol-MMT clay and 116% for CTAB-MMT. The ion extent of the ion exchange was calculated to be more than 100%

for each surfactant used to modify the sodium montmorillonite clay. This denotes the possibility that the surfactant intercalated could have formed bilayers inside the galleries. Therefore, this would mean that although there were enough ion-exchange sites (96.2 meq/100 g) on the clay surface for surfactant ion exchange, excess surfactant was adsorbed inside the silicate galleries.

The surfactants could have formed a bilayer by adsorbing a second layer on the silicate bonded surfactant chain. This postulation would be further motivated by the fact that excess surfactant was thoroughly washed during the preparation of the organoclay, and was further tested for the presence of excess surfactant in the suspension. In that instance, no excess surfactant was detected. However, intercalated excess surfactants could not be washed by the de-ionized water, as it was ionically bonded inside the galleries. A possibility of adsorption outside the clay galleries was also reported by Rausell-Colom and Serratosa.[10] Large cations containing long chain lengths can be adsorbed in excess over the clay CEC, regardless of whether they have been exchanged with the inorganic cations.

4.3.2 Analysis of surface properties by scanning electron microscopy

The organoclay samples and Na-MMT were analyzed for surface properties using SEM. The surface characteristics of the Na-MMT, as shown in Figure 4.8, were found to be granular in nature and they were irregular in sizes and shapes. The sizes were expected to vary since the samples were analyzed as received from supplier. Few flaky particles were observed (Figure 4.8-d), which showed the layered-nature of the clay particles. However, the other particles showed agglomerated particles. The oven-dried and sieved ethyl-MMT had no distinct differences in terms of the grain shapes and the size distribution was variable, as shown in Figure 4.9 a-d. The particles in this sample also showed similarity to the Na-MMT sample. Oven drying, with the escape of water in the galleries, led to shrinkage, and hence the agglomerated particles. The particles were smaller (less than 63 μm) because of the grinding and sieving, but the sizes were not evenly distributed.

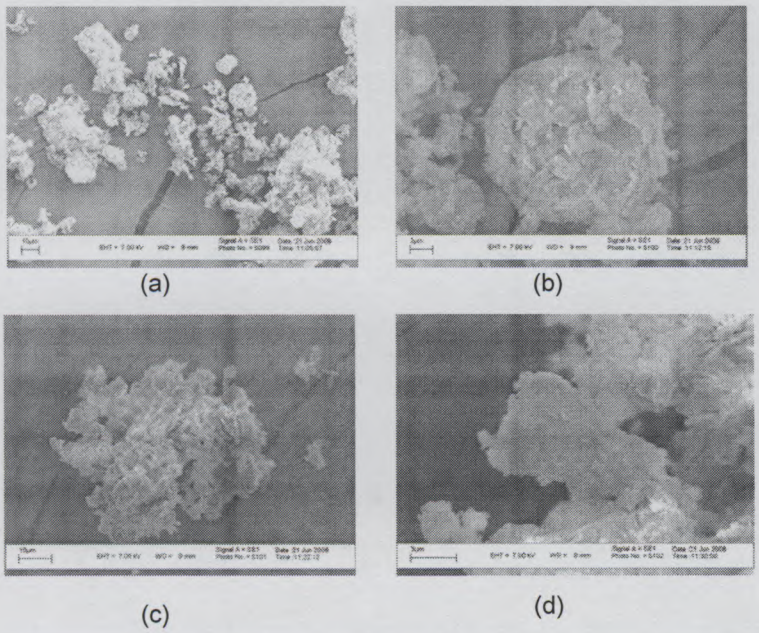

Figure 4.8 : SEM micrograph of Na-MMT sample at (a) 10 μm, (b) 2 μm, (c) 10 μm and (d) 3 μm magnifications.

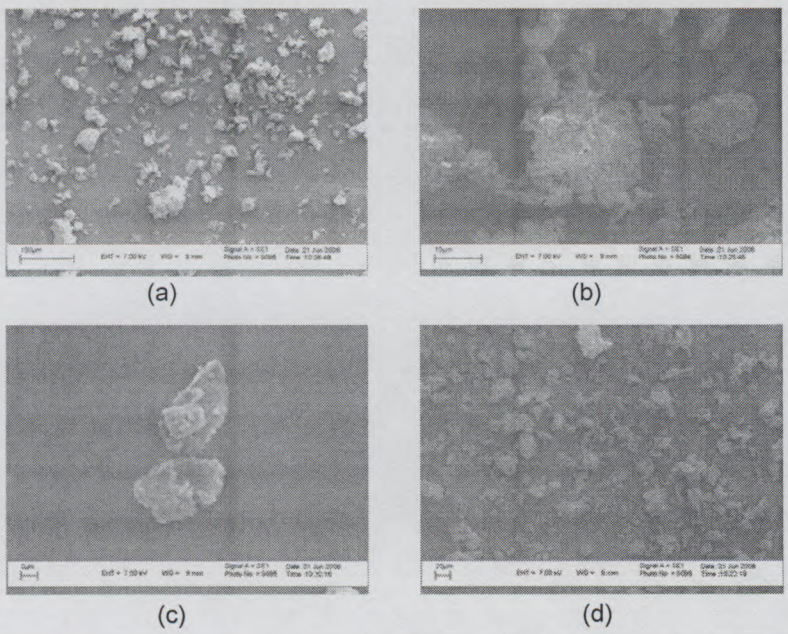

Figure 4.9: SEM micrograph of an oven-dried and sieved ethyl-MMT sample at (a) 100 μm, (b), 2 μm (c) 10 μm and (d) 20 μm magnifications.

The micrographs of the freeze-dried sample (Figure 4.10) showed that the grains of the sample were more spherical, with average sizes of between 10-20 μm. The cluster of the grain particle sizes of the freeze-dried samples looked more uniformly distributed compared to the oven-dried and sieved samples.

The finer and evenly distributed particles obtained from freeze-drying are an important result for sample preparation of the organoclays. This is because there is less work involved in preparing the fine powder product for synthesis and analysis. Grinding and sieving, or milling, would no longer be required, as it is laborious and time consuming. The loose packing of the particles gives a larger surface area that makes it more efficient to run analysis such as TGA which requires larger surface area.

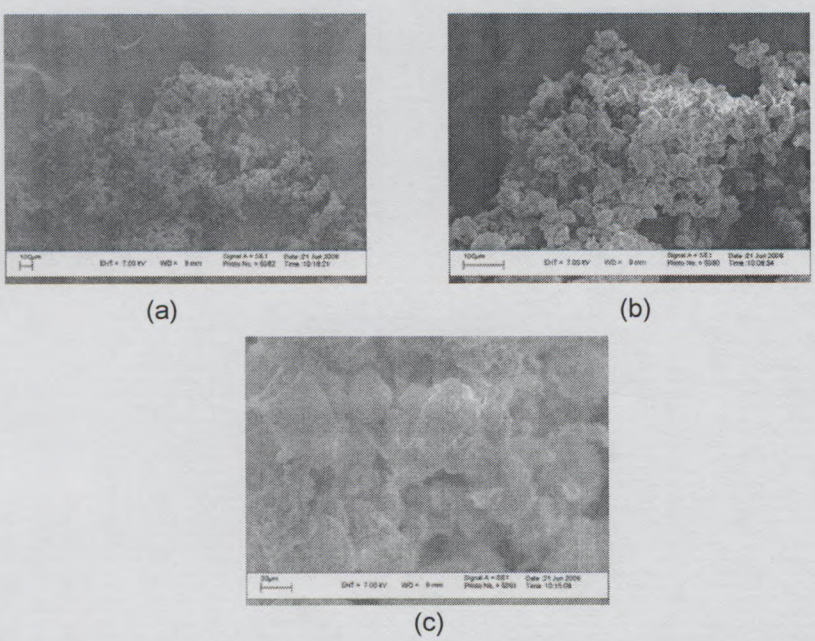

Figure 4.10: SEM micrograph of a freeze-dried ethyl-MMT sample at (a) 100 μm, (b) 100 μm, (c) 20 μm magnifications.

More importantly, the packed (tactoid) structure that was found in oven-dried organoclays was not observed in the freeze dried samples. This makes the dispersion of

organoclays in a liquid phase to make a suspension much easier, without prior preparation. Polymerization reactions for nanocomposite preparations are conducted in solution, emulsions, or in bulk (where the clay is in direct contact with a viscous monomer, without a supplementary medium). The ease of dispersion is important for the latter, since viscosity will only increase on polymerization and will yield a more difficult system to disperse.

4.3.3 Morphological properties

4.3.3.1 Fourier transform infrared spectroscopy

The FTIR absorption spectra (Figure 4.11 to Figure 4.14) show direct influences of the ethyl and hydroxyethyl surfactants on the modified clay. The characteristic absorption bands of the surfmers (Table 4.1) reappeared in the organoclay spectra. The absorption bands of the three organoclays were compared to those of the pristine Na-MMT, and tabulated in Table 4.7.

Several reports in the literature agree on the characteristic absorption band of the clay materials.[2,8,12,18] The most prominent and identifiable are Si-O in-plane vibrations at 1062 and 1054 cm^{-1}, Al-O at 620 cm^{-1} and -OH structure at 3600-3700 cm^{-1}. A water absorption band at around 3400cm^{-1} is always observed if no drying has been done. Newman and Brown[26] indicated that clays always adsorb atmospheric moisture in their steady state, depending on the humidity. This was observed in all the spectra of the samples since no extra caution was taken to protect the samples from the room humidity. However the organoclays showed minimized moisture peaks, with ethyl-MMT showing the least (Figure 4.13). The presence of the hydroxyl based organoclay may be leading to the adsorption of the atmospheric water molecules since its structure can allow for hydrogen bonding of the latter.[10] The FTIR spectra clearly indicate the presence of the surfactant groups in the clay structure.

Table 4.6: Table showing the characteristic absorption band of ethyl and hydroxyethyl surfmers.

Functional group	-CH ($-CH_3$, $-CH_2$)	-CH	C=C	-C-O-C-	>C=O	-OH
Absorption band (cm^{-1})	**2850-2960**	**1410**	**1290-1300**	**1050-300**	**1700**	**3000-3500**
Ethyl surfmer	2922 2852	1404	1291	1195	1722	3431 weak
Hydroxyethyl surfmer	2922 2853	1409	1291	1191	1725	3316 strong

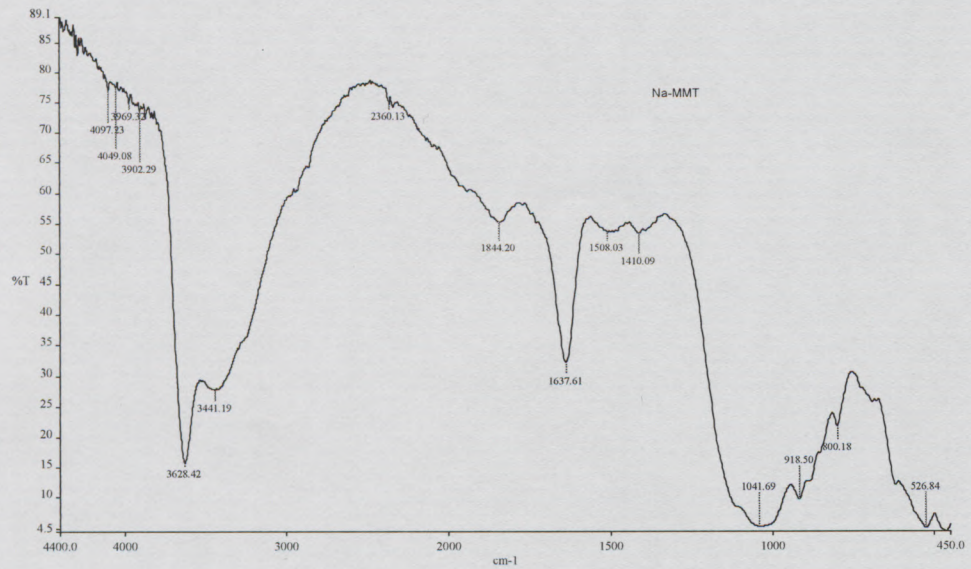

Figure 4.11: FTIR spectrum of a pristine Na-MMT.

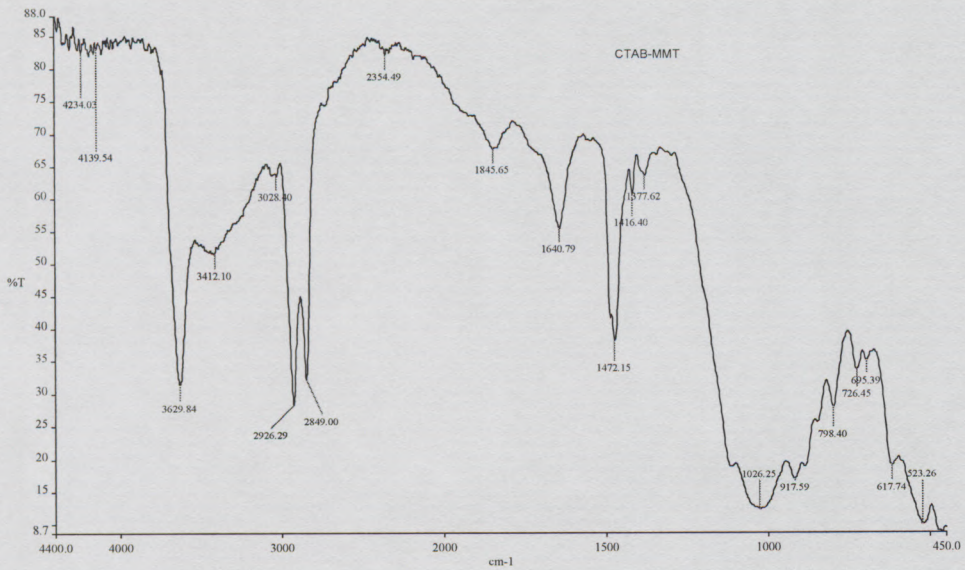

Figure 4.12 : FTIR spectrum of a CTAB-MMT organoclay.

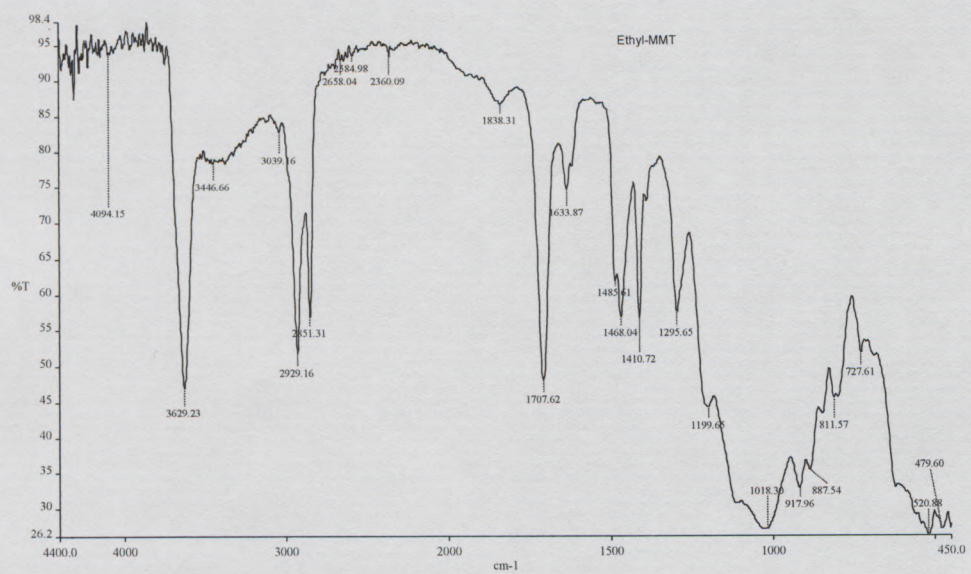

Figure 4.13: FTIR spectrum of an ethyl-MMT organoclay.

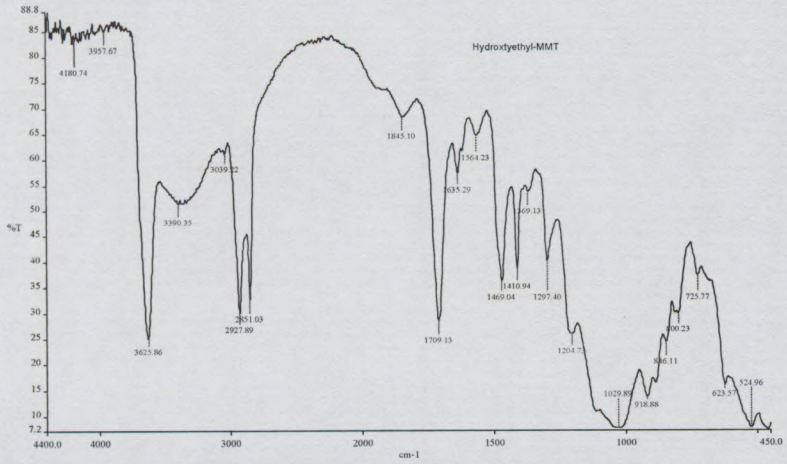

Figure 4.14: FTIR spectrum of a hydroxyethyl-MMT organoclay.

Table 4.7: Characteristic absorption bands of organoclays.

Functional group	Absorption band (cm^{-1})	Na-MMT	Ethyl-MMT	Hydroxyethyl-MMT	CTAB-MMT
Water -OH stretching	**3000-3500**	3429	3446	3390	3412
Structural -OH	**3600-3700**	3627	3629	3626	3629
Water -OH stretching	**1640**	1650	1635	1633	1640
-CH ($-CH_3$, $-CH_2-$)	**2850-2960**	none	2851 2929	2851 2927	2849 2926
-C-O-C-	**1050-300**	None	1199	1204	None
>C=O	**1700**	None	1707	1709	None
- CH_3	**1410**	None	1410	1410	1416
R-CH=CH_2	**1290-1300**	None	1296	1297	None

4.3.3.2 Small angle X-ray scattering

The SAXS results [Figure 4.15 (a)-(d)] showed that the interlayer distances increased, as calculated from the Bragg equation. The information from the SAXS diffractograms is summarized in Table 4.8. The basal spacing or *d*-spacing (d_{001}) for a vacuum dried pristine Na-MMT clay was 1.11 nm. This value compares with the value obtained in the literature, in which 0.99 nm[27] and 1.21 nm[8] were reported for the *d*-spacing of Na-MMT. The *d*-spacing values for the organoclays increased considerably because of the intercalated alkylammonium surfactants. CTAB-MMT had the largest d_{001} value (1.84 nm) compared to the two surfmers. CTAB has a longer alkyl chain length than its acrylate-based chain surfactant counterparts.[27] The d-spacing value of hydroxyethyl-MMT (1.69 nm) was also higher than that of the ethyl-MMT clay (1.55 nm). The presence of hydroxyethyl surfmer leads to larger amounts of atmospheric water to be adsorbed into the galleries from at ambient conditions. This is due to the presence of the –OH groups in the structure of hydroxyethyl surfmer, which could easily be absorption sites for water molecules.

Table 4.8: Interlayer spacing of clay and organoclay samples obtained from SAXS data.

Clay	Intensity	q (nm^{-1})	d_{001} (nm)	Interlayer spacing (nm)
Na-MMT	1.869	5.68	1.11	0.15
Ethyl-MMT	2.367	4.06	1.55	0.59
Ethanol-MMT	2.344	3.72	1.69	0.73
CTAB-MMT	2.907	3.42	1.84	0.88

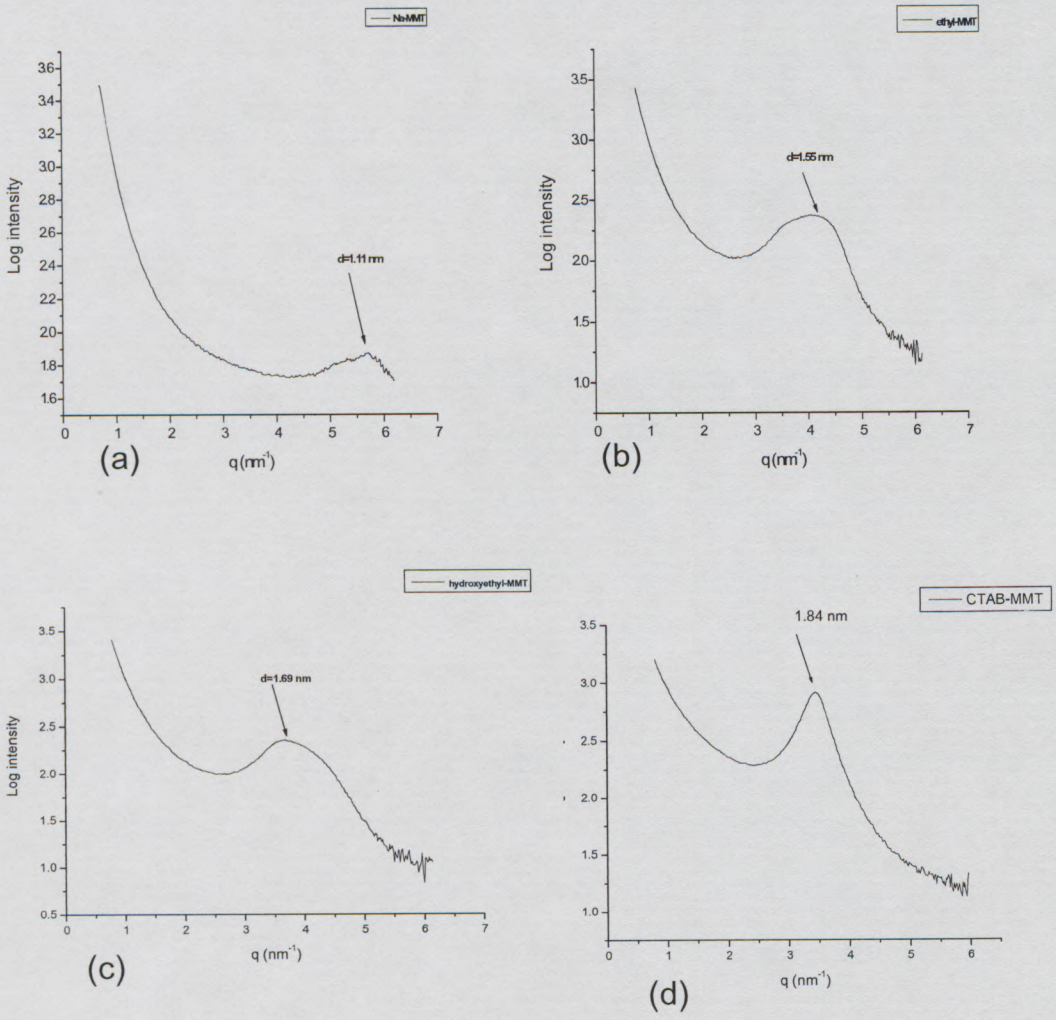

Figure 4.15: SAXS patterns of (a) Na-MMT, (b) ethyl-MMT, (c) hydroxyethyl-MMT and (d) CTAB-MMT.

The differences in the SAXS peak were shown by plotting overlain graphs of all four clay samples (Figure 4.16). The peak broadness for the surfmer organoclays (ethyl and hydroxyethyl) was due to the loss of ordering in the silicate layers, and may also be due to the variation in interlayer distances, as q depends on the basal spacing. The CTAB-

MMT organoclay showed a more acute peak, which depicted the similarity in the averaged basal spacings.

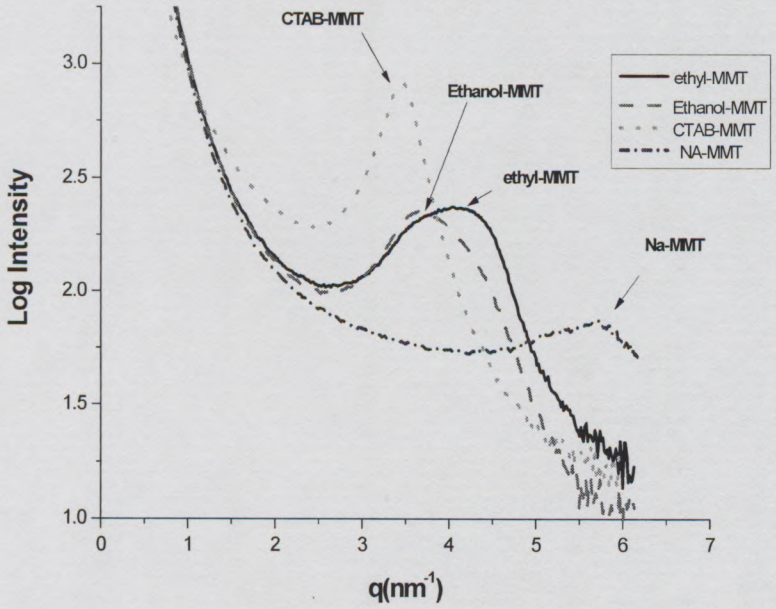

Figure 4.16: Overlain SAXS patterns for the organoclays and a pristine Na-MMT clay.

4.4 Conclusions

Organoclays were successfully synthesized and characterized by SAXS, TGA, and FTIR. Surface properties of the organoclays were also determined using SEM. The overall preparation and characterization was a preparation for the synthesis of polymer-layered silicate nanocomposites (PLSNs). A better understanding of the prepared organoclay characteristics gives a better perspective of the observed structure and the properties of the PLSNs.

The TGA results showed a similar degradation trend for all the organoclays. However, there was a difference in the onsets of degradation for organic components between the organoclays. This meant that the thermal stability of the surfactants also played a role in the degradation trend of the final organoclay. The total weight loss for organic components in the organoclays showed that the surfactants were adsorbed in excess over the cation-exchange capacity (CEC). This was attributed to the intercalation of the surfactant as bilayers in the galleries.

SEM showed that freeze-dried samples were more uniform in particle size and shape. It was also shown that loosely packed particles were about 20 μm, which would be easier to disperse in a monomer for bulk polymerization.

FTIR confirmed the presence of organic molecules in the galleries of layered silicates. It also showed that the presence of alkyl ammonium ions chains reduced the ability of clay to adsorb atmospheric moisture. However, the hydroxyethyl-MMT organoclay provided sites for water adsorption when compared to the other organoclays. This was attributed to the presence of the –OH group in the structure of the hydroxyethyl surfmer.

Through SAXS, the interlayer distances were calculated. The CTAB-MMT organoclay showed the largest interlayer spacing, and also more uniform distribution of the spacings. The surfmer based organoclays showed a wider distribution of the interlayer distances.

4.5 List of References

1. Zhu, L.; Chen, B.; Tao, S.; Chiou, C. T. *Environmental Science and Technology* **2003,** 37, 4001-4006.

2. He, H.; Yang, D.; Yuan, P.; Shen, W.; Frost, R. L. *Journal of Colloid and Interface Science* **2006,** 297, 235-243.

3. Alexandre, M.; Dubois, P. *Materials Science and Engineering: R (Reports)* **2000,** 28, 1-63.

4. Schmidt, D.; Shah, D.; Giannelis, E. P. *Current Opinion in Solid State & Materials Science* **2002,** 6, 205-212.

5. Ray, S. S.; Okamoto, M. *Progress in Polymer Science* **2003,** 28, 1539-1641.

6. Gao, F. *Materials Today* **2004,** 7, 50-55.

7. Zeng, H. Q.; Yu, A. B.; LU(Max), G. Q.; Paul, D. R. *Nanoscience and Nanotechnology* **2005,** 5, 1574-1592.

8. Wang, H.-W.; Chang, K.-C.; Yeh, J.-M.; Liou, S.-J. *Journal of Applied Polymer Science* **2004,** 91, 1368-1373.

9. Luckham, P. F.; Rossi, S. *Advances in Colloid and Interface Science* **1999,** 82, 43-92.

10. Raussell-Colom, J. A.; Serratosa, J. M., Reactions of Clays with Organic Substances. In *Chemistry of Clays and Clay Minerals*, 1st ed.; Newman, A. C. D., (Eds). Wiley-Interscience: New York, **1987**; pp 371-422.

11. Xie, W.; Gao, Z.; Liu, K.; Pan, W.-P.; Vaia, R.; Hunter, D.; Singh, A. *Thermochimica Acta* **2001,** 367-368, 339-350.

12. Xie, W.; Xie, R.; Pan, W.-P.; Hunter, D.; Koene, B.; Tan, L.-S.; Vaia, R. *Chemistry of Materials* **2002,** 14, 4837 - 4845.

13. Joynes, D.; Sherrington, D. C. *Polymer* **1997,** 38, 1427-1438.

14. Shang, C.; Rice, J. A.; Lin, J. S. *Soil Science Society of America Journal* **2002,** 66, 1325-1230.

15. Samakande, A.; Hartmann, P. C.; Sanderson, R. D. *Journal of Colloid and Interface Science* **2005,** 269, 316-323.

16. Mermut, A. R.; Lagaly, G. *Clays and Clay Minerals* **2001,** 49, 393-397.

17. Hartmann, P. C.; Dieudonné, P.; Sanderson, R. D. *Journal of Colloid and Interface Science* **2005,** 284, 289-297.

18. Dharaiya, D.; Jana, S. C. *Polymer* **2005,** 46, 10139-10147.

19. Xie, W.; Gao, Z.; Pan, W.-P.; Hunter, D.; Singh, A.; Vaia, R. *Chemistry of Materials* **2001,** 13, 2979-2990.

20. Osman, M. A.; Ploetze, M.; Suter, U. W. *Journal of Materials Chemistry* **2003,** 13, 2359-2366.

21. Chigwada, G.; Jiang, D. D.; Wilkie, C. A. *Thermochimica Acta* **2005,** 436, 113-121.

22. Davis, R. D.; Gilman, J. W.; Sutto, T. E.; Callahan, J. H.; Trulove, P. E.; De Long, H. C. *Clay and Clay Minerals* **2004,** 52, 171-179.

23. Madejova, J. *Vibrational Spectroscopy* **2003,** 31, 1-10.

24. Shah, R. K.; Paul, D. R. *Polymer* **2006,** 47, 4075-4084.

25. Samakande, A. Synthesis and Characterization of Surfmers for the Synthesis of Polystyrene-Clay Nanocomposites. MSc Thesis, University of Stellenbosch, Stellenbosch, **2005**.

26. Newman, A. C. D.; Brown, G., The Chemical Constitution of Clays. In *Chemistry of Clays and Clay Minerals*, 1st ed.; Newman, A. C. D., (Eds). Wiley-Interscience: New York, 1987; pp 1-116.

27. Fu, X. A.; Qutubuddin, S. *Journal of Colloid and Interface Science* **2005,** 283, 373-379.

Chapter 5

Preparation and characterization of polystyrene-layered clay nanocomposites

Abstract

Polystyrene-layered silicate nanocomposites (PS-LSN) were synthesized and characterized. The PS-LSNs were prepared using the in-situ intercalative polymerization method in bulk. The structure of the obtained was characterized with small-angle X-ray scattering (SAXS) and transmission electron microscopy (TEM). The techniques were used complementarily to deduce the nanocomposite morphologies, and to determine the extent of clay dispersion. EthylMMT-PS nanocomposites were mostly exfoliated, hydroxyethylMMT-PS nanocomposites were a combination of exfoliated and intercalated morphologies (exfoliated-intercalated) and CTABMMT-PS nanocomposites were intercalated. Increasing clay loading in the nanocomposites leads the presence of agglomerated organoclay particles. Fourier transform infrared spectroscopy (FTIR) was used to determine the changes in the vibrational spectroscopic bands as a result of the dispersion of organoclay in the polymer matrix. The formation of new bands, and the disappearance of peaks observed in the organoclay spectra, was due to new interactions as a result of the presence of the layered silicates.

5.1 Introduction

Polymer layered-silicate nanocomposites (PLSNs) based on different polymers have been studied, since improvements in nylon-6 were reported a few years ago by the Toyota research group.[1] Polymers that have been researched range from thermoplastics to thermosets including nylon, poly(methyl methacrylate) (PMMA), epoxies, polyacrylonitrile (PAN) and polystyrene (PS), to mention but a few.[2-5] Different methods that can be used to synthesize PLSNs are discussed in detail in Chapter 2, Section 2.4.

In the current study PS based nanocomposites (PS-LSNs) were synthesized and characterized. The PS-LSNs were prepared by the in-situ intercalative polymerization (bulk polymerization). Preparation and characterization of organoclays used for the preparation of the PS-LSNs is discussed in Chapter 4. In-situ intercalative polymerization (illustrated in Figure 5.1) is the method commonly used when the intercalation is done at the same time as the polymerization. The monomer is intercalated into the galleries, followed by polymerization, in a single preparative procedure. The final product can have three possible morphologies. The formation of each of which is influenced by the interfacial interactions between the monomer/polymer and the layered silicate surfaces. This first one, exfoliated morphology, is a highly sought after morphology, with layers delaminated to form a random distribution, thereby maximizing the interfacial interaction between the silicate layers and the polymer matrix.[6] The second one is the intercalated morphology, where the polymer chains have penetrated the galleries. The polymer penetration leads to larger intergallery spacing but the layers do not lose their organization of the layered lattice. The last one is obtained when the layers are agglomerated in the matrix, similarly to the classical microcomposites and, is known as the phase separated morphology.

It is hypothesized that the presence of polymerizable modifiers in the galleries promotes exfoliation, even though their mere presence does not guarantee exfoliation.[7] The polymerizable groups in the modifier (surfmers in the case of the current study) take part in

the polymerization reaction to form copolymers with the main polymer, and the chain growth in the galleries exerts pressure on the adjacent layers.[8] This would then lead to delamination of the layers, thereby promoting exfoliated morphology. However, this has been proved otherwise for solution polymerized PLSNs.[7]

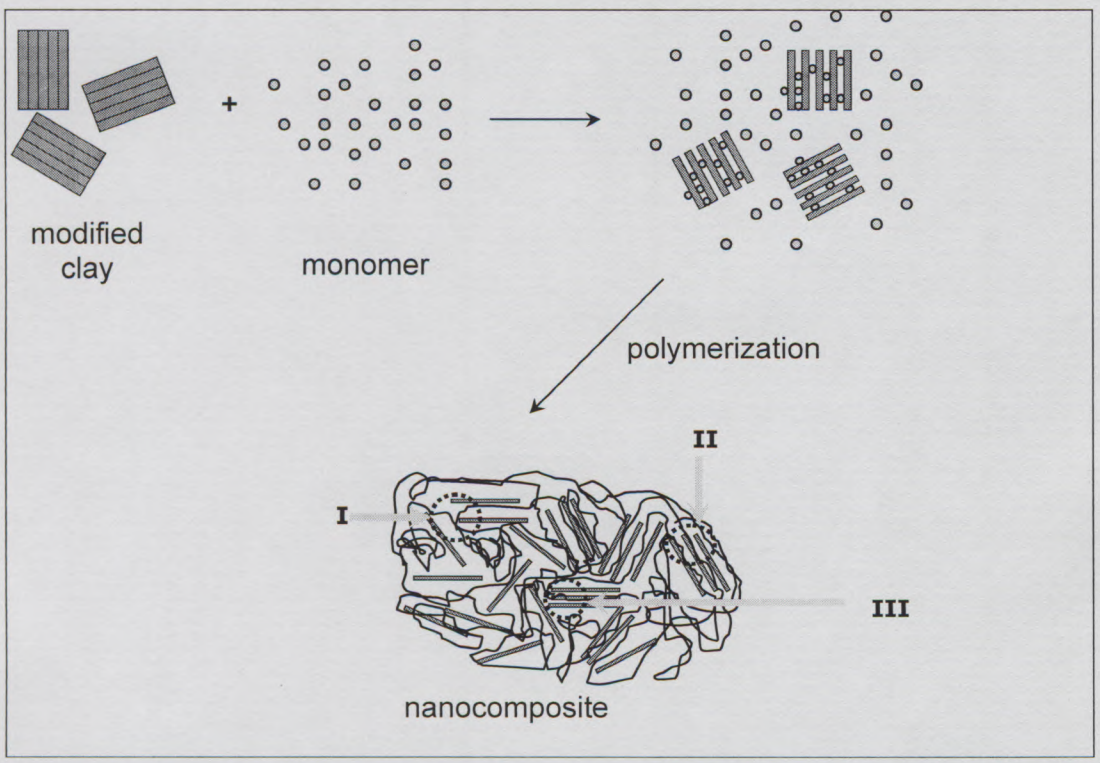

Figure 5.1: Illustration of in-situ intercalative polymerization producing a nanocomposite with three morphologies; (I) exfoliated, (II) intercalated and (III) agglomerated (phase separated).

The main focus of this chapter is the synthesis and characterization of PS-LSN. The preparation of the organically modified clays (organoclays) used was reported in Chapter 4. The structures and properties of the prepared PS-LSNs were characterized by small-angle X-ray scattering (SAXS) analysis, transmission electron microscopy (TEM), gel permeation chromatography (GPC) and Fourier transform infrared spectroscopy (FITR).

5.2 Experimental

5.2.1 Materials

The following materials were used for the synthesis of PS homopolymer and PS-LSNs. A styrene monomer was prepared for polymerization by first removing the inhibitor. This was done by washing the monomer three times with a 30% KOH solution. The monomer was then purified by distilling under reduced pressure at 30 °C. A *2,2*-azobis (isobutyronitrile) (AIBN) initiator was purified by recrystallization in hot methanol. Organoclays were prepared by a method described in Chapter 4, via the ion-exchange of sodium montmorillonite with the surfactants: cetyl trimethyl ammonium bromide (CTAB), 11-acryloyloxy undecyl dimethyl ethyl ammonium bromide (ethyl surfmer) and 11-acryloyloxy undecyl dimethyl hydroxyethyl ammonium bromide (hydroxyethyl surfmer), to yield CTABMMT, ethylMMT and hydroxyethylMMT, respectively.

5.2.2 Synthesis and characterization

The synthesis of PS and PS-LSNs was conducted in bulk by the following procedure: ethyl-MMT (0.050 g) and AIBN initiator (0.025 g) were added to a Schlenk tube containing 4.940g (0.046 mol) of freshly distilled styrene monomer. The Schlenk tube was immersed in liquid nitrogen and the contents frozen. Vacuum suction was then applied to the frozen mixture for 5 minutes to remove any oxygen from the Schlenk tube. The frozen mixture was allowed to return to ambient temperature. The process was repeated twice (freeze and thaw). Thereafter, the mixture was stirred and sonicated for 4 hours, after which the Schlenk tube was placed in an oil bath in which polymerization was carried out at 60 °C for 72 hours. The solid bulk polymer was dissolved in chloroform to form a suspension, followed by precipitation in excess methanol. After filtration and vacuum drying at ambient temperature, and a white powdered 1 wt% ethylMMT-polystyrene (1% ethylMMT-PS) nanocomposite was obtained. The amount of organoclay was varied to yield increasing clay loadings of 1 wt%, 3 wt% and 5 wt% in separate experiments. Lower clay loading amounts (less than 5 wt%) are sufficient to induce significant changes in the properties of the PS-

LSNs.[9,10] A 10 wt% loading in the ethylMMT was synthesized to determine the amount at which the organoclay would start to show phase separated morphology, and as a relatively higher loading reference.

A similar synthesis procedure was carried out for hydroxyethylMMT and CTABMMT based nanocomposites. 1 wt%, 3 wt% and 5 wt% hydroxyethylMMT-PS and 1 wt%, 3 wt% and 7 wt% CTABMMT-PS nanocomposites were produced. The synthesis of PS homopolymer was carried out using a similar procedure but no clay was added and no sonication was done.

SAXS and TEM were used to characterize the morphology, and to evaluate the extent of dispersion of the clays in the matrix. FTIR was used to determine the functional groups and the bonding properties between the organoclay and the polymer matrix. GPC was used to determine the molecular weight and molecular weight distribution of the polymer. In preparation for GPC, a Soxhlet extraction was done to obtain unattached (clay-free) polymer chains.[7] Details on the techniques and applications in the characterization of PLSNs were discussed in Chapter 3. The characterization of the structure contributes vitally to the current study as the materials' morphology is correlated to findings of the physical measurements (Chapter 6).

5.3 Results and discussion

5.3.1 Small-angle X-ray scattering

Wide-angle X-ray diffraction (WAXD) is a commonly used technique for the determination of the morphology of PLSNs.[11-15] In 2005, Causin et al.[16] proposed a method for the use of small-angle X-ray scattering (SAXS) as a tool for the quantitative assessment of the morphology of PLSNs. In their study, they pointed out the shortcomings and inconsistencies in the use of WAXD for the characterization of the PLSN structure. In the current study, SAXS in conjunction with TEM was used to characterize the morphology of

PS-LSNs. SAXS determination for the PS-LSNs was still at angles that still overlapped with WAXD lower threshold. SAXS is a better tool to study the exfoliated morphology, as the absence of diffraction peaks in WAXD does not always indicate exfoliation of the silicate layers.[16] Intercalated morphology with larger interlayer spacing can be determined by SAXS (diffraction peak), without assuming exfoliation. The SAXS data is combined (correlated) with TEM studies, as no conclusive determination of the structure could be done by X-ray diffraction (XRD) only.[2,17]

The SAXS analysis results were treated with great care, since they are crucial to the determination of the exact structure of the nanocomposites. In a study by Samakande[18], ethylMMT-PS nanocomposites samples mostly gave exfoliated nanocomposites, and no diffraction peak was observed up to 18 wt% clay loading. However, the data obtained in this present study was not consistent with that finding. This could be attributed to minor differences in preparative methods. The diffractograms of 1 wt% and 3 wt% clay loadings showed the absence of the diffraction peaks (Figure 5.2). This means that there are no patterned silicate layers in the polymer matrix. A study by Morgan and Gilman[17] suggested the fact that the absence of peaks is not always equivalent to exfoliated morphology. Other factors that can be influential to the absence of diffraction peaks include undetectable levels (for low clay loading) and disorder (also present in immiscible and intercalated systems). The morphology of the nanocomposites was later confirmed by TEM studies.

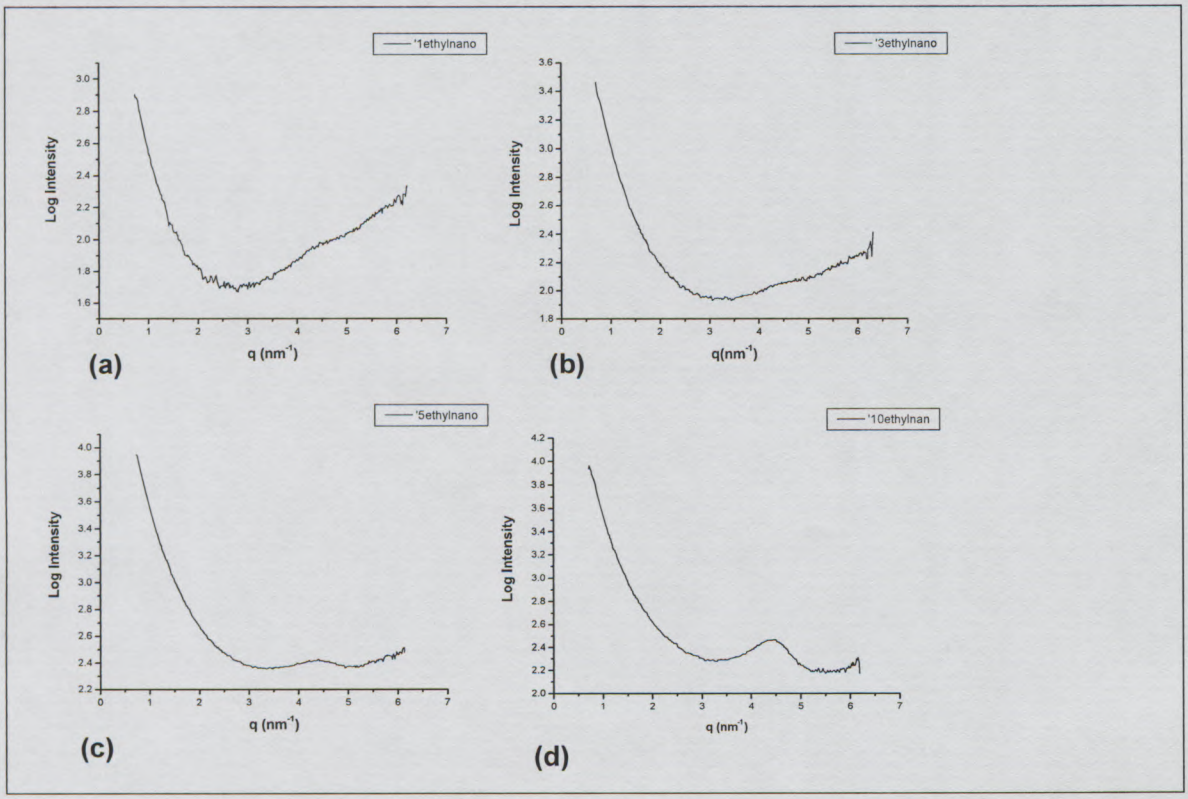

Figure 5.2: Diffractograms of ethylMMT-PS nanocomposites with log intensity vs wave vector *q*: (a) 1% ethylMMT, (b) 3% ethyl MMT, (c) 5% ethylMMT and (d) 10% ethylMMT.

The diffraction patterns of 5 wt% and 10 wt% clay loadings showed diffraction peaks with the latter showing a prominent peak with a maximum at $q = 4.42$ nm^{-1} ($d = 1.42$ nm)[#]. The 5 wt% sample had a diffraction pattern that showed a rather minute "bump", also at around the same q-value as the 10 wt% sample. The modified clay (ethylMMT) used to prepare the nanocomposite had shown the same diffraction peak $q = 4.06$ nm^{-1} ($d = 1.55$ nm), as shown in Figure 5.3. This implied that, with varying extent, the two nanocomposites had some immiscible organoclay tactoids. TEM later confirmed this conclusion. Even though the lower clay loading nanocomposites were intended for the purposes of this study, 10 wt% was included in the ethylMMT-PS range to clearly observe the appearance of the diffraction peak, as it was not the case with 5 wt%. It was not expected that the 5 wt% nanocomposite would show a peak, but going to higher clay loading would show signs of

[#] *d*-spacing obtained from the formula: $q = 2\pi/d$ (See Chapter 3, Section 3.2.1.3)

immiscibility. The presence of phase-separated morphology at 10 w% loading for PS-LSNs was consistent with the findings in the literature.[19]

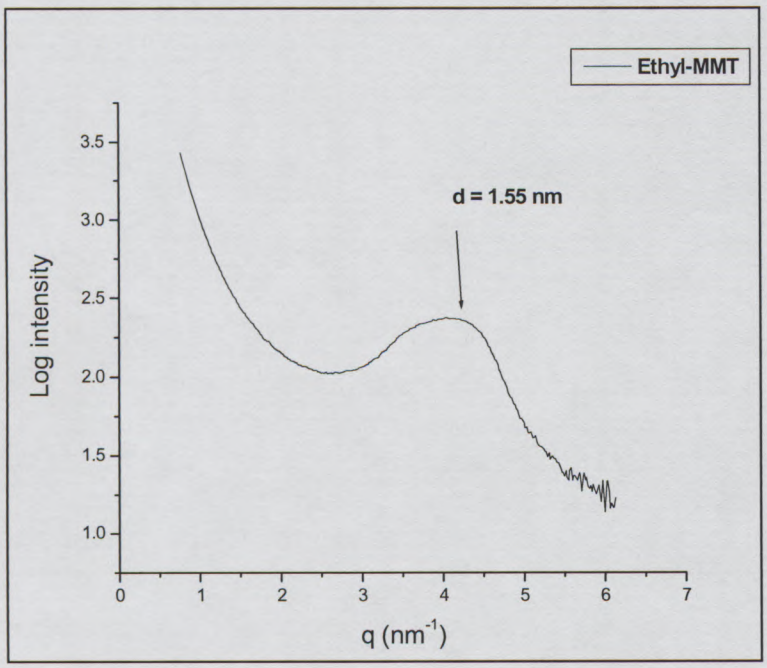

Figure 5.3: A SAXS diffraction pattern of an ethylMMT organoclay.

The hydroxyethylMMT based nanocomposites have also been studied and were said to have a mixed intercalated/exfoliated morphology.[18] A minute "bump" was observed for 1 wt% clay loading and a small but prominent peak was observed for 5 wt% loading (Figure 5.4). The minute peak for the 1 wt% clay loading was at lower q values (3.49 nm^{-1}) than its higher loading counterpart, which had a surprisingly higher value (4.23 nm^{-1}), even higher than the parent organoclay (3.72 nm^{-1}). This means that the diffraction peak for the 5% hydroxyethylMMT-PS nanocomposite has some tactoids with layers closer to each other; even less than the intercalation of the parent organoclay (d = 1.69 nm) (see Chapter 4, Section 4.3.32). The decrease in the interlayer spacing was attributed to thermal desorption of the organic modifier, where it can diffuse out of the layers due to high temperature effects.[20] It was also observed that even thought the peak maximum was at the said q value, some area under the peak overlapped with the q value of the organoclay peak maximum.

This suggests that there was a wider distribution of the *d*-spacing as the broadness of the hydroxyethyl diffraction peak depicted (Chapter 4, Figure 4.15-b).

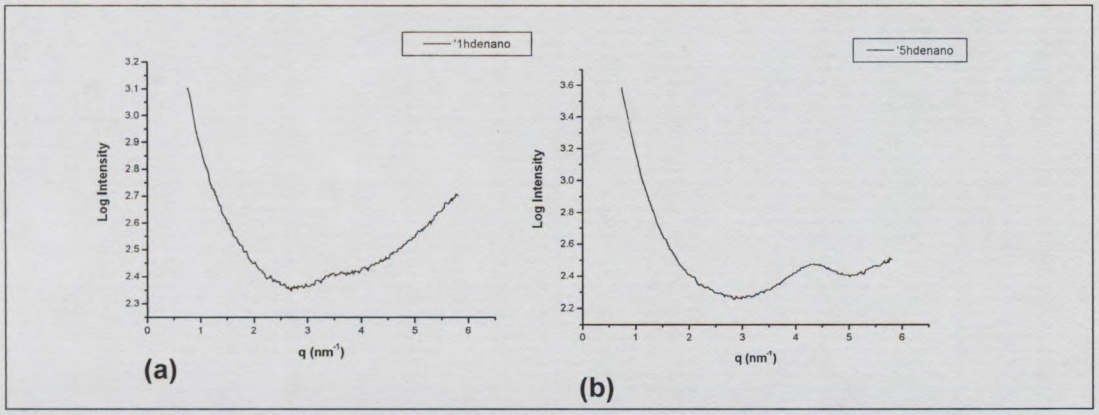

Figure 5.4: Diffractograms of hydroxyethylMMT-PS nanocomposites, log intensity vs *q*: (a) 1% hydroxyethylMMT and (b) 5% hydroxyethylMMT.

A rather surprising finding was exhibited by the CTABMMT-PS nanocomposites. CTAB is a non-polymerizable quaternary ammonium ion, and a different trend from that shown by the previous two modifiers was expected. The 1 wt% showed a very minute peak (Figure 5.4-a) in the same region as the parent organoclay (Chapter 4, Figure 4.15-c), CTABMMT. The 3 wt% clay loading nanocomposite showed a pronounced and acute diffraction peak (Figure 5.4-b). This was attributed to the ordered silicate layers in the nanocomposite. The diffraction pattern (peak) was very different from that of the parent clay (q = 3.49 nm^{-1} compared to q = 3.42 nm^{-1}, respectively). This feature depicted that the interlayer spacing widened due to the intercalation of polymer chains. A diffraction peak for the 7 wt% loading sample (Figure 5.4-c) was rather small (low intensity) compared to its nanocomposite counterparts but it was also at the same region as the parent clay. At this loading (higher than 5 wt%), a more pronounced diffraction peak was anticipated. The rather small peak was attributed to disorder, as there were more polymer chains intercalating the galleries.

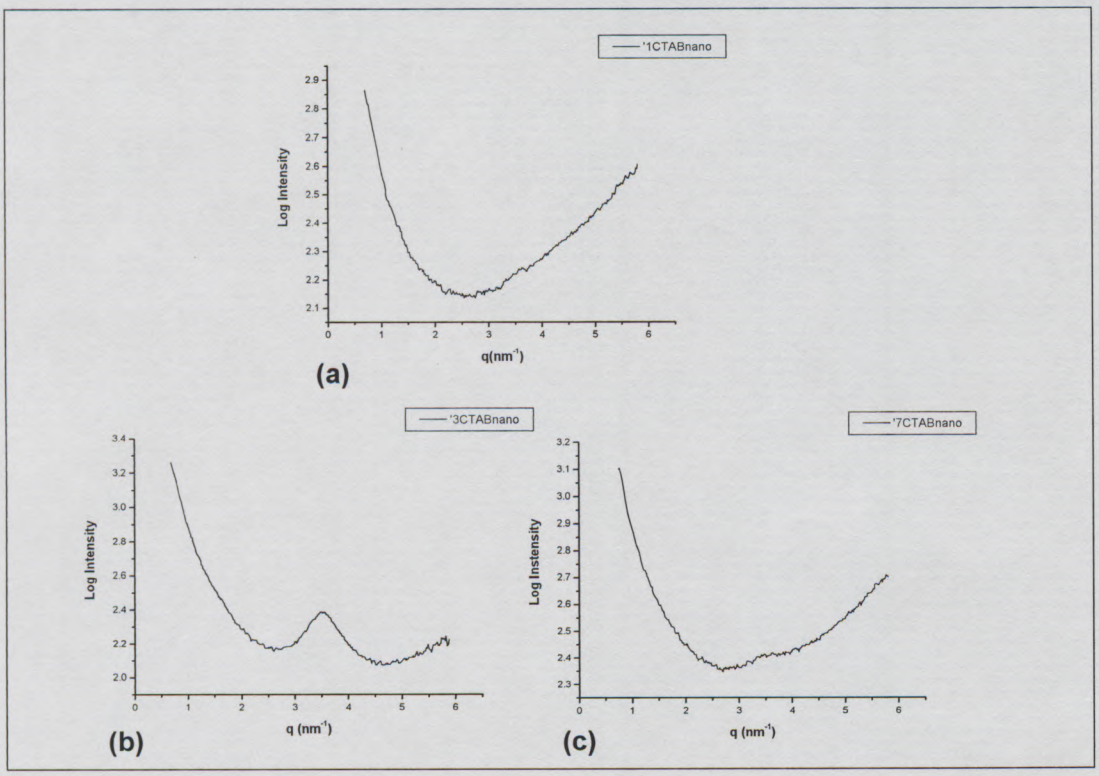

Figure 5.5: Diffractograms of CTABMMT-PS nanocomposites with log intensity vs *q*: (a) 1% CTABMMT, (b) 3% CTABMMT and (c) 7% CTABMMT.

5.3.2 Transmission electron microscopy

5.3.2.1 Exfoliated and exfoliated-intercalated nanocomposites

TEM analysis gave a visual perspective to the SAXS data enabling a more accurate determination of the type of morphology each nanocomposite exhibited. The dark lines in the micrographs showed the silicate layers and the polymeric parts were the lighter regions, which could also be the resin in which the samples were embedded. The use of this analytical technique is considered to be crucial in following the relationship between the structure and the physical properties.[21]

TEM images of the 1% ethylMMT-PS and 3% ethylMMT-PS nanocomposites showed total exfoliation in their morphologies (Figure 5.6 a,b). Figure 5.6 also shows that the

matrix of the 3% ethylMMT-PS sample has uniform distribution of the silicates in the matrix. Most of the clay portions in the matrix show layers following the same direction of alignment, although there were some bent and disordered patches. These materials would fall into the exfoliated category of *ordered-exfoliated* according to the literature.[17] The 5% ethylMMT-PS nanocomposite (Figure 5.7) exhibited similar properties to that of 3 wt% loading but with an additional feature. The micrographs of the 5 wt% sample showed some dark patches in the matrix, which meant that there were some immiscible organoclay layers. These appeared as a few noticeable spots in the matrix. This information is consistent with what was depicted by SAXS analysis, namely a very minute bump in the same region as the ethylMMT organoclay. It was therefore concluded that 5% ethylMMT-PS was mostly exfoliated.

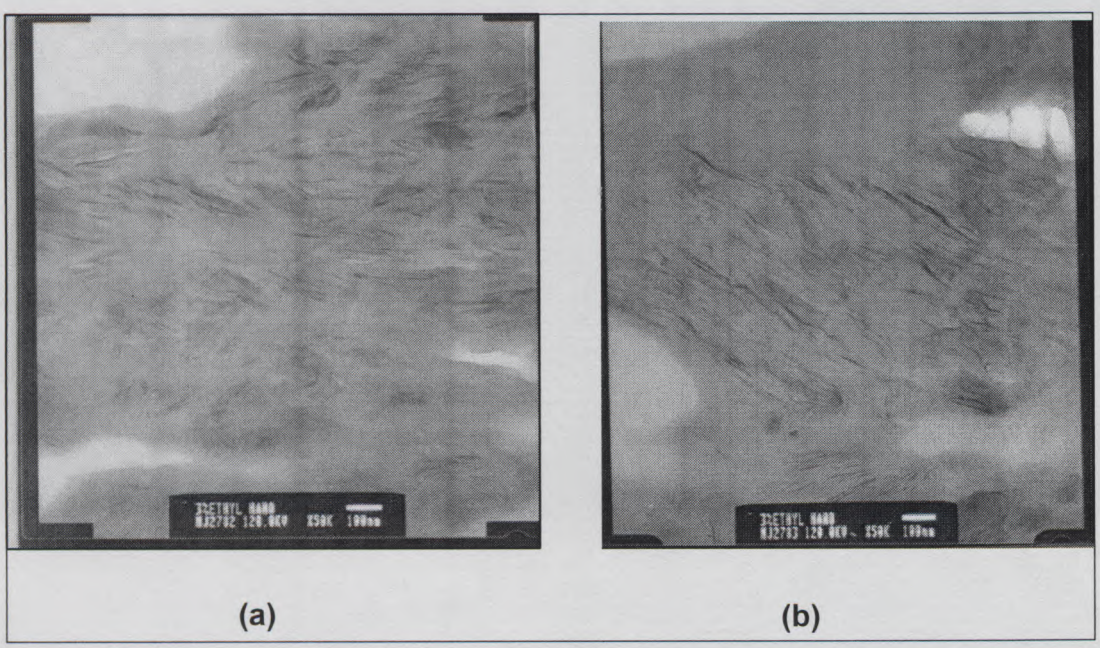

Figure 5.6: TEM images of 3% ethylMMT-PS nanocomposite, (a) and (b) portions with the same magnification (100 nm scale).

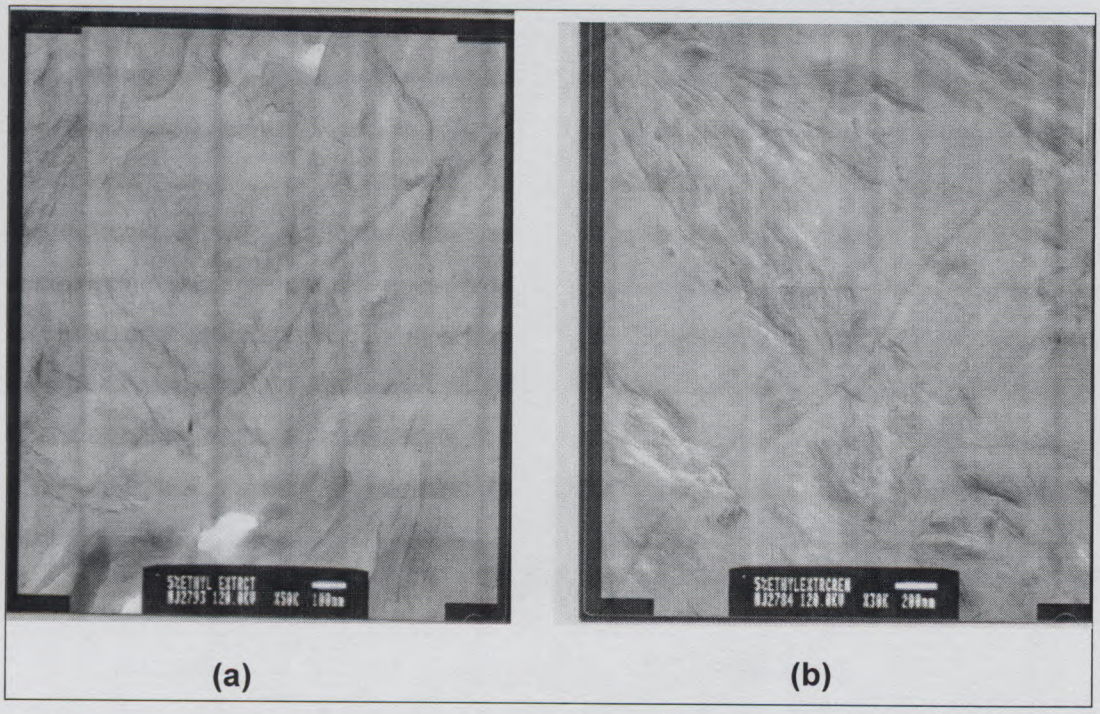

Figure 5.7: TEM images of 5% ethylMMT-PS nanocomposite, showing portions with different magnifications, (a) 100 nm scale and (b) 200 nm.

Large sections of dark parts were observed in the micrographs of the 10% ethylMMT-PS nanocomposite samples, as seen in Figure 5.8. This means that a large amount of the organoclay could not be intercalated by the polymer and hence there is no delamination of the polymers. However, the other fraction of the organoclays was exfoliated and dispersed in the polymer matrix (Figure 5.8). This means that the experienced immiscibility was not due to the incompatibility between the polystyrene and the organoclay, but rather influenced by the spatial factor. For example, the presence of large amount of clay may lead to poor mixing during polymerization, or the mixing may be influenced by high viscosity effects. The nanocomposite structure was consistent with the SAXS data which showed a diffraction peak as a result of the immiscible fraction of the organoclay. This was also a deviation from the findings of Samakande, where exfoliation was observed up to very high clay loading (18 wt%).[18]

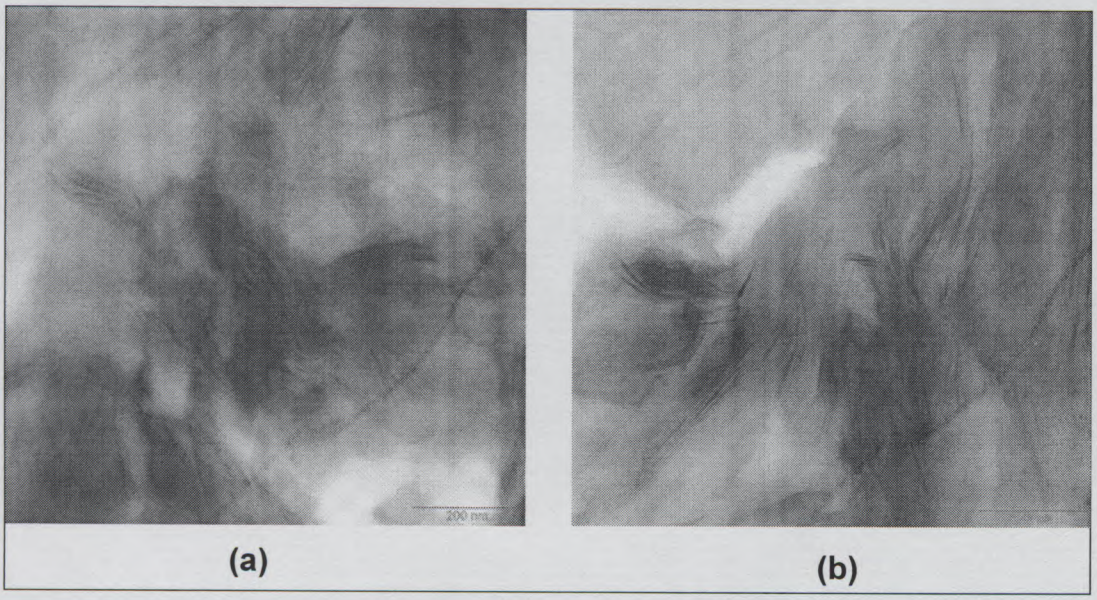

Figure 5.8: TEM images of 10% ethylMMT-PS nanocomposite, (a) and (b) showing portions with the same magnification (200nm scale).

TEM analysis (Figures 5.9 and 5.10) of the hydroxyethylMMT-based nanocomposites showed an agreement with the SAXS data. The morphology observed for the nanocomposites was an intermediate of intercalated and exfoliated (*exfoliated-intercalated*). In some cases, immiscible organoclay fractions were visible in the micrographs, especially for the 5 wt% sample (Figure 5.10). The 1 wt% sample showed uniform distribution of the clay layers in the matrix. The minute peak for the diffraction peaks of this nanocomposite was due to the intercalated and the immiscible organoclay.

Even though the surfmer organic modifiers were identical with a difference in one functional group, the nanocomposite structures obtained were not the same. The ethylMMT-based samples were better exfoliated and immiscible fraction of the organoclay was observed at 10 wt%, when compared to 5 wt% of the hydroxyethylMMT-PS nanocomposite. This means that the ethylMMT organoclay provided optimal conditions for the silicate layers to be exfoliated.

It is therefore speculated that the presence of the hydroxyl (-OH) group in the hydroxyethylMMT clay may have led to the formation of hydrogen bonds with the oxygen (-O) and (-OH) in the silicate structures. That would, then, lead to more attractive forces between the adjacent layers and would be relatively more difficult to push apart by the monomer/polymer.

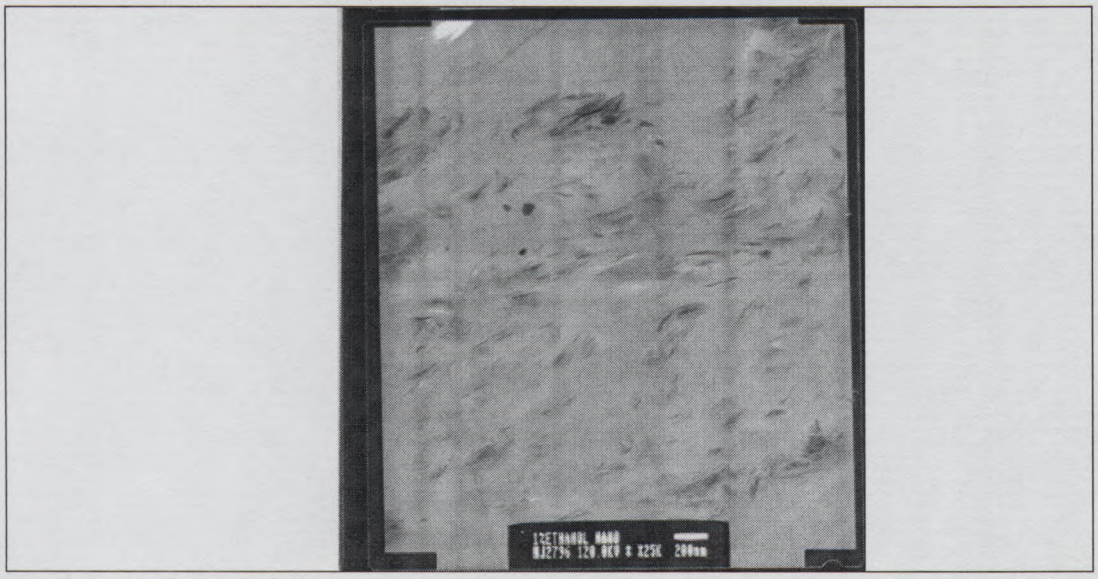

Figure 5.9: A TEM image of 1% hydroxyethylMMT-PS nanocomposite magnified at 200nm scale.

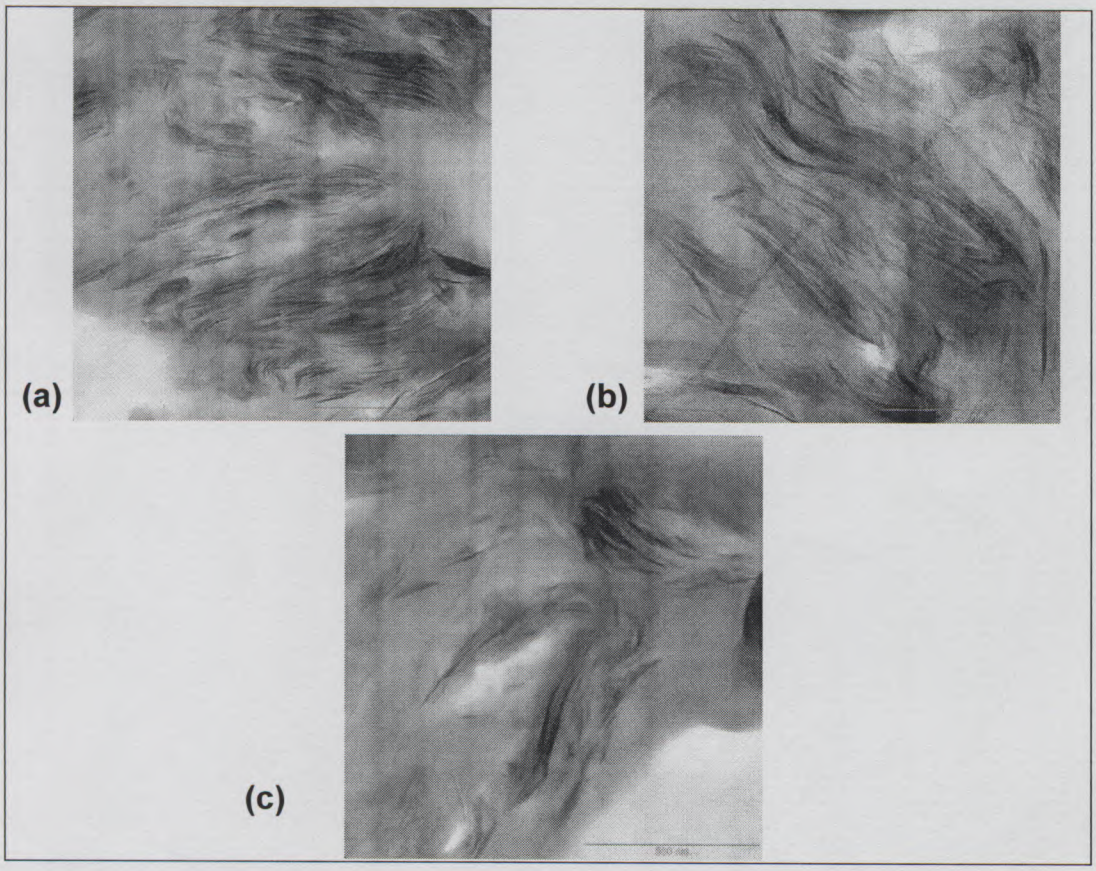

Figure 5.10: TEM images of 5% hydroxyethylMMT-PS nanocomposite, (a) and (c) showing portions with the same magnification (500nm scale) and (b) showing 200 nm.

5.3.2.2 Intercalated nanocomposites

From the TEM analysis, it was observed that the nanocomposites were intercalated and the distribution of the silicate layers was not constant throughout the matrix for the sectioned parts. Parts with only the polymer matrix were notable. However, even the nanocomposites that did not show peaks (1 wt% and 3 wt% CTABMMT) in SAXS analysis were intercalated. In the literature[17], the absence of peaks is attributed to the loss of ordering in the silicate layers, low amounts of clay and inefficiency of used method. Even though there is a definite intercalation of the polymer with layers lining parallel to each other, they are bent and in some instances, look twisted (Figure 5.11-b). The loss of ordering is the most likely factor that could have contributed to the reduced (in size) diffraction peak in the SAXS analysis. This is due to the fact the peak was not observed in 1 wt% and 7 wt%, and could have not been due to the undetectable amounts. Also, the instrument factor was

eliminated because of the quality of results in other measured samples, suggesting that the method was well optimized.

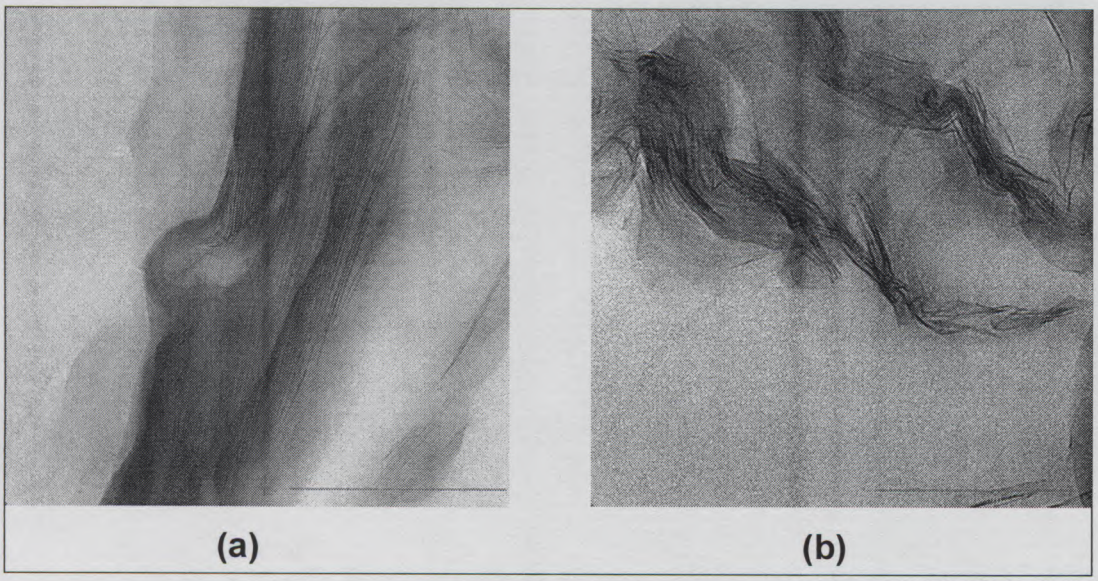

Figure 5.11: TEM images of 3% CTABMMT-PS nanocomposite, (a) and (b) showing portions with the same magnification (200nm scale).

5.3.3 Molecular weight determination

Gel permeation chromatography (GPC) provides information about the molecular weight (M_w), molecular number (M_n) and the molecular weight distribution (M_w/M_n), expressed as polydispersity index (PDI). GPC is technique in which polymer molecules are separated according to the hydrodynamic volumes (sizes). A porous gel is used as a stationary phase, where the smaller molecules get temporarily inserted in the pores. The larger molecules are eluted at shorter times since they have relatively less access to the pores. The lower molecular weight molecules spend more time in the column and are eluted last.

The preparation for molecular weight measurements by GPC was unsuccessful on the prepared nanocomposite samples. The Soxhlet extraction was made ineffective by the blockage of the thimble pore and thereby leading to overflow of the dissolved polymer. The dissolved polymer inside the thimble also constituted the silicate layers which were being filtered by the thimble. This led to the presence of the clay particles in the extracted polymer. This was confirmed by TEM measurement on the extracted polymer as shown in Figure 5.12 (well exfoliated nanocomposite, although was undesirable for the purpose). The extracted polymer was, therefore, not suitable for GPC analysis. However, a study the similar nanocomposites samples was done by a colleague and he successfully determined molecular weight properties by GPC.[18]

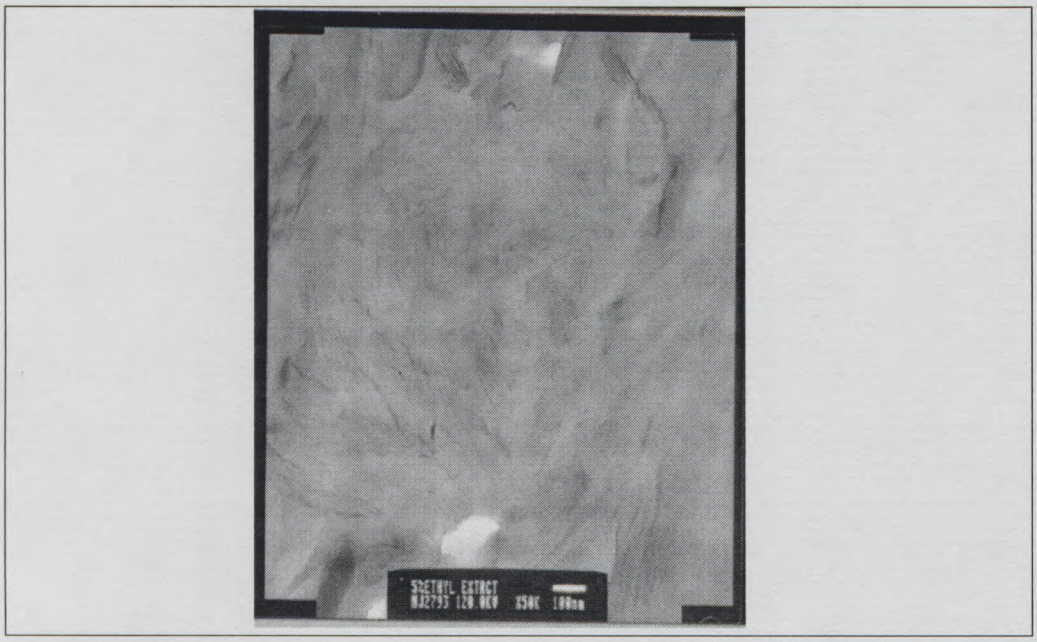

Figure 5.12: TEM images a polymer extracted 5% ethylMMT-PS nanocomposite showing traces of clay (100 nm scale).

The molecular weights of the polymers were generally high as expected of bulk polymerized materials, as shown in Table 5.1. Such properties that can be attributed to the characteristic nature of bulk polymerization include; (1) High viscosity, which affects the diffusion of the radical-activated monomer and propagating chains. Limited diffusion in high viscosity environment leads to the addition of the more agile radical-activated monomer to the less mobile propagating chain. This leads to chain growth and less termination, which is due to minimal head-to-head encounter of the propagating chains.
(2) Low temperature (i.e. 60 ^{o}C) of polymerization leads to fewer radicals in the reaction system and therefore, less radical-radical encounter for termination.

The PS homopolymer showed a lower molecular weight relative to the nanocomposites. This finding was attributed to two factors viz: (a) The pre-conditioning of the monomer-clay mixture by sonication increased the effects of viscosity discussed above (1). (b) The second factor is the nature of the layered clays, where an intercalated radical will create a chain-propagation inside the clay gallery. This means there will be less chance of a head-to-head termination, and chain growth will progress, as long as agile radical are still available.

Wang et al.[7] also reported an increase in the molecular weight for PS-LSNs synthesized in bulk. However, this is strongly opposed by Fu and Qutubuddin[22] whose study showed lower average molecular weights for bulk polymerized nanocomposites. Fu and Qutubuddin based their explanation on the difficulty of the initiator to diffuse into propagating chains due to the high viscosity, and also propagation restrictions. Our work disagrees with Fu and Qutubuddin's views based on the findings and explanation provided in above paragraph. The molecular weight of the polymer attached to the silicate layers or intercalated samples could not be extracted, therefore, it was unclear how much polymerization took place inside the galleries, or how much contribution was possible from the polymerizable groups on the organic modifiers.

Table 5.1: Variation of molecular masses and polydispersity index (PDI) with clay loading of the polystyrene-clay nanocomposites.[18]

Sample	**Clay content (%)**	**M_n x 10^3 (g/mol)**	**M_W x 10^3 (g/mol)**	**PDI (M_W/M_n)**
Polystyrene	-	170	510	3.1
Polystyrene-(Ethanol-MMT) Nanocomposite	1.5	230	740	3.2
	5.3	240	690	2.8
	7.1	200	860	4.2
	18.5	170	440	2.6
	21.3	400	1 190	3.0
Polystyrene-(Ethyl-MMT) Nanocomposite	2.1	190	690	3.7
	3.7	190	580	3.1
	5.7	210	630	2.9
	7.7	140	840	5.9
	18.5	240	1 120	4.7
Polystyrene-(CTAB-MMT) Nanocomposite	0.8	120	480	4.0
	1.2	80	540	6.8
	3.5	80	540	6.8
	6.0	80	540	6.4

5.3.4 FTIR Analysis

Fourier transform infrared (FTIR) determines the absorption and emission of the electromagnetic radiation by molecules in the infrared region. The molecules give different vibrational energies at specific infrared frequencies, and those characteristic can be vital tools in the determination and characterization of structure of molecules.

Polystyrene has characteristic vibration bands at 1450 cm^{-1}, 1500 cm^{-1}, 1600 cm^{-1} (aromatic C=C), 700 cm^{-1}, 750 cm^{-1} (monosubstituted benzene), and 2900 cm^{-1} to 3200 cm^{-1}, as shown in Figure 5.13. Montmorillonite bands are at 1100 cm^{-1} (Si-O), 500+ cm^{-1} (Al-O) and 400+ cm^{-1} (Mg-O).[10] Other absorption band assigned to the organoclays are shown in Chapter 4, Table 4.7. The IR spectra (Figure 5.14 and Figure 5.15) of the nanocomposites prepared from the surfmer-based organoclays did no show the absorption band at ~1290 cm^{-1}, which was due to the presence of the unsaturated double bond (C=C) in the surfmers. This would suggest that a larger fraction of the polymerizable groups was polymerized.

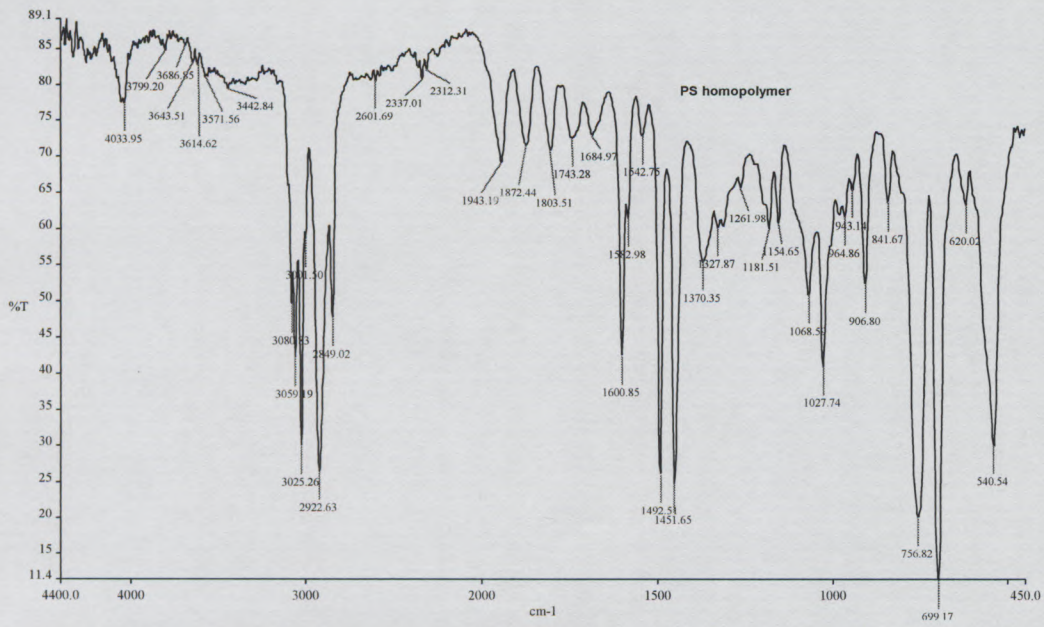

Figure 5.13: FTIR spectrum of polystyrene homopolymer.

Also, it was observed that there was a reduction in the structural OH bands (3600-3700cm^{-1}) in the spectra of the nanocomposites. This was attributed to the disruption of the silicate structures due to the intercalation of the bulky polymer chains in the galleries. A new vibration peak at ~ 1669 cm^{-1} appeared in the spectra of the nanocomposites. This peak was not seen in the organoclay or PS spectra. It was therefore concluded that the band was due to polymer-organoclay interaction. Due to the complexity of the

interactions that are present in the nanocomposite structure, it was not possible to conclude and suggest the source of the peak and would only be able to do so if and when further studies are taken up.

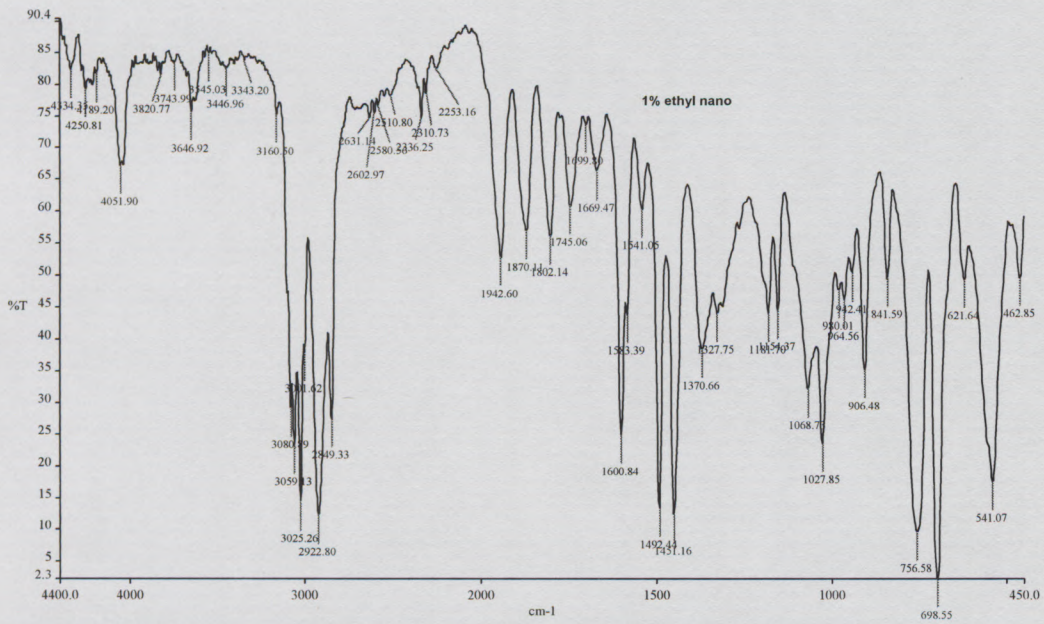

Figure 5.14: FTIR spectrum of FTIR spectrum a 1% ethylMMT-PS nanocomposite.

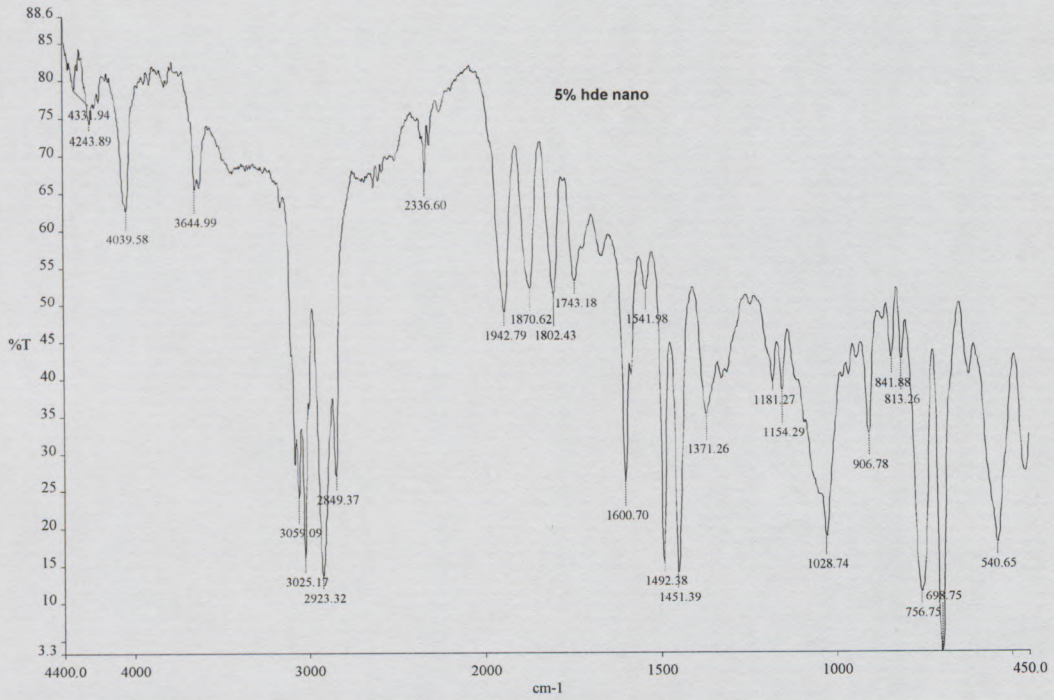

Figure 5.15: FTIR spectrum of a 5% hydroxyethylMMT-PS nanocomposite.

5.4 Conclusion

Polystyrene-layered silicate nanocomposites were successfully synthesized in bulk, using the in-situ intercalative polymerization method. Their structure was then characterized by using a complementary method of evaluating data from small-angle X-ray scattering (SAXS) and transmission electron microscopy (TEM) techniques. EthylMMT-PS nanocomposites showed an exfoliated morphology up to 5 wt% loading; immiscibility of the organoclay was determined by SAXS and TEM at 10 wt% loading. HydroxyethylMMT-PS nanocomposites showed an intermediate morphology between exfoliated and intercalated. This was attributed to the presence of the –OH group in the structure of the organic modifier, which may have led to the difficulty in the separation of the silicate layers due to the presence of hydrogen bonds. CTABMMT-PS nanocomposites showed an intercalated morphology.

Molecular weight studies for the nanocomposites showed that the extracted polymer, which was unattached to the silicate layers, had higher molecular weight compared to the PS homopolymer. This was attributed to the advantage provided by lower temperature (60 °C) of polymerization, which needed longer reaction times and less radical presence in the system at a specific time. This led to less radical-to-radical encounter, and therefore, less probability for reaction termination. The second motivation for higher molecular weight was the viscosity of the system, which led to immobility of the growing and bigger chains; this led to the more agile monomer adding up on the growing chain.

Fourier transform infrared spectroscopy (FTIR) studies showed the disappearance of the unsaturated double bond peak, which was initially observed in surfmer-modified organoclays. This was attributed to the reaction of the double bond during polymerization. The structural OH group band was diminished as a result of the loss of regularity in the silicate structures.

5.5 List of references

1. Kojima, Y.; Usuki, A.; Kawasumi, M.; Okada, A.; Fukushima, Y.; Kurauchi, T.; Kamigaito, O. *Journal of Materials Research* **1993,** 8, 1185-1189.

2. Chigwada, G.; Jiang, D. D.; Wilkie, C. A. *Thermochimica Acta* **2005,** 436, 113-121.

3. Fu, X. A.; Qutubuddin, S. *Journal of Colloid and Interface Science* **2005,** 283, 373-379.

4. Laus, M.; Camerani, M.; Lelli, M.; Sparnacci, K.; Sandrolini, F.; Francescangeli, O. *Journal of Materials Science* **1998,** 33, 2883-2888.

5. Abot, J. L.; Yasmin, A.; Daniel, I. M. In *Mechanical and thermoviscoelastic behavior of clay/epoxy Nanocomposites*, Materials Research Society Symposium Proceedings, 2003; (Eds), Materials Research Society: **2003**; 16.5.1-16.5.6.

6. Sarathi, R.; Sahu, R. K.; Rajeshkumar, P. *Materials Science and Engineering: A* **2007,** 445-446, 567-578.

7. Wang, D.; Zhu, J.; Yan, Q.; Wilkie, C. A. *Chemistry of Materials* **2002,** 14, 3837-3843.

8. Mijovic, J.; Lee, H.; Kenny, J.; Mays, J. *Macromolecules* **2006,** 39, 2172-2182.

9. Su, S.; Wilkie, C. A. *Journal of Polymer Science Part A: Polymer Chemistry* **2003,** 41, 1124-1135.

10. Wang, H.-W.; Chang, K.-C.; Yeh, J.-M.; Liou, S.-J. *Journal of Applied Polymer Science* **2004,** 91, 1368-1373.

11. Noh, M. W.; Lee, D. C. *Polymer Bulletin* **1999,** 42, 619-626.

12. Aphiwantrakul, S.; Srikhirin, T.; Triampo, D.; Putiworanat, R.; Limpanart, S.; Osotchan, T.; Udomkichdecha, W. *Journal of Applied Polymer Science* **2005,** 95, 785-789.

13. Alexandre, M.; Dubois, P. *Materials Science and Engineering: R (Reports)* **2000,** 28, 1-63.

14. Ray, S. S.; Okamoto, M. *Progress in Polymer Science* **2003,** 28, 1539-1641.

15. Qutubuddin, S.; Fu, X.; Tajuddin, Y. *Polymer Bulletin* **2002,** 48, 143-149.

16. Causin, V.; Marega, C.; Marigo, A.; Ferrara, G. *Polymer Communication* **2005,** 46, 9533-9537.

17. Morgan, A. B.; Gilman, J. W. *Journal of Applied Polymer Science* **2003,** 87, 1329-1338.

18. Samakande, A. Synthesis and Characterization of Surfmers for the Synthesis of Polystyrene-Clay Nanocomposites. MSc Thesis, University of Stellenbosch, Stellenbosch, **2005**.

19. Wang, H.-W.; Chang, K.-C.; Chu, H.-C.; Liou, S.-J.; Yeh, J.-M. *Applied Polymer Science* **2004,** 92, 2402-2410.

20. Park, C. I.; Choi, W. M.; Kim, M. H.; Park, O. O. *Journal of Polymer Science Part B: Polymer Physics* **2004,** 42, 1685-1693.

21. Morgan, A. B.; Gilman, J. W.; Jackson, C. L. *Macromolecules* **2001,** 34, 2735-2738.

22. Fu, X.; Qutubuddin, S. *Polymer* **2001,** 42, 807-813.

Chapter 6

Effects of morphology on the physical properties:

Structural correlations

Abstract

Three types of nanocomposites with different morphologies were characterized by dynamic mechanical analysis (DMA), thermomechanical analysis (TMA) and dielectric analysis (DEA). EthylMMT-PS nanocomposites, having an exfoliated morphology, showed improved properties relative to the homopolymer, with a systematic dependence on the clay loading. The semi exfoliated-intercalated hydroxyethylMMT-PS nanocomposites showed a variation of superior and inferior properties relative to the PS homopolymer, but there was less dependence on the clay loading. CTABMMT-PS nanocomposites exhibited an intercalated morphology and showed less dependence of the properties on the clay loading.

Improved DMA and TMA properties were generally observed in the nanocomposites. Confinement studies, carried out using by using the DMA, demonstrated molecular restrictions in the exfoliated nanocomposites and increased glass transition temperature (T_g). The intercalated-exfoliated composites also showed increase in the T_gs, which was dependent on the individual clay loadings. Reinforcement was observed, although a plasticizing effect was determined for the exfoliated-intercalated nanocomposites from the TMA measurements.

Confinement studies were also determined by DEA. The dielectric relaxation results indicated the presence of ionic polarization and ionic conductivity effects in the nanocomposite matrix. The hydroxyethylMMT-PS nanocomposites exhibited the least change in the dielectric response relative to the PS homopolymer, and when compared to other nanocomposites. The effects of the different organic modifiers and resultant morphologies on the eventual properties on the nanocomposites were demonstrated.

6.1 Introduction

Polymer-layered silicate nanocomposites (PLSNs) are materials that are useful in many areas of application due to their improved properties with relatively very low level of clay loading. Improvements in a variety of properties of PLSNs have been reported.[1-6] There have been major improvements in their electrical, mechanical and thermal properties. In terms of the mechanical properties, the focus has mainly been on static tensile, and flexural measurements. Dynamic mechanical analysis (DMA)[2,7-11], dielectric relaxation spectroscopy (DEA)[11-15] and nuclear magnetic resonance (NMR)[16,17] are some of the techniques that have been used to investigate local molecular dynamics in polymers and PLSNs. DMA and DEA are analytical techniques that are used to study relaxation processes and molecular motions in the PLSNs.[11,14] Relaxation and molecular motion studies are able to probe the free volume and confinement effects of polymer chains between and around the dispersed layered silicates. A detailed DMA study on different PLSNs, based on different polymers, has been reported.[2]

Literature reviews (Chapter 2, Section 2.4.4) show that the effects of the presence of clay in the polymer matrix are variable. However, in most cases the effects of the presence of the layered silicates are prominent at the α-relaxation/glass transition region (T_g). This is due to the fact that it is during the motions of the segments and chains of the polymer that the effect of the presence of clay is increased. The short-range effect of the chains and the nano-scale dispersed particles is most likely to be prominent when there is flow. Melt rheology has been used to study the influence of dispersed particles on the melt flow of the matrix of PLSNs.[2,3]

This chapter focuses on the determination of the physical properties of the polystyrene-layered clay nanocomposites (PS-LSNs) and the correlation between these properties and the structure of the nanocomposites.

6.2 Experimental

6.2.1 Materials

PS-LSNs based on organically modified clay were used (synthesis reported in Section 5.2.2, Chapter 5). Montmorillonite (MMT) clay was modified using three organic surfactants, as discussed in Section 4.2.2, Chapter 4. Two polymerizable, in-house synthesized surfactants and one non-polymerizable, commercial surfactants were used in the organic modification of MMT. The surfactants are 11-acryloyloxy-undecyl dimethyl ethyl ammonium bromide, 11-acryloyloxy-undecyl dimethyl hydroxyethyl ammonim bromide (polymerizable) and cetyl trimethyl ammonium bromide (non-polymerizable) and were shortened to *ethyl*, *hydroxyethyl* and *CTAB* surfactants, respectively. The subsequent nanocomposites were named based on these shortened names. For instance, a nanocomposite based on one weight percent (wt%) ethyl-modified MMT and polystyrene is called *1% ethylMMT-PS*.

6.2.2 Measurements

Dynamic measurements were done on a Perkin Elmer 7e using a parallel plate measuring system with 3-mm diameter probe with a controlled dynamic force applied at 1 Hz frequency. A strain control was set to an amplitude limit of 10 μm to ensure that the measurement was within the linear viscoelastic region of the polystyrene-based samples. A temperature scan from 25 °C to 250 °C, with a ramp rate of 5 °C/min, was programmed. A nitrogen gas with a flow rate of 28 ml/min was used to purge the measurement system. Storage modulus, loss modulus and tan delta were reported as functions of temperature.

For thermomechanical analysis (TMA), both the penetration and thermal expansion behaviors were determined, at a temperature scan of between 20 °C and 220 °C was used, with a ramp rate of 3°C/min. The TMA measurements were also done on the Perkin

Elmer DMA7e system on static mode. The penetration measurements were done with a 1 mm diameter flat-front penetration probe with a 5000 mN force applied. The change in the sample height was measured and reported as a percentage of the initial height, as a function of temperature. Thermal expansion measurements were done with a 3 mm diameter probe with zero stress applied on the sample. The dimensional change was also reported as a percentage of the initial sample height, as a function of temperature.

Dielectric measurements were carried out on a Novocontrol Broadband Dielectric Converter (BDC) connected to a Solatron Gain/Phase analyzer for a larger frequency range. A parallel plate measuring system was used. 13-mm diameter cylindrical samples were coated with an alcohol-based conducted silver paint applied on both sides. A full frequency scan measurement was done at isothermal points. The temperature isothermal points were set from -50 °C to 225 °C for PS homopolymer, and 25 °C to 150 °C for thereafter for the nanocomposites, at 25 °C increments.

6.3 Results and discussion

6.3.1 Dynamic mechanical analysis

In this current study the mechanical damping properties of the PLSN materials were used to study the suppression of the mobility of the chains near the interfaces of the silicate layers. Tan δ was used to observe the measured mechanical damping properties. The tan δ peak, at the T_g, was used as an indicator of the molecular motions[18] of the polymer as affected by the presence of: (1) the layered silicates and (2) the organic modifier, especially the polymerizable groups. The lower temperature inflection point (first onset/T_{onset1}) of the peak was marked as the first gradual point of motion of the main chains of the polymer at the T_g. This point is a better indicator for T_g when using the tan δ curve on the DMA results.[19] The height of the peak, and the temperature at which the peak occurred (position), indicate the overall molecular motion behavior of the polymer.

The tan δ peak height is sensitive to material-dependent parameters such as cross-link density, filler content or blend morphology, but is less influenced by the glass transition itself.[19] Since tan δ is the ratio between the loss to the storage moduli, the peak properties are indicative of both elastic and flow properties.

The tan δ curves of the ethylMMT-based nanocomposites showed a remarkable increase in the T_{onset1} value compared to the PS homopolymer (Figure 6.1). The polymer chains start to be mobile at this temperature and the presence of the clay affects the mobility of the polymer chains. Another factor is the presence of the polymerizable groups in the nanocomposite system. The polymerizable groups introduce an anchoring effect of the chains as the organic cations are attached to the silicate layers and therefore contributing greater restriction (confinement) of the chain motions.[7] The morphologies of the ethylMMT-PS nanocomposites were determined to be mostly exfoliated, up to 5 wt% organoclay (Section 5.3, Chapter 5). At 10 wt% loading a large fraction of the composite has lost exfoliation, and the morphology of the sample was no longer regarded as an exfoliated nanocomposite system. An interesting observation was that all the T_{onset1} points for the lower clay loading ethylMMT-PS nanocomposites were very close to each other. The 3 wt% loading had the highest onset temperature (Table 6.1). The 10 wt% clay loading sample had a slightly lower T_{onset1} value (104.6 °C) than the values of other nanocomposite samples, which were between 106 °C and 107 °C.

A similar trend was observed for the temperature of the peak height maxima (T_{max}). The ethylMMT-PS nanocomposites showed an increase in T_{max} compared to the PS homopolymer. Although T_{max} for 10% ethylMMT-PS was not lower than other ethylMMT-PS nanocomposites, it was lower than for 5% ethylMMT-PS. This indicated that the nanocomposite system could be having a critical threshold for the increasing mechanical damping properties with increasing clay loading.[11] The tan δ peak maximum (tan δ_{max}) showed a gradual decrease with an increasing clay amount, as shown in Figure 6.2. The PS homopolymer showed a tan δ_{max} value that was similar to that of 1% ethylMMT-PS. The 3 wt% and 5 wt% samples had a much lower tan δ_{max} value but higher than 10% ethylMMT-PS. The decrease in the peak height corresponds to the

increase in the elastic factor due to reinforcement and/or a decrease in the flow characteristics, as a result of the suppression of mobility in the segments.[7,20] In the case of the ethylMMT-PS nanocomposites, the main contributing factor to tan δ was the loss modulus, as opposed to the storage modulus. The loss modulus contributes a larger factor as the materials are at the glass-rubbery transition, which is also characterized by elastic and flow behaviors. This contribution is shown by the values of tan δ_{max} that are all higher than 1 for the measured samples (see Table 6.1). The tan δ_{max} value is closer to 1 for 10% ethylMMT-PS, meaning that the elastic and fluid factors contribute almost equally to the mechanical damping properties of the material. In general, the presence of the filler (not necessarily nano-sized) would contribute to the lowering of the tan δ_{max}.[21] This is due to the fact that fillers provide the polymer matrix with reinforcement, and the overall hardness of the material is enhanced. The advantage with PLSNs is that the effect of reinforcement is observed at very low clay loadings. This reinforcement was effective at 3% and 5% clay loadings of the ethylMMT-PS nanocomposites.

At temperatures above 170 °C, where the base of the tan δ peak was, there were no interpretable trends. The curves crossed over, and had become noisy. This was the limitation of the measuring technique, where the viscosity of the sample dropped. Shear DMA measurements above the T_g have been reported.[2]

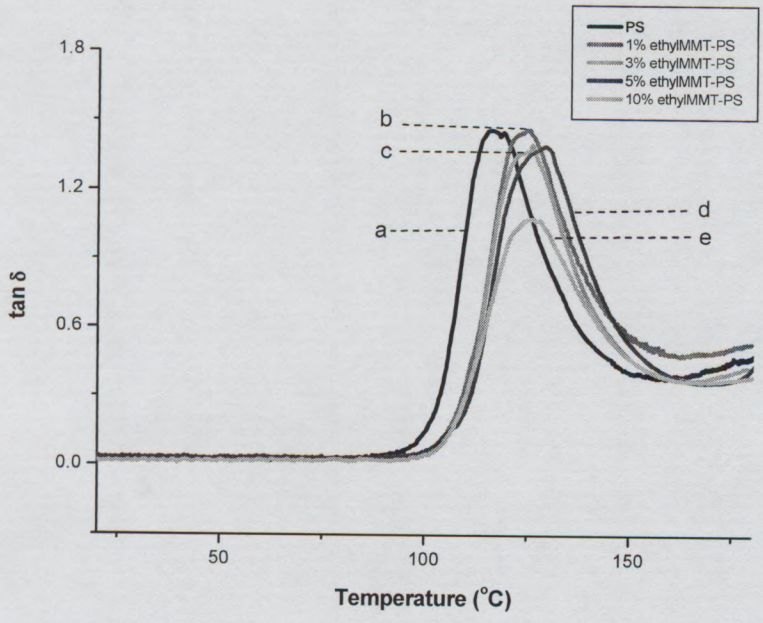

Figure 6.1: Tan delta peaks of (a) polystyrene homopolymer and ethylMMT-PS nanocomposites containing (b) 1 wt%, (c) 3 wt%, (d) 5 wt% and (e) 10 wt% organoclay.

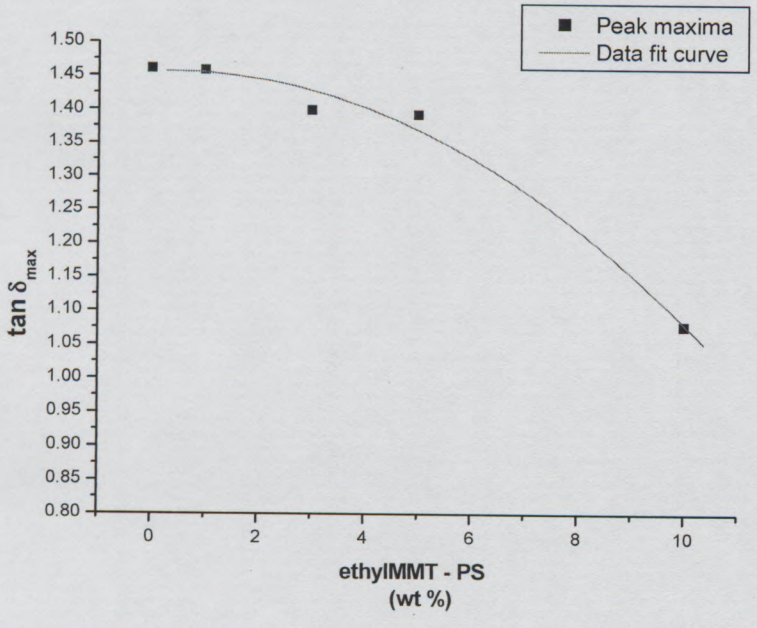

Figure 6.2: Dependence of the tan delta peak maxima on the clay loading in ethylMMT-PS nanocomposites.

Table 6.1: tan δ properties of ethylMMT-PS nanocomposite samples at the T_g

EthylMMT-PS wt%	**T_{onset1}(tan δ) (°C)**	**T_{max} (°C)**	**Tan δ_{max}**
0	101.2	116.6	1.461
1	105.9	124.4	1.459
3	107.2	126.0	1.400
5	106.9	129.5	1.393
10	104.6	126.6	1.079

Similar findings to that of ethylMMT-based nanocomposites were observed for hydroxyethylMMT-based samples. The onset values for the nanocomposites had increased compared to that of PS homopolymer (Figure 6.3). The same explanation for the increase in the onset was deemed applicable since the organic modifiers used in the clays were similar in chemistry; i.e. both had polymerizable functional groups. The anchoring of the polymer chains is mediated by the organic modifiers, which are attached to the silicate layers by the electrostatic attraction and covalently bonded to the polymer. However, the morphology of these nanocomposites was characterized as intercalated-exfoliated (Section 5.3.2, Chapter 5).

The increase in the T_{onset1} values for the nanocomposites was attributed to the confinement of the molecular segments. This is because the presence of silicate layers reduces the free volume needed for the molecular movement.[22] Another possibility is that the formation of a copolymer of the PS and the acrylic based surfactant at the interfacial region leads to immobility of the molecular chains in the composite. Rao and Pochan[20] studied the mechanics of PLSNs, by focusing on the effects of the interfacial phase. The 1 wt% loading was intermediate between the PS homopolymer and other ethylMMT-PS nanocomposites. The 3 wt% and 5 wt% loading nanocomposites had almost similar T_{onset1} values, as seen in Table 6.1.

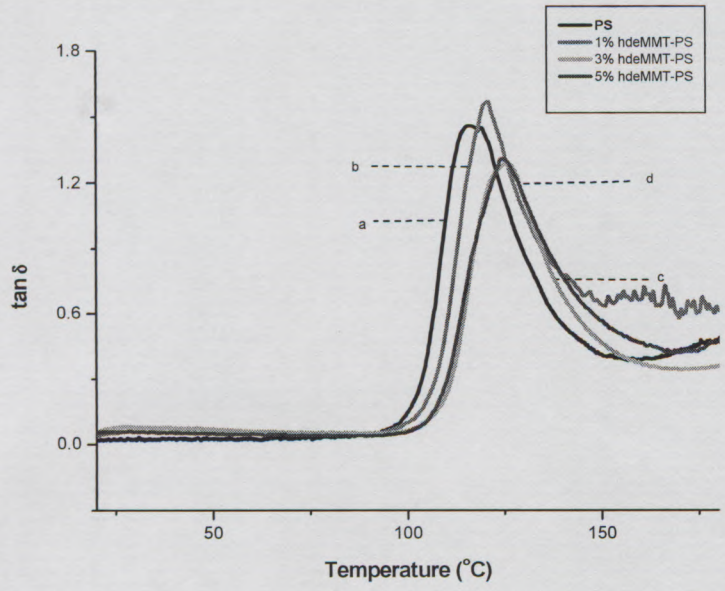

Figure 6.3: Tan delta peaks of (a) polystyrene homopolymer and hydroxyethylMMT-PS nanocomposites containing (b) 1 wt%, (c) 3 wt% and (d) 5 wt%.

The tan δ_{max} values for the 3 wt% and 5 wt% hydroxyethylMMT-PS nanocomposites were lower than that of the homopolymer and the 1 wt% sample, and similarly for the ethylMMT-PS nanocomposites. However, the tan δ_{max} value for 1% hydroxyethylMMT-PS was higher than that of the PS homopolymer. This was rather questionable for the hydroxethylMMT-PS nanocomposites as the damping was expected to be less than that of the pure homopolymer, given the general observation that hardened fillers tend to lead to an increase in the elastic modulus.[18,19]

Table 6.2: tan δ properties of hydroxyethylMMT-PS nanocomposite samples at the T_g

hydroxyethylMMT-PS (wt%)	**T_{onset1}(tan δ) (°C)**	**T_{max} (°C)**	**Tan δ_{max}**
0	101.2	116.6	1.461
1	105.1	120.8	1.570
3	106.3	125.4	1.295
5	106.5	124.8	1.309

The CTAB-based nanocomposite samples showed significant improvements in the T_{onset1} values for the 1 wt% and 3 wt% loadings. The 7 wt% CTABMMT-PS nanocomposite only showed an intermediate improvement compared to the PS homopolymer (Figure 6.4). There was about 9 °C and 10 °C difference for the 1 wt% and 3 wt% nanocomposites, respectively, when compared to the PS homopolymer. On the other hand, the 7 wt% showed only about 4 °C increase in the T_{onset1} value, as shown in Table 6.3.

The tan δ_{max} values for the 1 wt% and 3 wt% CTABMMT-PS nanocomposites were much smaller compared to the homopolymer, indicating the fact that there was more elasticity at the α-relaxation region due to the presence of the organoclay in the matrix. This was not the case with the 7 wt% sample as there was no change in the peak maximum height compared to the homopolymer. The higher level of organoclay in the matrix led to the presence of a larger fraction of the CTAB surfactant in the matrix, which brought about a plasticizing effect at the α-relaxation region. This means that the effort of the silicate layers to improve the T_g and elasticity properties was counter-balanced by the presence of a larger surfactant fraction. Since the CTAB fraction was not co-polymerized to the PS chains, it brought about a 'slippage effect' as the temperature increased and the T_g behaviors were negatively influenced by this (slippage) effect. The influence of intercalated morphology was considered as a critical factor, since the structural studies (SAXS and TEM) showed that the nanocomposite was well intercalated with minimal agglomerated organoclay (Section 5.3, Chapter 5).

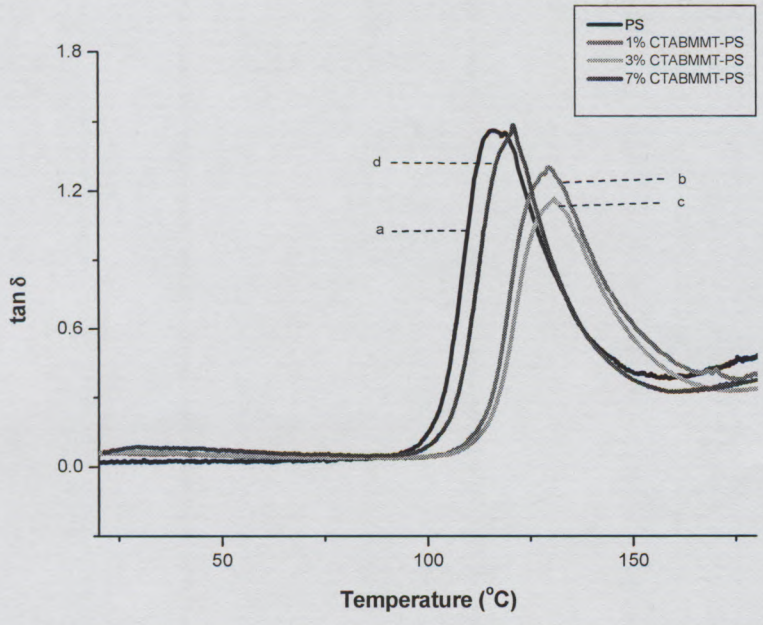

Figure 6.4: Tan delta peaks of (a) polystyrene homopolymer and CTABMMT-PS nanocomposites containing (b) 1 wt%, (c) 3 wt% and (d) 7 wt% organoclay.

Table 6.3: tan δ properties of CTABMMT-PS nanocomposite samples at the T_g

CTABMMT-PS (wt%)	T_{onset1}(tan δ) (°C)	T_{max} (°C)	tan δ_{max}
0	101.2	116.6	1.461
1	109.9	129.7	1.302
3	111.9	131.0	1.169
7	105.5	121.0	1.485

The overall DMA results (Table 6.4) show that the morphology of the nanocomposite has a major effect on the dynamic properties below the T_g. For each nanocomposite type (based on surfactant), the elastic modulus (E') values taken at 30 °C are generally similar. The E' values of the ethylMMT-PS nanocomposites do not differ significantly from those of the PS homopolymer. However, the 1 wt% sample had a lower E' value due to the

stress in the sample. Besides the low values, E' showed a peak before the inflection point at the T_g, usually associated with stress relaxation. Although the samples had been thermally conditioned before the measurements, the storage modulus of 1% ethylMMT-PS showed stress relaxation characteristics. However, the sample was not reconditioned, in order to maintain consistency of thermal history with other nanocomposites.

Table 6.4: Dynamic mechanical properties of the PLSNs samples at the $T < T_g$

Sample	E' at 30 °C (10^6 Pa)	E'' at 30 °C (10^6 Pa)	E''_{max} (10^6 Pa)
PS	410	9.77	131
1 wt% ethylMMT-PS	271	5.72	115
3 wt% ethylMMT-PS	410	12.09	124
5 wt% ethylMMT-PS	442	14.90	118
10 wt% ethylMMT-PS	455	6.93	115
1 wt% hydroxyethylMMT-PS	320	15.42	138
3 wt% hydroxyethylMMT-PS	226	14.31	81
5 wt% hydroxyethylMMT-PS	317	15.60	87
1 wt% CTABMMTPS	291	14.14	93
3 wt% CTABMMTPS	251	13.92	78
7 wt% CTABMMTPS	229	13.46	82

The hydroxyethylMMT-PS samples had slightly lower E' values compared to the PS homopolymer. The 3 wt% sample had a stress relaxation peak, and although not pronounced, it did affect the E' value. The E' value of 3% hydroxyethylMMT-PS was lower than that of the other hydroxyethylMMT-PS nanocomposite samples. This means that the presence of the hydroxyethyl surfmer in the matrix introduces an effect that reduces the overall hardness of the materials. This reduction in hardness was considered to be a surfactant dependent factor as the effect was even greater in the case of the CTABMMT-PS nanocomposites. The E' values were about half the value for the pure PS sample. This was in disagreement with some findings in the literature that show an increased value of the storage modulus in the clay nanocomposites.[10] The presence of an excess of surfactants in some nanocomposites can bring about the so called "slippage effect" in the matrix, which plasticizes the composites.[23] These findings raise the question of the extent of polymerization inside the galleries. The extent of co-polymerization with the hydroxyethyl surfmer can, possibly, be less than that of the ethyl surfmer. The question of plasticized nanocomposite matrix can also be related to a low T_g that is formed at the polymer-layered silicate interfaces. The surfmers do not yield similar nanocomposite morphologies although their parent structures are similar, differing with only one functional group.

The loss modulus showed some inconsistency of the results for the same types of nanocomposites and between the different morphologies. This was observed at temperatures lower than the T_g of the nanocomposites. Since there is very limited flow of the molecular segment below the T_g, there is little changes that could be determined on the loss modulus. However, it was observed that most of the nanocomposite samples had generally higher loss modulus value than the pure polymer, with the exception of two samples. 1 wt% and 10 wt% ethylMMT-PS samples had similar values but different clay loadings, which made it difficult to assign a correlation to this property. Ray et al.[3] indicated that the increase of the loss component can be related to large anisotropy of the clays.

Inconsistencies in the loss modulus values were observed around the T_g. At this region the polymer chains start to be mobile and show viscoelastic properties. This meant that the most significant contribution to the tan δ values was from the elastic component. The PS homopolymer and 1% hydroxyethylMMT-PS had greater contributions from the loss modulus in the tan δ than other nanocomposites.

6.3.2 Thermomechanical analysis

TMA techniques are generally considered as general characterization tools rather than useful for in-depth analysis of complex polymer structure.[24] However, they are very useful for measuring physical changes that may describe the effects of certain structural elements, such as for filled plastics. In this study, TMA was used to determine the effects of the presence of the organoclays in the PS matrix. A penetration probe was used to do a static force measurement with changes in temperature. The changes in the sample dimensions were measured as a function of temperature.

TMA results showed that the penetration response of the ethylMMT-PS nanocomposites was dependent on the clay loading (Figure 6.1). The temperature at the onset of penetration (T_{onset}) did not differ significantly from the PS homopolymer (Table 6.5). However, the dependence of the penetration on the clay loading was observed at over 50% of the normalized sample dimension (% height). The PS homopolymer showed a lower T_{onset} value than for the ethylMMT-PS nanocomposites. The penetration temperature increased with the increase in the clay loading. Due to the presence of organoclay, the flow of the matrix is restricted, thereby leading to resistance in penetration as the amount is increased. The 10 wt% sample showed a higher T_{onset} value than other nanocomposites. The presence of the polymerizable groups in the surfactant promotes "anchoring" of the silicate layers to the matrix through copolymerization with PS.

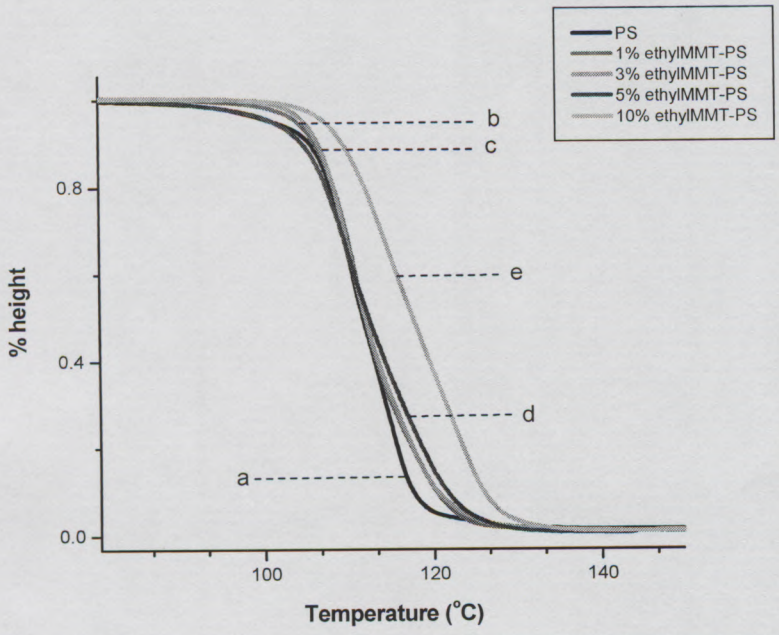

Figure 6.5: TMA curves of (a) polystyrene homopolymer and ethylMMT-PS nanocomposites containing (b) 1 wt%, (c) 3 wt%, (d) 5 wt% and (e) 10 wt% organoclay.

Table 6.5: Thermomechanical properties of ethylMMT-PS nanocomposite samples

EthylMMT-PS (wt%)	T_{onset} (°C)	$\%height_{onset}$	$T_{Penetration}$ (25%) (°C)	$T_{Penetration}$ (90%) (°C)
0	105.9	96.8	108.7	117.5
1	105.9	99.3	109.1	120.3
3	105.6	99.6	109.0	120.4
5	104.3	97.1	108.3	121.6
10	108.2	99.8	113.0	125.9

The TMA findings for the hydroxyethylMMT nanocomposites were very interesting, leading to the point discussed earlier in the DMA of hydroxyethylMMT-PS nanocomposites (Section 6.3.1). The penetration trend for the hydroxyethylMMT-PS nanocomposites increased with increasing clay loading, similarly to the ethylMMT-PS nanocomposites. However, the penetration curves for the 1 wt%, 3 wt% and 5 wt% hydroxyethylMMT-PS nanocomposites were at lower temperatures than for the PS homopolymer, as shown in Figure 6.6. It was deduced that hydroxyethyl surfmer might have copolymerized with PS in the nanocomposite, as no unsaturated bonds were detected by FTIR (Chapter 5, Section 5.3.4). However, a low T_g copolymer could have been formed at the inter-phase between the homopolymer and the layered silicate. Since the interface properties in the composite contribute to the bulk properties, this effect can diminish the reinforcing capability of the layered silicate. Similar inferior reinforcing effects were found in the dynamic mechanical measurements.

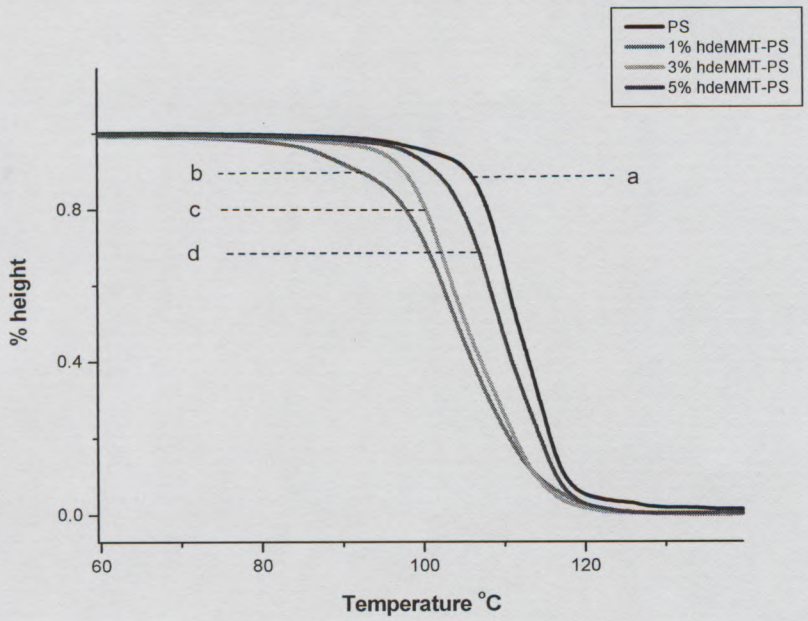

Figure 6.6: TMA curves of (a) polystyrene homopolymer and nanocomposites containing (b) 1 wt%, (c) 3 wt% and (d) 5 wt% hydroxyethylMMT organoclay.

Table 6.6: Thermomechanical properties of hydroxyethylMMT-PS nanocomposites

hydroxyethylMMT-PS (wt%)	T_{onset} (°C)	%height$_{onset}$	$T_{Penetration}$ (25%) (°C)	$T_{Penetration}$ (90%) (°C)
0	105.9	96.8	108.7	117.5
1	94.9	95.9	99.3	114.0
3	97.5	97.4	101.2	113.9
5	102.6	98.0	105.8	116.4

The CTABMMT-PS nanocomposites containing 1 wt% and 3 wt% showed significant improvement in the penetration properties (Figure 6.7). At 90% penetration, there was a considerable difference in the penetration temperatures when compared to that of the PS homopolymer, as shown in Table 6.7. The difference in $T_{Penetration}$ (90%) between the 3% CTABMMT-PS and the sPS homopolymer was about 3 °C, and also that of 3% ethylMMT-PS.

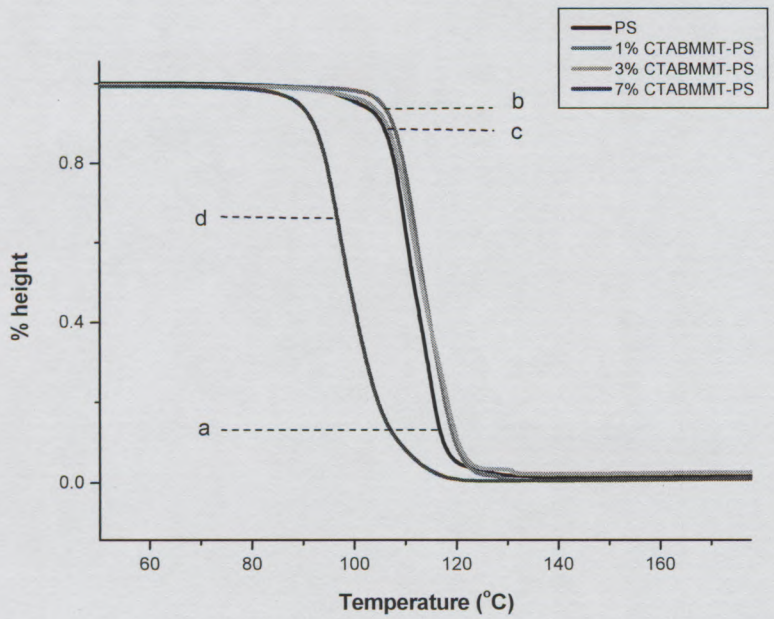

Figure 6.7: TMA curves of (a) polystyrene homopolymer and CTABMMT-PS nanocomposites containing (b) 1 wt%, (c) 3 wt% and (d) 7 wt% organoclay.

A more interesting observation was that the 7 wt% nanocomposite sample showed a far lower T_{onset} value than the PS homopolymer and nanocomposite samples, as seen in Figure 6.7. The low T_{onset} value of the sample indicated that it was not physically reinforced and the matrix was plasticized. Although the DMA results also showed less improvements of 7% CTABMMT-PS, the TMA values were very low compared to the PS homopolymer (Table 6.7). This effect was attributed to the presence of more surfactant fraction in the matrix and acting as plasticizer, thereby minimizing the reinforcement effect of the silicate layers.

Table 6.7: Thermomechanical properties of CTABMMT-PS nanocomposites

CTABMMT-PS (wt%)	T_{onset} (°C)	%height$_{onset}$	$T_{Penetration}$ (25%) (°C)	$T_{Penetration}$ (90%) (°C)
0	105.9	96.8	108.7	117.5
1	107.5	98.4	110.5	119.8
3	106.4	96.7	109.7	120.4
7	91.5	98.3	95.5	108.8

6.3.3 Thermal expansion

Thermal expansion studies were done to determine the coefficient of linear thermal expansion (CLTE) of the nanocomposites when dimensional change (L/L_o) is measured as a function of the programmed temperature. Changes in the dimensions of the samples were measured with no stress applied. During the thermal heating, a polymer expands at a certain rate and as there is greater free volume the rate of expansion is increased.[25] The convergence of the two different expansion slopes in a measurement has been classically used to determine the T_g of the polymeric material being tested.[22] In this study, the expansion slopes of the measured samples were extrapolated to obtain $T_{g\ extrapolated}$ (Figure

6.8). The overall CLTE values of the nanocomposites were less than that of the PS homopolymer, and is summarized in Table 6.8.

A decrease of about 46% in the CLTE was obtained for 1% ethylMMT-PS nanocomposite relative to the PS homopolymer. There was no trend that showed any dependence on the amount of organoclay in the nanocomposite (Figure 6.9). There was also no correlation established for the different types of nanocomposites. 10% ethylMMT-PS and 5% hydroxyethylMMT-PS showed the most significant decrease when compared to the other nanocomposites and the homopolymer. The 5% hydroxyethylMMT-PS showed a decrease in CLTE (88.8 $x10^{-6}$/ °C) relative to the homopolymer.

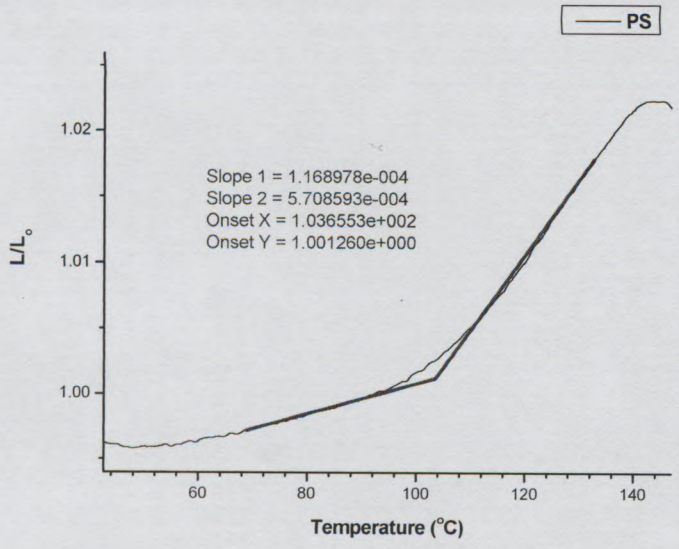

Figure 6.8: Thermal expansion curve of a polystyrene homopolymer with an extrapolated T_g from two expansion slopes.

When heating continued during a measurement, the dimensions of the sample eventually collapsed as the material starts to flow. In this study measurements were continued past the thermal expansion region, to about 230 °C, where the sample dimensions declined due to the flow of the polymer. Since there was no force applied, the resistance of the

samples to heating was determined, and then related to the dimensional stability of the nanocomposites and compared to that of the homopolymer (Figure 6.10).

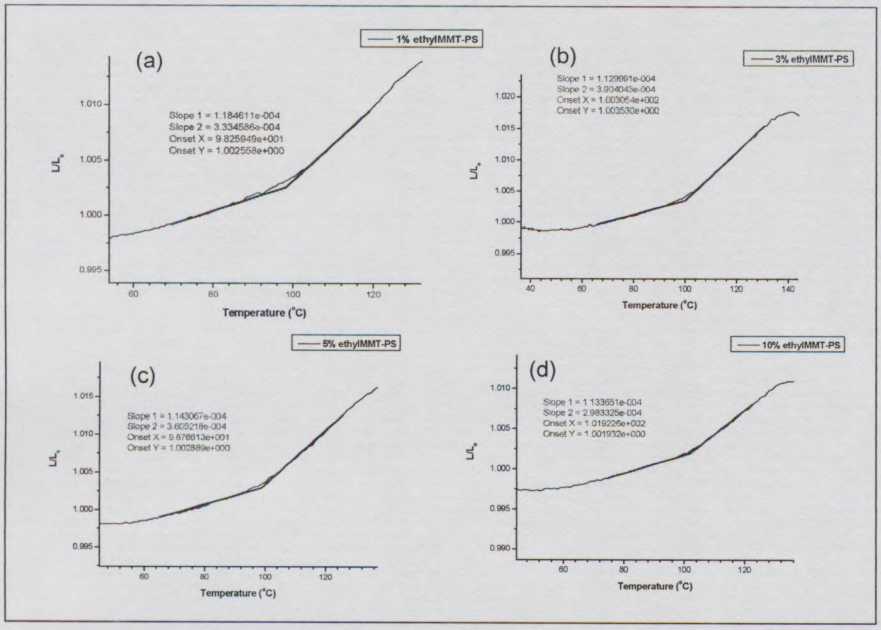

Figure 6.9: Thermal expansion curves of ethylMMT-PS nanocomposites containing (a) 1 wt%, (b) 3 wt% and (c) 5 wt% and (d) 10 wt% organoclay.

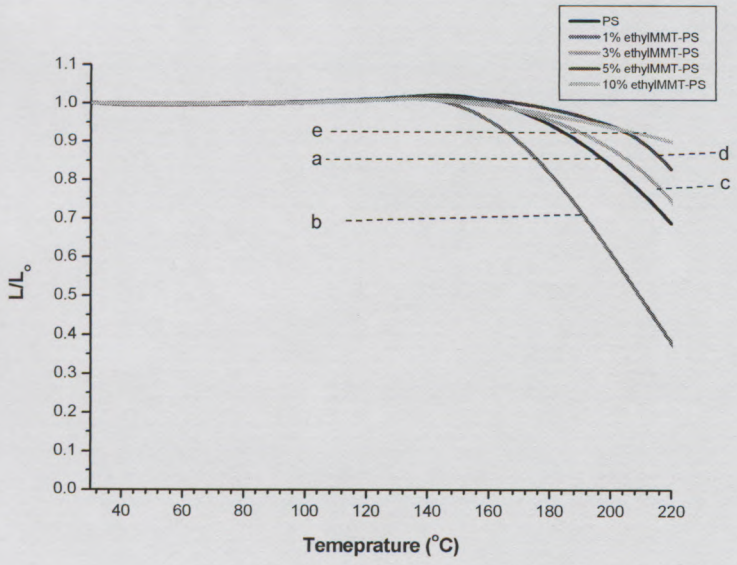

Figure 6.10: Overlaid thermal expansion curves of (a)polystyrene and ethylMMT-PS nanocomposites containing (b) 1 wt%, (c) 3 wt% and (d) 5 wt% and (e) 10 wt% organoclay.

The nanocomposites samples, mostly, showed more dimensional stability compared to the PS homopolymer when the sample dimension (L/L_o) was recorded at 220 °C. However, at the 1 wt% loading different nanocomposite samples showed a lower value (at 220 °C) compared to the PS homopolymer. The reason for this effect is unclear. The 10 wt% ethylMMT nanocomposite showed more stability when compared to other measured samples, as 90% of the original height was determined at 220 °C.

Table 6.8: Thermal expansion properties of nanocomposite samples compared to PS homopolymer

EthylMMT-PS (wt%)	**T_g extrapolation (°C)**	**Slope 1 (10^{-6}/ °C)**	**Slope 2 (10^{-6}/ °C)**	**Expansion coefficient (10^{-6}/ °C)**	**L/L_o (220 °C)**
0	103.7	116.9	570.8	211.5	0.68
1	98.3	118.4	333.4	144.3	0.38
3	100.3	112.9	390.4	161.9	0.75
5	98.8	114.3	360.5	168.8	0.83
10	101.9	113.3	298.3	103.0	0.90
hydroxyethylMMT-PS (wt%)	**T_g extrapolation (°C)**	**Slope 1 (10^{-6}/ °C)**	**Slope 2 (10^{-6}/ °C)**	**Expansion coefficient (10^{-6}/ °C)**	**L/L_o (220 °C)**
0	103.7	116.9	570.8	211.5	0.68
1	84.4	24.2	357.0	118.2	0.28
3	84.2	46.5	340.0	121.8	0.76
5	91.2	42.3	289.0	88.8	0.70
CTABMMT-PS (wt%)	**T_g extrapolation (°C)**	**Slope 1 (10^{-6}/ °C)**	**Slope 2 (10^{-6}/ °C)**	**Expansion coefficient (10^{-6}/ °C)**	**L/L_o (220 °C)**
0	103.7	116.9	5.708	211.5	0.68
1	114.1	146.5	447.6	127.6	0.43
3	104.0	118.3	326.9	124.3	0.83
7	90.9	74.6	410.8	156.7	0.79

6.3.4 Dielectric relaxation and conductivity studies

Dielectric analysis (DEA) or dielectric relaxation spectroscopy (DRS) is a very powerful characterization technique whose functionality is best described by William and Thomas[26] as *"...provides a means of determining the average rate of molecular tumbling motions in different materials (e.g. dipolar liquids, rotatophase molecular crystals, amorphous, crystalline and liquid-crystalline solid polymers)."* When polymers and composites are subjected to an electric field, they are subjected to ionic (space-charge), interfacial and dipole polarizations, which affect the overall dielectric properties.[11] The above polarization processes are exhibited at lower frequencies. Dipole polarization is due to dipoles attempting to follow an applied electric field, the ionic polarization is due to mobile charge-conduction processes and the interfacial polarization is due to the presence of the silicate layers in the polymer matrix.

DEA studies of PLSNs have been reported, both in terms of the general bulk behavior and also the molecular scale confinement.[11-14] Rao and Pochan[20] stated the need to address the effects of the presence of the interfacial phase in PLSNs. They also indicated the difficulty in understanding the mechanics of nanocomposite systems due to the presence of various distribution states (i.e. partially exfoliated-intercalated, partially pristine). The DEA in the present study was more focused on the bulk properties of the nanocomposites and the effects of the underlying structure (exfoliated and intercalated) while consideration was given to the underlying physics and mechanics on the molecular level. Polarization and conductivity effects were studied as a function of frequency and temperature, and were associated with the relaxation and mobility of the chain segments of the nanocomposite matrix.

The following parameters were measured at frequencies ranging from 10^{-2} to 10^{8} Hz for the nanocomposite samples and the homopolymer: real permittivity or dielectric constant (ε'), imaginary permittivity or dielectric loss (ε'') and real conductivity (σ'). The

measurements for polystyrene homopolymer were done at isothermal temperature points, from -50 °C to 225 °C, with 25 °C increments for optimization. The temperature isothermal points were then limited to 25 °C to 150 °C since temperature below 25 °C showed insignificant measurements, and were subjected to noise. At temperature points above 150 °C, the sample changed its dimensions, which started to take effect and this affected the results, especially permittivity. This was ascertained by repeating the measurements at 25 °C. The value obtained at 25 °C was different (higher) to the initial values due to the permanent changes in the sample dimensions, which started to manifest at 170 °C, as shown in Figure 6.11. The frequency was restricted to a higher margin of 10^5 Hz, since the signals were very noisy above this frquency especially for the composites. The ε' value obtained for the pure PS sample was approximately 8. This was in the frequency range between 10^{-2} and 10^5 (Figure 6.11). The ε' value was consistent through most of the temperature range (25 °C – 150 °C) until the sample dimensions changed due to high temperatures. These optimization results showed that the ε' value of PS was not temperature or frequency dependent at the selected ranges.

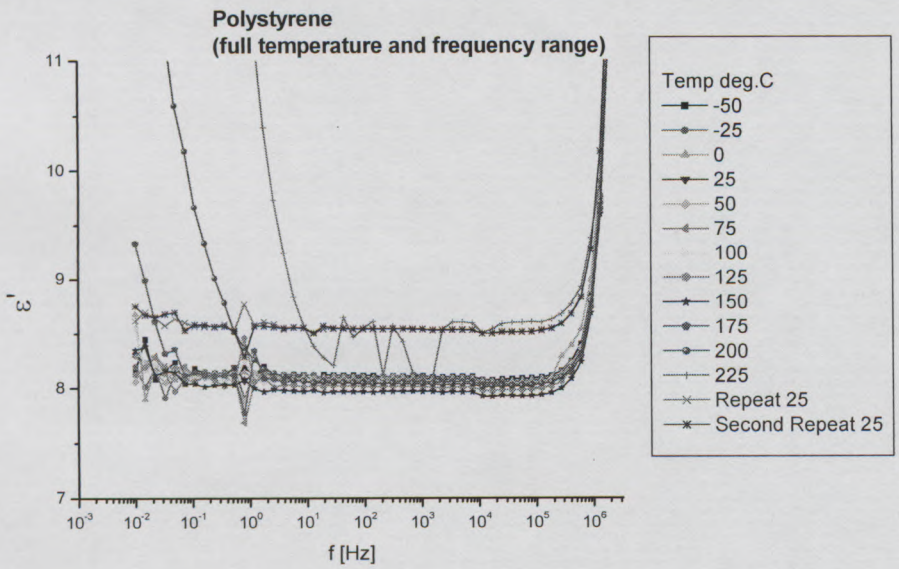

Figure 6.11: An optimization measurement: a real permittivity plot as a function of frequency for pure PS sample over the full isothermal range.

6.3.4.1 Dipole orientation

Dipolar relaxations of PLSNs have been studied through the dielectric loss factor ε" versus frequency plots.[11,20] The relaxation can be due to molecular relaxation processes, the result of the motion of dipole groups, as a whole or as polymer chain segments.[26] In this present study, the dipolar and relaxation processes of the composites were compared to that of PS homopolymer through the plots of real permittivity as a function of frequency (at temperature range of 25 °C to 150 °C).

The ε' values at 25 °C for all the measured nanocomposites decreased compared to that of a PS homopolymer (see Figures 6.12 to 6.14). Lower ε' values for PS-LSNs than for the PS homopolymer were reported by Wang et al.[13] However, there were no clear trends in the current study and no correlation could be made between the ε' values at 25 °C and the amount of clay loading.
It was subsequently determined that variation in ε' values of the nanocomposites at 25 °C was related to their sample thicknesses. This is because ε' is a quantity that is normalized with a sample geometric factor, area-over-thickness (A/L). However, the actual determinant of the ε' values of the samples was an intrinsic one, rather than sample thicknesses, although they are related.

The ε' curves at 25 °C for the nanocomposites remained flat and constant over the measured frequency range, as for the pure PS. This finding was also not totally consistent with what was reported Wang et al.[13] They reported higher ε' values at frequencies of about 100 Hz (at temperature less than 30 °C) for PS, which gradually decreased as the frequency increased. This dependence of dielectric permittivity on the frequency is known as the dielectric dispersion.

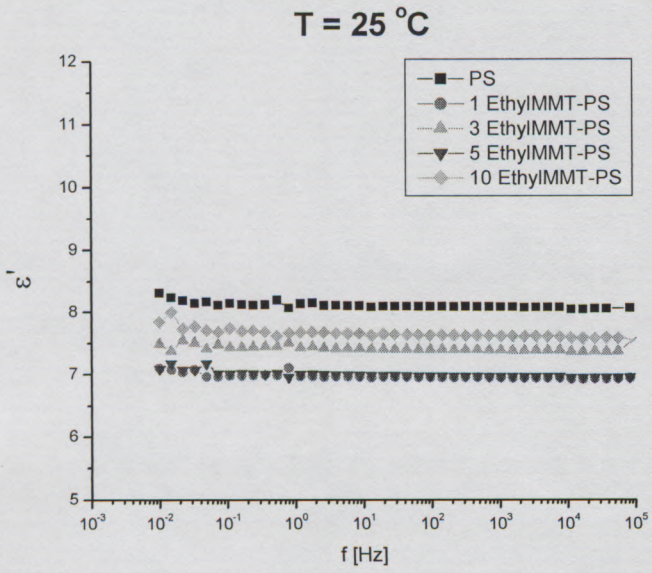

Figure 6.12: Real permittivity plot as a function of frequency for pure PS and ethylMMT-PS nanocomposite samples at 25 °C.

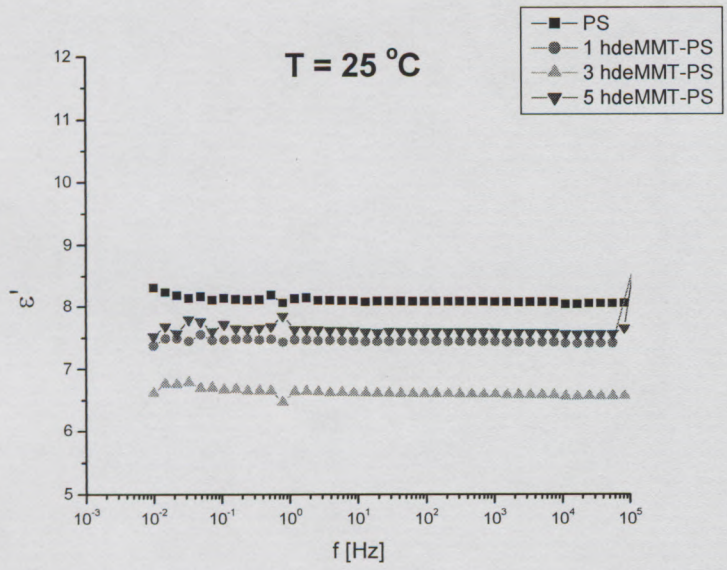

Figure 6.13: Real permittivity plot as a function of frequency for pure PS and hydroxyethylMMT-PS nanocomposite samples at 25 °C.

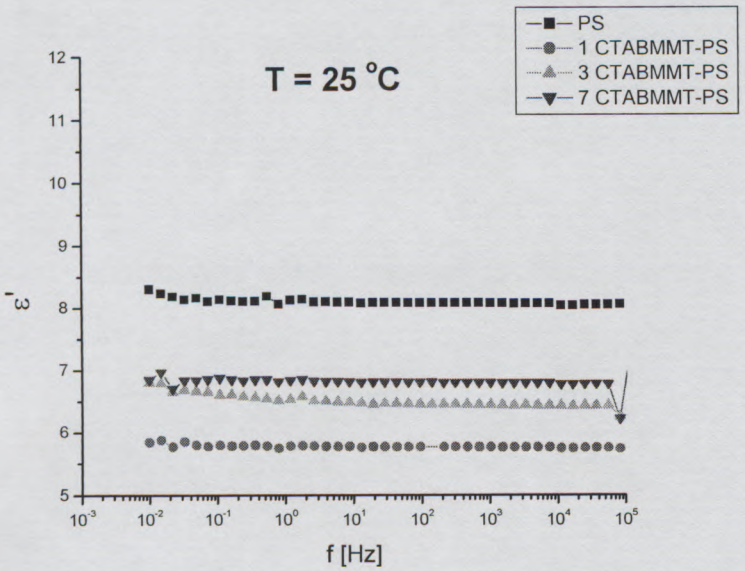

Figure 6.14: Real permittivity plot as a function of frequency for pure PS and CTABMMT-PS nanocomposite samples at 25 °C.

The nanocomposites showed low frequency dispersion with increasing temperature. The ε' values for the nanocomposites started to increase (dispersion) at 75 °C (Appendix B1). The dispersion was dependent on the increasing amount of clay loading in nanocomposites matrix. The 1 % ethylMMT-PS had a lower ε' value than for the PS homopolymer. Even though the 1 wt% sample showed ε' value less than for the pure PS, the curve still showed dependence on the low frequency. The 3 wt%, 5 wt% and 10 wt% ethylMMT-PS samples showed higher ε' values than for the pure PS at lower frequencies. The ε' curves cross over and become lower than the PS at frequency points higher than 1 Hz. The ethylMMT-PS nanocomposites showed ε' values that increased with increasing clay loading at low frequencies (Figure 6.15).

The above feature was understood as increased dipole orientation with increasing clay loading, due to the presence of the interfacial region in the nanocomposite matrix. The increase of ε' values with increasing clay amount is a temperature-dependent effect because it was not exhibited at low temperatures. It was associated with segmental motions as the temperature approached the T_g of the nanocomposites. This finding does

not agree with the literature, in which it is reported that the presence of clay in the matrix suppresses the dipole orientation because of the intercalation/exfoliation confinement.[13] The presence of clay allowed for more dipole orientation as the temperature was increased. Also, the increase ε' values was also ascribed to the ionic polarization at lower frequencies, brought about by the presence of layered silicates.[27] The layered silicates are, possibly, attached to the un-exchanged cations or to the unwashed surfactant ions, which may contribute to unbound ions and hence, ionic polarization. From a relaxation point of view, polymer chains between the silicate layers (intercalated) are more confined than the ones in an exfoliated system.[11]

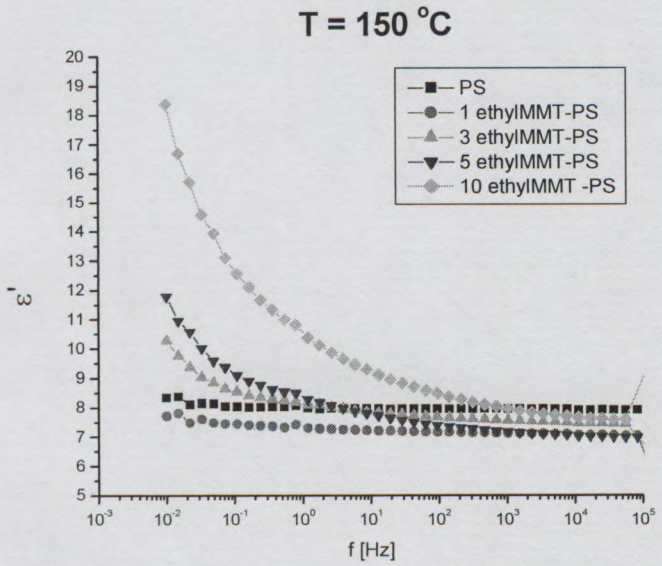

Figure 6.15: Real permittivity as a function of frequency at 150 °C for pure PS and ethylMMT-PS nanocomposites.

The hydroxyethylMMT-PS nanocomposites showed a different trend when compared to the ethylMMT-PS nanocomposites. The overall ε' values at 150 °C were lower than for the pure PS. At lower frequencies the ε' values for the nanocomposites were close to that of pure PS. The curves become significantly lower than that of the homopolymer as the frequency increased.

This is an interesting phenomenon as it was seen that the dipole orientation of the composites increased with temperature. The 3% hydroxyethylMMT-PS showed the largest dependence of ε' on the temperature. The ε' value for the 3% hydroxyethylMMT-PS increased from 6.6 to 8.7 at temperatures between (25 °C to 150 °C), measured at 10^{-2} Hz. 1 wt% and 5 wt% samples, at the same frequency and temperatures, exhibited an increase of 1.3 and 0.6, respectively. Another interesting observation was that the hydroxyethylMMT-based nanocomposites had similar low frequency (10^{-2} Hz) ε' values at 150 °C but different at lower temperatures. The 3 wt% sample showed the lowest ε' value when compared to other nanocomposites and the homopolymer (Figures 6.16 and 6.17).

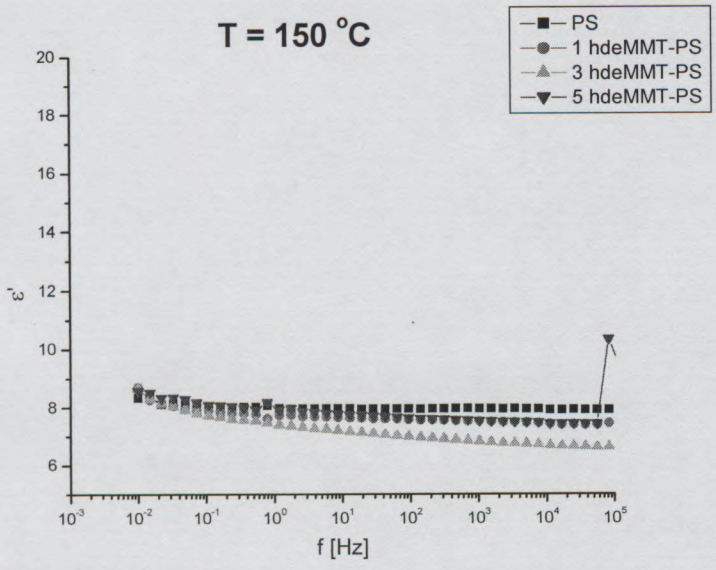

Figure 6.16: A real permittivity plot as a function of frequency at 150 °C for pure PS and hydroxyethylMMT-PS nanocomposites.

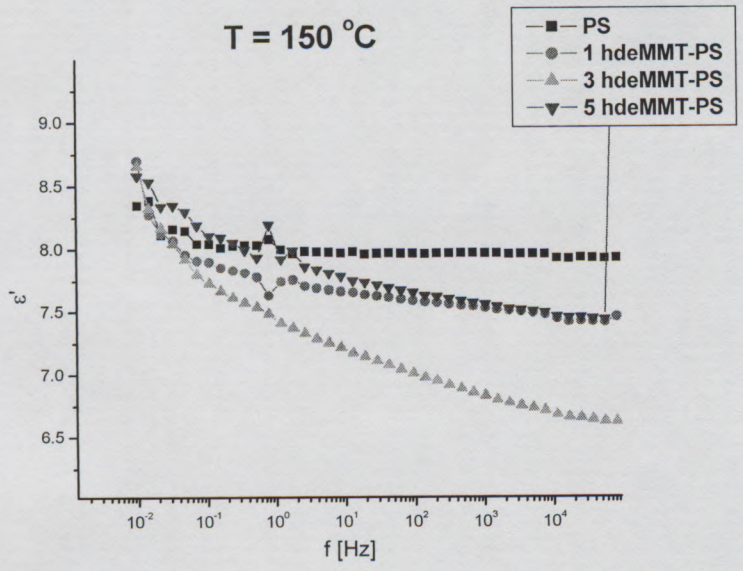

Figure 6.17: A magnified scale of permittivity versus frequency plot at 150 °C for PS and hydroxyethylMMT-PS nanocomposites.

CTABMMT-PS nanocomposites showed different results for ε' at 150 °C when compared to the other types of nanocompostes. Considerable changes in the low frequency permittivity curve were observed for the 3 wt% sample when compared to the 7 wt% and 1 wt% samples (Figure 6.18). The real permittivity curve for the 1 wt% CTABMMT-PS remained lower than that of the PS homopolymer. While the 5 wt% CTABMMT-PS sample's ε' curve was higher than the PS curve, it was lower for the 3 wt% sample. The real permittivity curves for CTABMMT-PS nanocomposites were lower than that of the PS homopolymer at frequencies higher than 10^{-2} Hz.

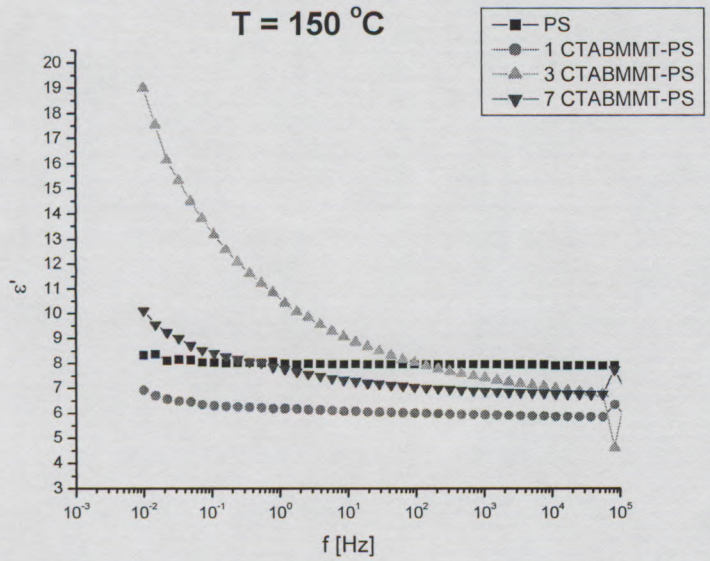

Figure 6.18: A Real permittivity plot as a function of frequency at 150 °C for pure PS and CTABMMT-PS nanocomposites

6.3.4.2 Conductivity behavior of the PS-LSNs

Permittivity and conductivity determine the same dielectric properties of materials but look at different presentation to highlight particular features. Kanapitsas et al.[15] employed DEA to study the morphology of epoxy resin-clay nanocomposites, during which they used both permittivity and conductivity in their investigation. Conductivity, as a function of frequency and temperature, was used a tool to study interface properties. This was achieved by studying the motion of charge carriers over various distances above the molecular level (mesoscopic). In the current study a plot of σ' as a function of frequency at 25 °C for the composites was similar to that of PS homopolymer (Figures 6.19 and 6.20). Relatively, the PS-LSN materials are highly insulating as the conductivity was in the range of 10^{-14} to 10^{-8} S/cm. The bulk behavior of the composites at lower temperatures resembled that of the pure PS, since there were no conducting influences from either the silicate layers, organic modifiers, or nanocomposite structure. The σ' curves showed that there was less conductivity at lower frequencies. Then, σ' curve

gradually increased up to about 1Hz where the slope became steeper. This feature in which the conductivity versus frequency (in a log-log scale) curves show two slopes is known as the universal dielectric response function for amorphous materials.[26]

At the lower temperatures the polymer chains are locked and have no intrinsic molecular mobility, as a result there was no considerable contribution of the presence of the layered silicate to the conductivity factor of the nanocomposites. Pristine clays have interlayer cations that may contribute to the conductivity when they are dispersed in a polymer matrix. The conductivity increases due to the conductive nature of the interlayer cations.[28] In the case of organically modified clays the smaller alkali and alkaline earth cations are substituted by the bulky alkylammonium groups, which are less mobile. A study by Jacobs et al.[29] on the dielectric relaxation of organoclays showed a temperature-dependence of a transition, from static and glass-like to molten, determined by a considerable increase in the mobility of organoclays. The study also shows that excess surfactant and residual electrolytes enhance direct current conductivity and increase in low frequency ionic (space-charge) polarization.

Conductivity for the PS homopolymer showed total independence on changes in temperature (between 25 °C and 150 °C). Plotting the conductivity versus frequency measured at different temperatures on the same system of axes did not show any considerable changes (Figure 6.19). It was then concluded that the pure PS conductivity did not change as a result of the increase in temperature. However, the conductivity curves became noisy at higher temperatures without even shifting considerably from the initial values.

There are a number of different variables that can affect the relaxation processes in PLSNs. These variables may be unique to a particular system and they include experimental conditions, type of confinement, extent of intercalation/exfoliation, surface properties, and interfacial interactions.[11] Conductivity at lower temperatures for the nanocomposites did not show any changes when compared to the PS homopolymer. This phenomenon is illustrated in Figure 6.20 for the ethylMMT-PS nanocomposites at 25 °C.

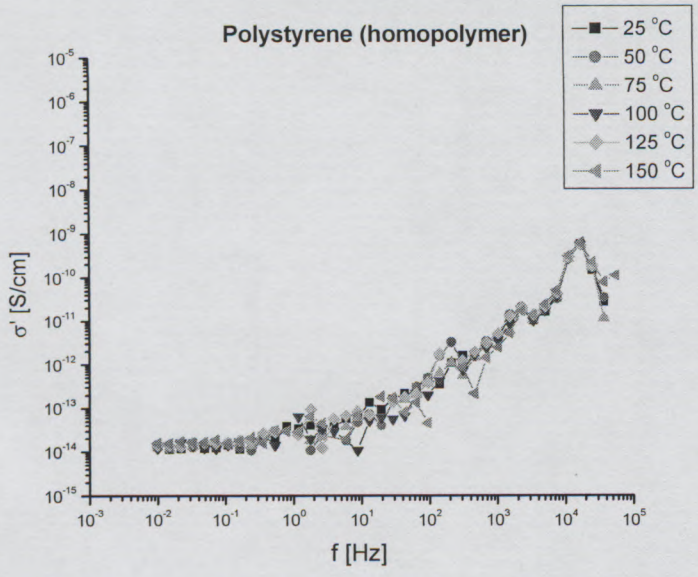

Figure 6.19: Overlaid curves of conductivity versus frequency measured at different temperatures.

Conductivity measurements with increasing temperature show a dependence on the type of nanocomposite and the also clay loading. The ethylMMT-PS nanocomposites showed an increase in the conductivity with increase in clay loading (Figure 6.21). As the clay amount was increased from 1 wt% to 10 wt%, conductivity increased from 1.5 $X10^{-14}$ to 1.4 $X10^{-13}$ S/cm. The conductivity gradually increased as the temperature was increased. According to Jacobs et al.[29] bound and unbound surfactant molecules facilitate charge transport and act as the mobile charge-carrying species.

Morphology dependence of conductivity was observed when comparing the ethylMMT-PS nanocomposites to the hydroxyethylMMT-PS nanocomposites. The nanocomposites did not show major enhancement of the conductivity at similar temperatures. At 150 °C the conductivity curves for hydroxyethylMMT-PS nanocomposites did not show any appreciable changes from each other, as shown in Figure 6.22. CTABMMT-PS nanocomposite showed an increase in the conductivity, as shown in Figure 6.23. The dependence of the conductivity on clay loading at high temperatures was such that the 3 wt% loading showed the highest σ' value. On the other hand, the conductivity curve for 7% CTABMMT-PS was above that of 1 wt% CTABMMT-PS.

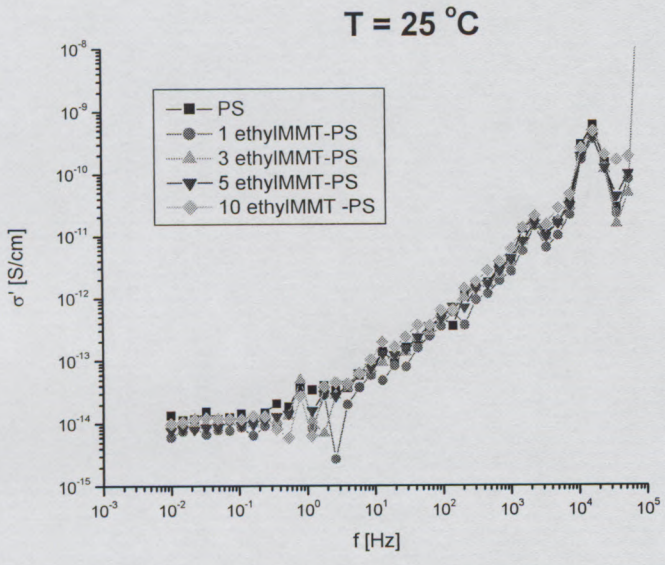

Figure 6.20: A plot of real conductivity as a function of frequency at 25 °C for pure PS and ethylMMT-PS nanocomposites.

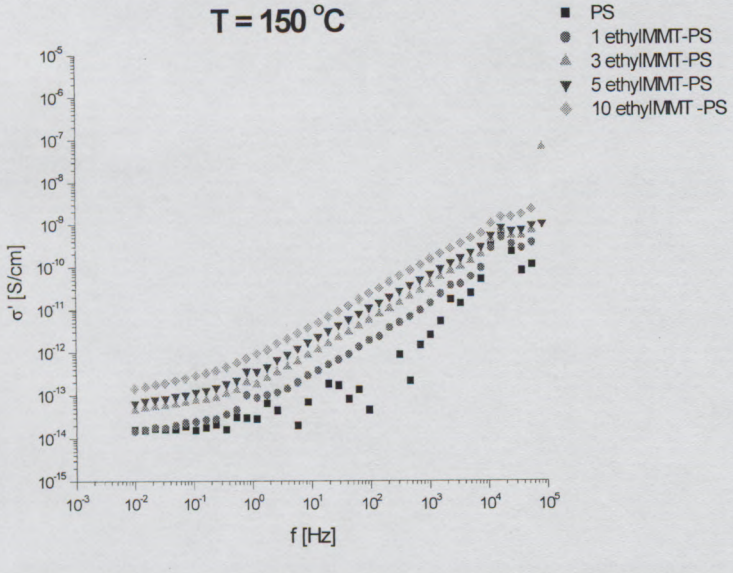

Figure 6.21: A plot of real conductivity as a function of frequency at 150 °C for pure PS and ethylMMT-PS nanocomposites.

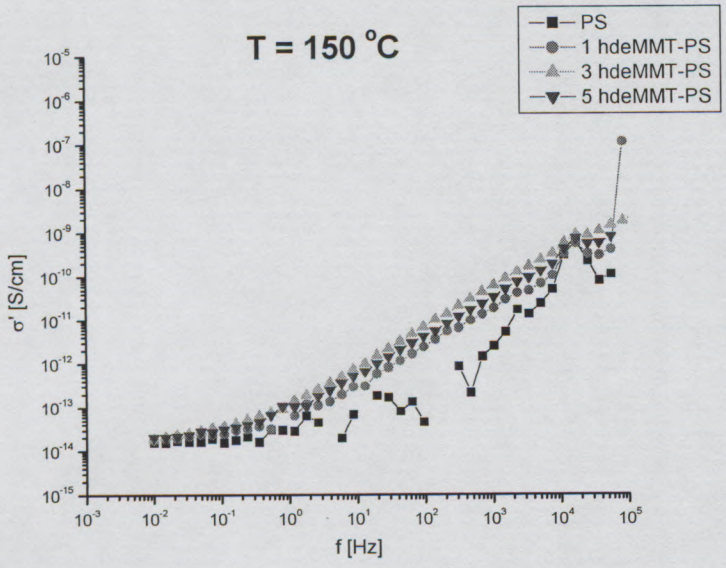

Figure 6.22: A plot of real conductivity as a function of frequency at 150 °C for pure PS and hydroxyethylMMT-PS nanocomposites.

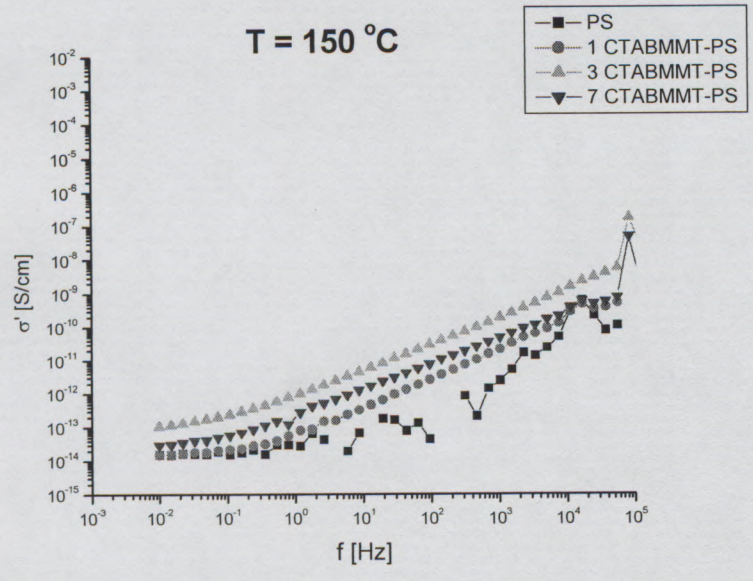

Figure 6.23: A plot of real conductivity as a function of frequency at 150 °C for pure PS and CTABMMT-PS nanocomposites.

The dependence of dielectric properties on the different organic modifiers was evident from the results shown, since each nanocomposite type showed its own dielectric effects. The enhancement of the ionic conductivity was the most prominent feature in the dielectric properties of the nanocomposites. It could be observed that the most exfoliated systems (ethylMMT-PS) showed the most systematic responses from the measured properties. This observation was also true for DMA results. The DEA results for hydroxyethylMMT-PS nanocomposites were strongly contrasted by the DMA results. The DEA results of the hydroxyethylMMT-PS nanocomposites showed immobility of the dipolar components, whereas the DMA showed plasticizing effects. The CTABMMT-PS nanocomposites showed dependence of the properties on the clay loading, but this was not systematic.

6.4 Conclusions

The DMA, through the use of tan δ, was successfully used to study the molecular mobility of the nanocomposite matrix, and to determine the effects of the organic modifier. The tan δ peak was also used as an indicator for the T_g. The ethylMMT-PS nanocomposites showed improvements in T_g relative to the PS homopolymer. The viscoelastic properties, at the T_g, showed that the molecular mobility of the composite matrix was reduced, as depicted by the reduction in the tan δ peak height. This suppression in matrix mobility was exhibited with increasing clay loading. This was attributed to confinement brought about by the distribution of the silicate layers in the matrix.

The hydroxyethylMMT-PS and CTABMMT-PS nanocomposites also showed an increase in the T_g relative to the PS homopolymer. However, the extent of the increase was dependent on the clay loading. The trends were variable between the two nanocomposite types. On the other hand, the suppression of the molecular mobility was only exhibited at

3 wt% and 5 wt% loadings for the hydroxyethylMMT-PS, and 1 wt% and 3 wt% loadings for the CTABMMT-PS nanocomposites.

TMA results for ethylMMT-PS nanocomposites showed an increase (dependent on clay loading) in the penetration temperature relative to the PS homopolymer. The hydroxyethylMMT-PS nanocomposites showed an increase in the penetration temperature, and the increase was dependent on the clay loading. The finding for this nanocomposite system was different from the above, as penetration temperature for the nanocomposites was relatively lower than that of the PS homopolymer. This was attributed to a plasticizing effect that could have been brought about by the organic modifier, or the copolymer at the polymer-clay interface. The copolymer might exhibit lower T_g, and that would affect the bulk properties. The TMA results of CTABMMT-PS nanocomposites did not show much change relative to those of the PS homopolymer. The only change in the results was seen with a 7 wt%, which was highly plasticized, with penetration at lower temperature relative to the homopolymer and other composites.

Thermal expansion measurements demonstrated a reduction in the coefficient of linear thermal expansion when compared to that of the homopolymer. From the current study, the nanocomposites exhibited thermal dimensional stability when compared to the parent homopolymer. This improved property is suitable for high temperature applications. The nanocomposites also showed an enhanced ionic mobility at high temperatures, as determined by DEA. This was shown through the low frequency dispersion of the real permittivity and the increased real conductivity. These changes were observed at temperatures above 75 ^{o}C. The dependence of the above dielectric properties was systematic for the ethylMMT-PS nanocomposites. The hydroxyethylMMT-PS nanocomposites exhibited the least changes in the dielectric responses.

The three different modifiers, which had produced different nanocomposite morphologies, influenced the mechanical and dielectric responses in different ways. This difference in properties/responses originated from the different nanocomposite morphologies exhibited. Although there was just a single different molecule in the

structure of the surfmers, the eventual morphologies were different and hence subsequent properties of the nanocomposites. The effect of the nanocomposite morphology, is evidently, a major factor in the final properties.

6.5 List of references

1. Alexandre, M.; Dubois, P. *Materials Science and Engineering: R (Reports)* **2000,** 28, 1-63.

2. Ray, S. S.; Okamoto, M. *Progress in Polymer Science* **2003,** 28, 1539-1641.

3. Ray, S. S.; Okamoto, K.; Okamoto, M. *Macromolecules* **2003,** 36, 2355-2367.

4. Agag, T.; Koga, T.; Takeichi, T. *Polymer* **2001,** 42.

5. Fischer, H. *Materials Science and Engineering: C* **2003,** 23, 763-772.

6. Yei, D.-R.; Kuo, S.-W.; Fu, H.-K.; Chang, F.-C. *Polymer* **2005,** 46, 741-750.

7. Laus, M.; Camerani, M.; Lelli, M.; Sparnacci, K.; Sandrolini, F.; Francescangeli, O. *Journal of Materials Science* **1998,** 33, 2883-2888.

8. Noh, M. W.; Lee, D. C. *Polymer Bulletin* **1999,** 42, 619-626.

9. Qutubuddin, S.; Fu, X.; Tajuddin, Y. *Polymer Bulletin* **2002,** 48, 143-149.

10. Fu, X.; Qutubuddin, S. *Polymer* **2001,** 42, 807-813.

11. Mijovic, J.; Lee, H.; Kenny, J.; Mays, J. *Macromolecules* **2006,** 39, 2172-2182.

12. Wang, H.-W.; Chang, K.-C.; Chu, H.-C.; Liou, S.-J.; Yeh, J.-M. *Applied Polymer Science* **2004,** 92, 2402-2410.

13. Wang, H.-W.; Chang, K.-C.; Yeh, J.-M.; Liou, S.-J. *Journal of Applied Polymer Science* **2004,** 91, 1368-1373.

14. Anastasiadis, S. H.; Karatasos, K.; Vlachos, G.; Manias, E.; Giannelis, E. P. *Physical Review Letters* **2000,** 84.

15. Kanapitsas, A.; Pissis, P.; Kotsilkova, R. *Journal of Non-Crystalline Solids* **2002,** 305, 204-211.

16. Bertmer, M.; Wang, M.; Kruger, M.; Blumich, B.; Litvinov, V. M.; van Es, M. *Chemistry of Materials* **2007,** (In Press), (5 pages).

17. Grandjean, J. *Clay Minerals* **2006,** 41, 567-586.

18. Al Arbash, A.; Ahmad, Z.; Al-Sagheer, F.; Ali, A. A. M. *Journal of Nanomaterials* **2006,** 2006, 1-9.

19. Nielsen, L. E.; Landel, R. F., *Mechanical Properties of Polymers and Composites.* 2nd ed.; Marcel Dekker, Inc.: New York, **1994**; p 557.

20. Rao, Y.; Pochan, J. M. *Macromolecules* **2007,** 40, 290-296.

21. Mernad, K. P., *Dynamic Mechanical Analysis: A Practical Introduction.* 1st ed.; CRC Press LLC: Boca Raton, Florida, **1999**; p 208.

22. Nielsen, L. E., *Mechanical Properties of Polymers.* 1st ed.; Van Nostrand Reinhold Company: New York, **1962**; p 274.

23. Meneghetti, P.; Qutubuddin, S. *Thermochimica Acta* **2006,** 442, 74-77.

24. Shah, V., *Handbook of Plastics Testing Technology.* 2nd ed.; John Wiley & Sons, Inc: New York, **1998**; p 527.

25. Turi, E. A., *Thermal Characterization of Polymeric Materials: Vol 1.* 2nd ed.; Academic Press, Inc.: San Diego, California, USA, **1997**; p 1378.

26. Williams, G.; Thomas, D. K. *Phenomenological and Molecular Theories of Dielectric and Electrical Relaxation of Materials*; Application Note Dielectrics no.3: Novocontrol GmbH: **1998**; pp 1-29.

27. Jordan, J.; Jacob, K. I.; Tannenbaum, R.; Sharaf, M. A.; Jasiuk, I. *Materials Science and Engineering: A* **2005,** 393, 1-11.

28. Cadène, A.; Rotenberg, B.; Durand-Vidal, S.; Badot, J.-C.; Turq, P. *Physics and Chemistry of the Earth, Parts A/B/C* **2006,** 31, 505-510.

29. Jacobs, J. D.; Koerner, H.; Heinz, H.; Farmer, B. L.; Mirau, P.; Garrett, P. H.; Vaia, R. A. *Journal of Physical Chemistry B* **2006,** 110, 20143 -20157.

Chapter 7

Conclusion and recommendations

7.1 Conclusions

The main objectives of the study (Chapter 1, Section 1.3) is to determine the structure-property relationships of PLSN materials. These materials have already been studied in terms of preparation and applications.[1] However, the uniqueness of each individual PLSN materials system provides for an opportunity to study each material's properties, and how the morphology influences those properties. The successful preparation of polymerizable surfactants (surfmers) paved way for the preparation and characterization of the PLSNs, and to further investigate the subsequent properties.

Montmorillonite (MMT) was successfully functionalized using the surfmers and a classical surfactant, cetyl trimethyl ammonium bromide (CTAB). The properties of the organically-modified clays (organoclays) were determined by small-angle X-ray scattering (SAXS), Fourier transform infrared spectroscopy (FTIR), to observe the characteristic vibration bands of the molecules. Thermogravimetric analysis (TGA) was used to study thermal stability characteristics, and to determine the amount of the exchanged surfactant, through thermally-induced weight loss. Surface properties were characterized using scanning electron microscopy (SEM). These properties were very vital in understanding the organoclays, before dispersing in the polymer matrix.

Polystyrene-layered silicate nanocomposites were successfully synthesized in bulk using an *in-situ* intercalative polymerization. Exfoliated, intercalated-exfoliated and intercalated morphologies were determined by SAXS and transmission electron microscopy (TEM). A good balance between the driving factors and interfacial properties leads to an exfoliated morphology. These factors include type organic modifier, clay type, polymerization reaction, processing conditions, to mention a few. The matrices of the nanocomposites had higher average molecular weight compared to the homopolymer, as determined by gel permeation chromatography (GPC). FTIR confirmed the participation of the surfmer double bonds in copolymerization. However, the extent of copolymerization could not be determined, as the GPC analysis was limited only to an unattached polymer. Each nanocomposite material is a unique system, which has own peculiar characteristics. This was demonstrated by remarkable findings in this study. In Chapter 6, the properties of the PS-LSNs were determined, employing temperature-based techniques. The improvement in bulk properties was mostly observed when there was large scale chain mobility. This is because viscous flow starts to show the confinement of the chains due to the presence of clay layers in the matrix. Although bulk properties were assigned to the structure, the dynamics of the interfacial region are still yet to be understood. Also, the nano-scale heterogeneity poses more challenges in the understanding of the bulk properties and in their correlation to the underlying structure. Dynamic mechanical analysis (DMA) showed better correlation in the amount of clay added for the ethylMMT-PS (exfoliated) when compared to the other nanocomposites.

The exfoliated nanocomposites showed a dependence of the properties on the amount of clay loading. Even though the 10 wt% ethylMMT-PS nanocomposite had shown the presence of immiscible clay agglomerates, the bulk properties were not greatly compromised. Exfoliated-intercalated nanocomposites exhibited variable dependencies of properties on the clay loading. Thermomechanical analysis (TMA) properties of the exfoliated-intercalated composites showed inferior properties relative to the PS homopolymer. This finding further demonstrated the complexity of the nanocomposite

matrices and the interaction between the phases. An overall improvement in the coefficient of linear thermal expansion was observed in all the types of nanocomposites prepared. The thermal expansion studies further demonstrated thermal and dimensional stability due to the silicate reinforcement.

The determination of new features in the properties and structure of the nanocomposite material was also one of the objectives. The systems were more complex and therefore more variables had to be taken into account. For instance, the properties of the copolymer formed at the polymer-silicate interface could not be determined due to the limitation of the extraction technique used. The information regarding the interfacial region was not well studied. It was, therefore, difficult to conclude the presence or absence of new features in the structure and properties of the materials. However, improvements in thermal, mechanical and dielectric properties were seen as some of the extra-ordinary properties of the nanocomposites.

The current study brought about new knowledge on how to improve properties of conventional polymer, without compromising other properties. PS is a high dielectric constant material (insulator) but its dielectric properties could be modified, giving more conductive features, with enhanced thermal and mechanical properties. It was demonstrated that less than 5 wt% clay could bring about the above-mentioned properties without adding more weight into the material. A more critical factor in the nanocomposite study is the ability for it to be modified in the structure of one or more of its components, in order to obtain the required properties. In the current study, it was observed that a single, small functional group could lead to a different structure and eventually, different properties. The -OH group in the structure of the hydroxyethyl surfmer produced a different nanocomposite morphology when compared to its counterpart with a $-CH_3$ group.

Even with these remarkable findings, more work would have to be undertaken in order to comprehensively understand the morphology, and more intensive study of the properties is needed for a better correlation. The suggested recommendations would strongly complement this study.

7.2 Recommendations

The complexity of the interactions experienced between the phases in the nanocomposites require a more comprehensive analysis, in order to understand the contribution of each component. Such endeavor would require the use of other analytical methods that would not have been possible, due to time and resource constraints, during the current study.

It would be an added advantage to include computational and modeling studies for the interaction of the nanocomposite phases. This would be vital in the prediction of the bulk behavior and the interaction of different phases of the nanocomposite systems. Furthermore, computational and modeling studies would be vital in depicting local structural details of the polymerizable surfactants in the galleries, similar to the study of the dynamics of intercalated alkyl ammonium ions in MMT by Heinz and Suter, cited by Jacobs et al.[2]

The effect of the variation of the surfactant concentration was not done. It would be relevant to follow a relationship between the intercalation dynamics and the variation of the nominal surfactant concentration in solution. It would also be a beneficial study to follow the intercalated organic amount to the clay CEC. This would give an indication of the configuration which the surfactant chains might assume inside the galleries. More importantly, the understanding of these dynamics would be critical in the synthesis or fabrication of PLSNs

In addition, comprehensive study to follow the intercalation chemistry, using adorption isotherms, during the ion-exchange in the organoclay synthesis could be an advantage. This would help in accurately quantifying the amount of surfactant in the galleries, and estimating the chain conformation. Obtaining a better estimation of the conformation and arrangement of the surfactant chains in the galleries would help understand the influence of the variation of the functional groups. The conformation studies would also help in the understanding the effect of the presence of a hydroxyl (-OH) group and just a methyl in the structures of the hydroxyethyl and ethyl surfmers, and how they contribute to the formation of the exfoliated and intercalated nanocomposite morphologies.

Frequency mode DMA measurement would reinforce the already obtained information in terms of understanding the contribution of chain mobility in bulk properties. It would also be advantageous to study the rheological properties of the nanocomposites in the viscoelastic region. Due to the limitation of the methods used, DMA (compressive mode) could only give reliable results only to a limited region after the T_g. Shear rheology measurements would definitely not be limited at temperatures above the T_g, and that could extend the understanding of chain mobility as affected by the presence of the silicate layers.

Reverse addition fragmentation chain-transfer (RAFT) incorporation in the synthesis of the nanocomposites would bring more control of the molecular weight. Less variation in the molecular weight would lead to less uncertainty of the bulk polymer properties.

7.3 List of references

1. Schmidt, D.; Shah, D.; Giannelis, E. P. *Current Opinion in Solid State & Materials Science* **2002,** 6, 205-212.

2. Jacobs, J. D.; Koerner, H.; Heinz, H.; Farmer, B. L.; Mirau, P.; Garrett, P. H.; Vaia, R. A. *Journal of Physical Chemistry B* **2006,** 110, 20143 -20157.

Appendix: A FTIR spectra of PS-LSNs

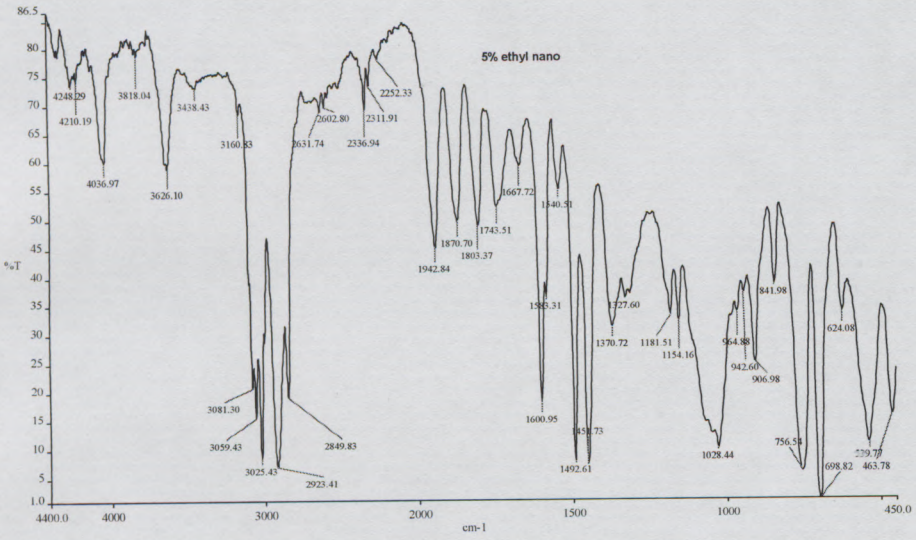

A1.1: FTIR spectrum of 5 wt% ethylMMT-PS nanocomposite

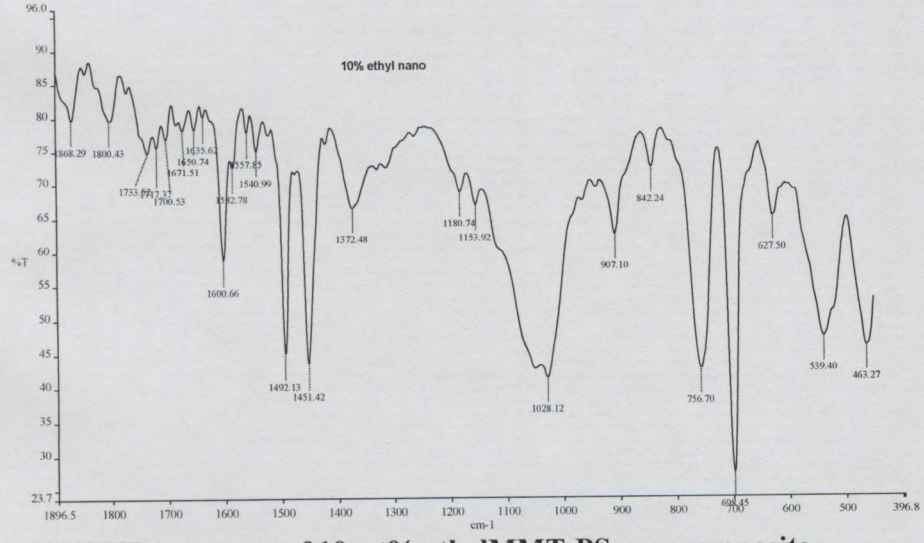

A1.2: FTIR spectrum of 10 wt% ethylMMT-PS nanocomposite

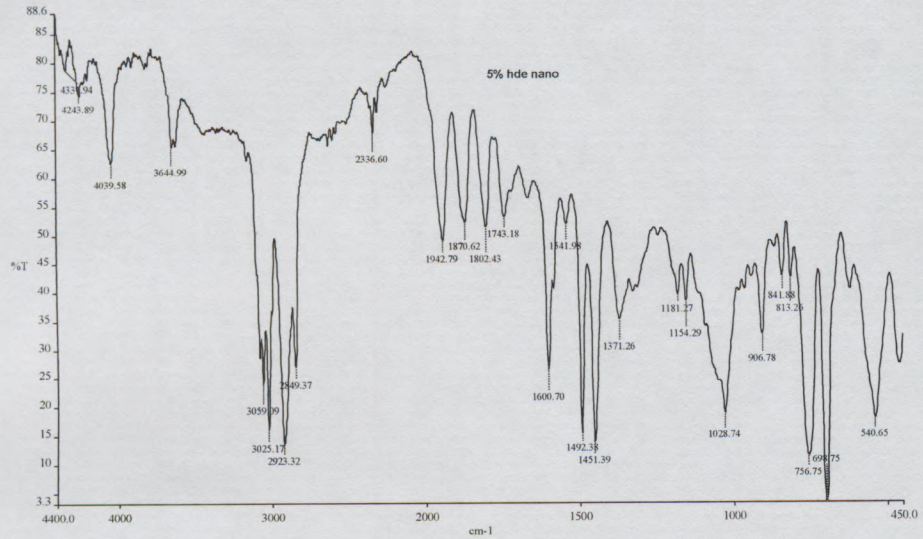

A1.3: FTIR spectrum of 5 wt% hydroxyethylMMT-PS nanocomposite

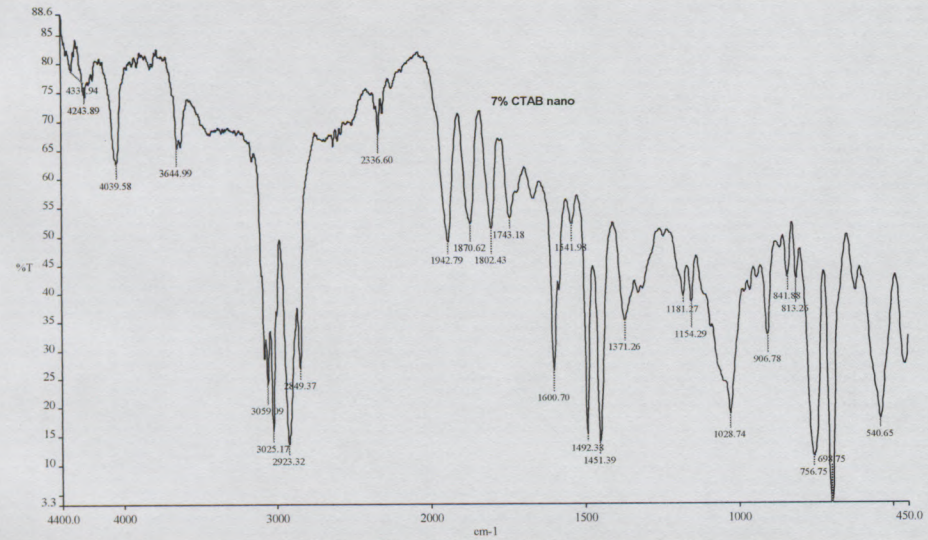

A1.4: FTIR spectrum of 7 wt% CTABMMT-PS nanocomposite

Appendix B Dielectric Analysis of Polystyrene-Layered Silicate Nanocomposite

B 1: Real permittivity plot (ε') versus frequency (f/Hz) plots at different temperatures (25 °C – 150 °C) for PS-LSNs

B1.1 – 1% ethylMMT-PS

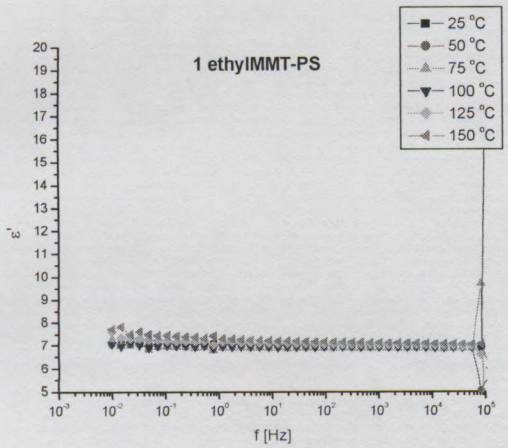

Real permittivity plot (ε') versus frequency (f/Hz) plots for 1% ethylMMT-PS

B1.2 – 10% ethylMMT-PS

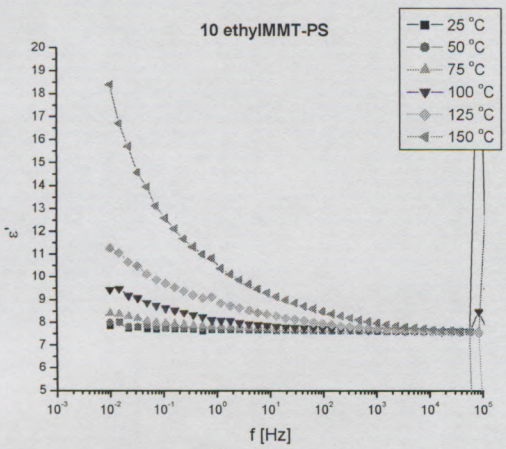

Real permittivity plot (ε') versus frequency (f/Hz) plots for 10% ethylMMT-PS

B1.3 – 1% hydroxyethylMMT-PS

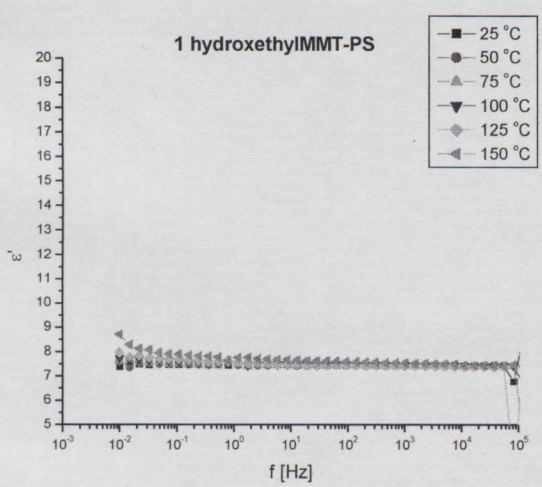

Real permittivity plot (ε') versus frequency (f/Hz) plots for 1% hydroxyethylMMT-PS

B2: Real conductivity plot (σ'/ S.cm^{-1}) versus frequency (f/Hz) plots at different temperatures for Polystyrene (-50 °C – 225 °C) and PS-LSNs(25 °C – 150 °C)

B2.1 – Polystyrene homopolymer

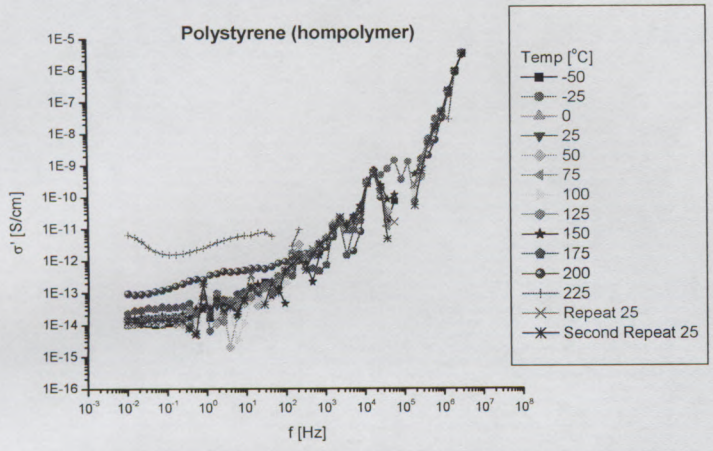

Real conductivity plot (σ'/ S.cm^{-1}) versus frequency (f/Hz) plots for polystyrene homopolymer

B2.2 – 1% ethylMMT-PS

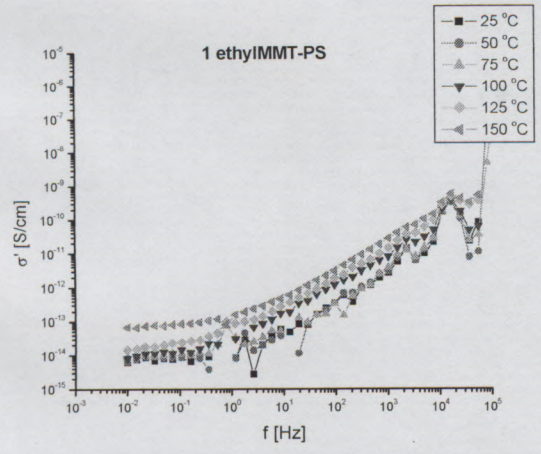

Real conductivity plot (σ'/ S.cm^{-1}) versus frequency (f/Hz) plots for 1% ethylMMT-PS

B2.3 – 10% ethylMMT-PS

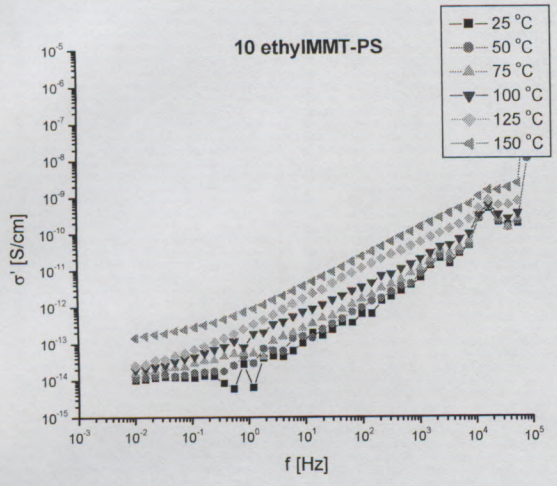

Real conductivity plot (σ'/ $S.cm^{-1}$) versus frequency (f/Hz) plots for 1% ethylMMT-PS

B2.4 – 1% hydroxyethylMMT-PS

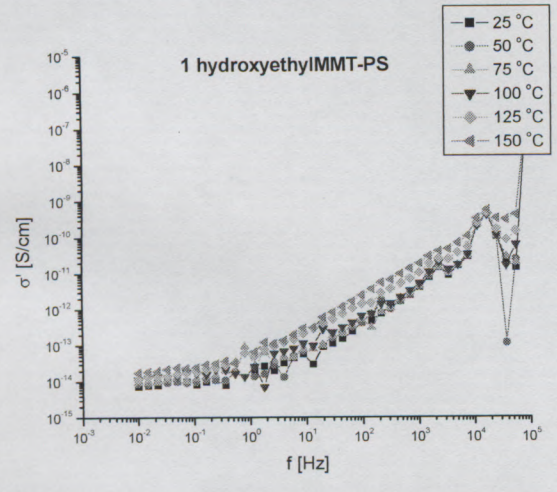

Real conductivity plot (σ'/ $S.cm^{-1}$) versus frequency (f/Hz) plots for 1% hydroxyethylMMT-PS

B2.5 – 7% CTABMMT-PS

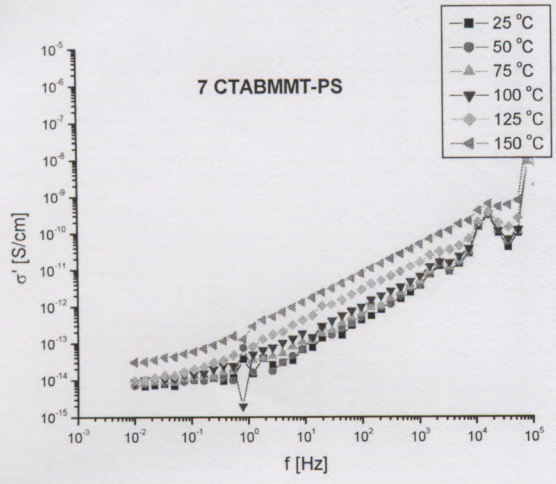

Real conductivity plot (σ'/ $S.cm^{-1}$) versus frequency (f/Hz) plots for 7% CTABMMT-PS